The role of short-term starvation in sensitizing breast cancer to chemotherapy

by

Yogeshni Govender

Thesis presented in fulfilment of the requirements for the degree of Master of Science in the Faculty of Science at Stellenbosch University

Supervisor: Prof. Anna-Mart Engelbrecht
Co-Supervisor: Dr. Benjamin Loos

Faculty of Science

Department of Physiological Sciences

March 2013

Declaration

By submitting this thesis, I declare that the entirety of the work contained therein is my own, original work, that I am the owner of the copyright thereof (unless to the extent explicitly otherwise stated) and that I have not previously in its entirety or in part submitted it for obtaining any qualification.

Date: March 2013

Abstract

Introduction: Breast cancer is a major contributor to mortality in women worldwide. Although, anthracyclines, such as doxorubicin, are among the most valuable treatments for breast cancer, their clinical use is limited due to detrimental side-effects such as cardiotoxicity. Additionally, evidence suggests that cancer cells are becoming increasingly resistant to chemotherapeutic agents. The consequence of poor vascularisation within tumours subsequently leads to a nutrient deprived microenvironment which cancer cells are known to adapt to via metabolic remodelling and increasing autophagy. Autophagy is an intracellular degradation system, which is induced as a survival mechanism in response to starvation and other environmental stressors. Recent studies have shown that starvation protects non-tumourigenic cells against chemotherapy-induced cell death. Furthermore, patients who starved prior to chemotherapy reported reduced side-effects. However, these studies investigated the effects of long-term starvation, which maybe clinically challenging. Therefore, this concept, under shorter and more tolerable periods of starvation still needs to be investigated. We hypothesis, that short-term starvation will sensitize breast cancer cells to doxorubicin-induced cell death. In order to test this hypothesis this study was approached by the following aims: (i) to establish a time point at which MCF12A breast epithelial cells are protected against starvation; (ii) to determine the effect of

short-term starvation on doxorubicin induced cell death; (iii) to assess autophagy and; (iv) to assess these above mentioned aims using an *in vivo* model.

Methods: MDAMB231 cells and MCF12A cells were starved for 0, 3, 6, 12, 24 and 48 hours using Hanks Balanced Salt Solution. Cell viability was assessed using the trypan blue, MTT and Caspase-Glo assays. MDAMB231 cells and MCF12A cells were subjected to the following conditions: (1) control; (2) 5 µM doxorubicin; (3) starvation of 3 hours and (4) a combination of starvation and doxorubicin. Following treatment an MTT assay to assess cell viability was performed. MDAMB231 cells were further examined using Live-Cell Imaging and western blot analysis. C57BL6 tumour bearing mice were treated with doxorubicin (5 mg/kg) or in combination with starvation of 24 hours. Upon termination of the protocol, tumour tissue was assessed using western blot analysis. In both *in vitro* and *in vivo* analyses cleaved-caspase 3 and cleaved-PARP were used as markers for apoptosis, LC3 and p62 as autophagic markers and p-AMPK and p-mTOR as markers of oxygen and energy sensing, respectively.

Results and discussion: Three hours of starvation was chosen for *in vitro* experiments since no significant reduction in cell viability or increases in apoptosis occurred at this time-point in the normal MCF12A breast epithelial cells. As expected, doxorubicin induced a significant decrease in cell viability in the cancerous MDAMB231 cells. Short-term starvation in combination with doxorubicin

treatment caused a further significant decrease in cell viability in MDAMB231 cells compared to the doxorubicin group alone. Interestingly, starved MCF12A cells were protected against doxorubicin-induced cytotoxicity as cell viability significantly increased. A significant decrease in autophagy was further observed with the combined treatment of doxorubicin and starvation which corresponded with a significant increase in cell death. In contrast, although the *in vivo* study also demonstrated a significant elevation in cell death and autophagy in response to doxorubicin treatment, the combined treatment (starvation and doxorubicin) did not have an additive effect when compared to the doxorubicin group alone.

Conclusion: Our *in vitro* results clearly demonstrate that short-term starvation sensitizes breast cancer cells to doxorubicin-induced cell death. Additionally, decreased levels of autophagy appear to contribute to this phenomenon of sensitization. Although doxorubicin treatment resulted in increased apoptosis *in vivo,* 24 hours starvation in combination with doxorubicin did not sensitize the tumours to doxorubicin treatment. Thus, for future *in vivo* studies more time points should be considered in order to translate the beneficial effects of short-term starvation observed in our *in vitro* study to an animal model.

Opsomming

Inleiding: Borskanker is ‘n belangrike faktor wat bydrae tot sterftes in vrouens wêreldwyd. Alhoewel antrasikliene soos doxorubicin, waardevol is vir die behandeling van borskanker, word die kliniese gebruik daarvan beperk deur newe-effekte soos kardiotoksisiteit. Verder, word daar al hoe meer bewys dat kankerselle toenemend weeerstandbiedend word teen chemoterapeutiese middels. Swak vaskularisasie van tumore lei tot ‘n mikro-omgewing met beperkte voedingstowwe waaby kankerselle kan aanpas deur middel van metaboliese hermodelering en ‘n toename in autofagie. Autofagie is ‘n intrasellulêre degraderingsisteem wat as ‘n oorlewingsmeganisme aangewend word tydens verhongering en ander omgewingstressors. Onlangse studies het getoon dat verhongering nie-tumourigeniese (normale) selle teen chemoterapie-geïnduseerde seldood beskerm. Verder is daar ook geraporteer dat pasiënte wat gevas het voor chemoterapie, verminderde newe-effekte getoon het. Hierdie studies het egter gefokus op ‘n relatief lang-termyn vas, wat klinies nogal uitdagend kan wees. Daarom moet hierdie konsep nog op korter, meer hanteerbare tye getoets word. Ons hipotese is dus dat kort-termyn vas borskankerselle kan sensitiseer tot doxorubicin-geïnduseerde seldood. Om hierdie hipotese te toets, is die volgende doelwitte gestel: (i) om ‘n tydspunt te bepaal waar MCF12A borsepiteelselle

beskerm is teen verhongering; (ii) om die effek van kort-termyn verhongering op doxorubicin-geïnduseerde seldood te toets; (iii) om autofagie te karakteriseer in ons model en; (iv) om hierdie doelwitte ook in ‘n *in vivo* model te toets.

Metodes: MDAMB231 en MCF12A selle is verhonger vir 0, 3, 6, 12, 24 and 48 ure deur van Hanks se gebalanseerde soutoplossing gebruik te maak. Sellewensvatbaarheid is bepaal deur middel van trypan blou, MTT en die Caspase-Glo tegnieke. MDAMB231 en MCF12A selle is onderwerp aan die volgende omstandighede: (1) kontrole; (2) 5 µM doxorubicin; (3) verhongering van 3 ure en (4) ‘n kombinasie van verhongering en doxorubicin. Na behandeling is die sellewensvatbaarheid deur middel van die MTT tegniek bepaal. MDAMB231 selle is verder ondersoek deur middel van “Live-Cell Imaging” en die westelike klad tegniek. C57BL6 tumor-draende muise is behandel met doxorubicin (5 mg/kg) of met ‘n kombinasie van verhongering van 24 ure en doxorubicin. Aan die einde van die protokol, is die kankerweefsel geanaliseer deur die westelike klad tegniek. In beide *in vitro* en *in vivo* analises, is gekliefde- caspase 3 en -PARP as merkers vir apoptose, LC3 and p62 as merkers vir autofagie en p-AMPK en p-mTOR as suurstof- en energie sensors respektiewelik gemeet.

Resultate en bespreking: Vir die *in vitro* eksperimente, is ‘n tydspunt van 3 ure gekies as gevolg van die feit dat geen afname in sellewensvatbaarheid en ‘n toename in apoptose in hierdie tydsgleuf tydens verhongering in die normale MCF12A borsepiteelselle plaasgevind het nie. Soos verwag, het doxorubicin

behandeling ‘n insiggewende afname in sellewensvatbaarheid in die kankeragtige MDAMB231 selle veroorsaak. Die kombinasie-terapie van verhongering en doxorubicin het ‘n verdere verhoging in seldood teweeg gebring in die MDAMB231 selle, maar het die normale MCF12A borsepiteelselle teen doxorubicin-geïnduseerde toksisiteit beskerm. Die kombinasie-behandeling is ook geassosieer met ‘n afname in autofagie. Alhoewel, die *in vivo* studie ook getoon het dat doxorubicin alleen insiggewende hoeveelheid seldood teweeggebring het, het die kombinasie-behandeling nie die additiewe effek, soos in die *in vitro* studie, teweeg gebring nie.

Gevolgtrekking: Die *in vitro* resultate het duidelik getoon dat kort-termyn verhongering borskankerselle kan sensitiseer vir doxorubicin terapie. Verder het dit geblyk dat ‘n afname in autofagie tot die fenomeen van sensitisering bygedrae het. Alhoewel doxorubicin behandeling *in vivo* tot ‘n toename in apoptose in die tumor gelei het, het die kombinasie behandeling nie die kankerweefsel ten op sigte van doxorubicin gesensitiseer nie. Daar sal dus vir toekomstige *in vivo* studies meer tydsgleuwe van behandeling ondersoek moet word om die optimum verhongeringsperiode te vind sodat die *in vitro* resultate ook *in vivo* van toepassing kan wees.

Acknowledgements

Thank you Heavenly Father for the strength and courage you have provided me with during challenging times.

I would like to thank the following people to whom I will be forever grateful:

My supervisor, Professor Anna-Mart Engelbrecht, for her constant guidance, patience, encouragement and for having faith in me at times when I had none. Thank you for all the time you sacrificed to assist me and for entrusting me with this project.

Dr Ben Loos: for all his assistance and guidance.

Members of DSG, thank you for all your support and for assisting me during this study. Special thanks to Heloise le Roux for her assistance with the animal study.

Academic Staff: for your great leadership.

My parents: for all their support, love, guidance and care. Thank you for all that you have sacrificed for me.

Andre de Bruyn: for his constant love, care and support. Thank you for all that you have assisted me with through the years and for your undivided attention during our conversations about cancer and lab-work.

Special thanks to the NRF and CANSA for your financial support which allowed me to continue studying.

TABLE OF CONTENTS

List of Figures

Abbreviations

A

α-KG	Alpha-Ketoglutarate
AMP	Adenosine monophosphate
AMPK	5' adenosine monophosphate-activated protein kinase
ADH	Atypical ductal hyperplasia
ANOVA	Analysis of variance
Apo-3L	Tumour necrosis factor (ligand) superfamily, member 12
ATG	Autophagy-related gene
ATM	Ataxia telangiectasia mutated
ATP	Adenosine triphosphate
AVO	Acidic vesicular organelle

B

Bak	Bcl-2 homologous antagonist/killer
Bax	Bcl-2–associated X protein
Bcl-2	B-cell lymphoma-2 homology
Bcl-X_L	B-cell lymphoma-extra large protein
BH_3	Bcl-2 homology domain 3
Bid	BH_3 interacting domain death agonist
BNIP3	Bcl-2/adenovirus E1B 19 kDa protein-interacting protein 3
BNIP3L	Bcl-2/adenovirus E1B 19 kDa protein-interacting protein3-like

C

c-Flip	Cellular FLICE inhibitory protein (apoptosis inhibitor)
CANSA	Cancer Association of South Africa
cDNA	complementary DNA
CD95	Cluster of differentiation 95
CTRL	Control
Cyt c	Cytochrome c

D

DCIS	Ductal carcinoma *in situ*
DED	Death effector domain
DICS	Death-inducing signaling complex
DMEM	Dulbecco's modified Eagle medium
DNA	Deoxyribonucleic acid
DNA-PKcs	DNA-dependent protein kinase catalytic subunit
DNMT1	DNA methyltransferase 1
DXR	Doxorubicin

E

ECACC	European Collection of Cell Cultures
ECG	Electrocardiography
EDTA	Ethylene diaminetetra-acetic acid
EGF	Epidermal growth factor
ERCC1	Excision repair cross-complementing
ERK1/2	Extracellular signal-regulated kinases

F

FADD	Fas-associated-death-domain
FBS	Foetal Bovine Serum

I

IAP	Inhibitor of apoptosis protein
IDC	Invasive (or infiltrating) ductal or lobular carcinoma
IGF-2	Insulin-like growth factor 2
IL-6	Interleukin-6

H

HIF1	Hypoxia Inducible Factor 1
HSF-1	Heat shock factor protein 1 HSF-1
Hsp25	Heat Shock protein 25- Hsp25

L

LC3	Microtubule-associated protein light chain-3
LIR	LC3-interacting regions

M

MAP	Mitogen activated protein
MPT	Mitochondrial permeability transition
mRNA	Messenger RNA
mTOR	Mammalian target of rapamycin
mTORC1	mTOR complex 1
MTT	3-(4,5-dimethythiazol-. 2-yl)-2,5-diphenyl tetrazolium bromide

N

NBR1	Neighbor of BRCA1 gene 1
NF-kB	Nuclear Factor-Kappa B

P

p38	p38 Mitogen-Activated Protein Kinase
p53	Tumour protein 53
p62/SQSTM1	Poly-ubiquitin protein 62/Sequestome 1
PARP	poly (ADP-ribose) polymerase cleavage
PBS	Phosphate Buffer Saline
PDGF-B	Platelet-derived growth factor B
Penstrep	Penicillin/Streptomycin
PI3K/Akt	Phosphatidylinositol 3-kinase/oncogenic kinase
PONR	'Point of no return'
PTEN	Tumour suppressor phosphatase and tensin homologue deleted from chromosome 10

R

REDD1	Regulated in development and DNA damage response 1
RIPA	Radio immunoprecipitation assay
ROS	Reactive oxygen species
RTK	Receptor tyrosine kinase

S

smac/DIABLO	The second mitochondria-derived activator of caspase/direct IAP binding protein with low pI
SEM	Standard error of mean
siRNA	Small interfering ribonucleic acid

STS	Short-term starvation

T

T25	25 cm^2 Flask
T75	75 cm^2 Flask
TGF-β	Transforming growth factor-β
TCA	Tri-carboxylic-acid
TN I	Troponin I
TNF-α	Tumour necrosis factor-α
TOP2A	DNA topoisomerase II
TP53	Tumour protein 53
TRIAL	TNF-related apoptosis-inducing ligand

V

VEGF	Vascular endothelial factor
VS	Versus

U

ULK1	Unc-51-like kinase (ULK1) complex
UBA	Ubiquitin-interacting domains

Units of Measurement

A	ampere
AU	arbitrary units
cm	centimetre
cm^2	centimetres squared
g	gravitational accerleration
hr/s	hour/s
kD	kilodalton
kg	kilogram
l/L	litre
M	molar
mg	milligram
mg/kg	milligram per kilogram
mg/m^2	milligram per metre squared
min	minutes
ml	millilitres
mm	millimetre
mM	millimolar
mmol/l	millimoles per litres
mm^2	millimetre squared
nm	nanometre
nM	nanomolar
rpm	revolutions per minute
sec	seconds
V	volt

%	percent/percentage
°C	degrees Celsius
µg	microgram
µg/ml	microgram per millilitre
µmol/L	micromoles per litre
µl	microlitre
µm	micrometre
µM	micromolar

Chapter 1 – Literature Overview

1.1: The Nature of Cancer

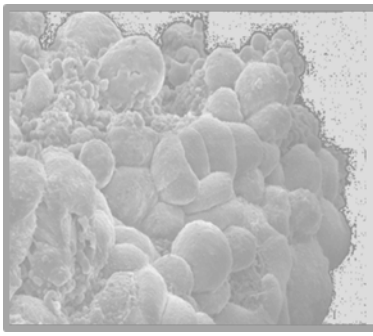

When I published the results of my experiments on the development of double-fertilised sea-urchin eggs in 1902, I added the suggestion that malignant tumours might be the result of a certain abnormal condition of the chromosomes, which may arise from multipolar mitosis…So I have carried on for a long time the kind of experiments I suggested, which are so far without success, but my conviction remains unshaken.

Theodor Boveri, pathologist, 1914

The cell: The single most fundamental unit of life. Each of the 100 trillion building blocks which constitute the human body, are endowed with an array of organelles which display great autonomy, versatility and function collectively to sustain the existence of life. Throughout the life span of an organism, cells possess the remarkable ability to proliferate, playing a critical role in tissue morphogenesis and maintaining the adult tissue by replacing cells that have become damaged or suffered attrition after many years of service. This process of cell proliferation is subjected to strict homeostatic control; cell death must exactly balance cell proliferation in order to maintain a constant number of cells in the human body (Evan and Vousden, 2001). A minor disruption in this tightly regulated process can trigger the onset of diseases such as cancer which is characterised by continuous cell proliferation (Fulda and Debatin, 2006).

The multifaceted complexity of this disease challenges a precise definition; however there are key characteristics that are inherent to all human cancers. These characteristics can be used to describe cancer as an abnormal growth of cells caused by multiple changes in gene expression (Evan and Vousden, 2001). Such genetic mutations lead to an evolving population of cells that can invade tissues and metastasize to distant sites, causing significant morbidity and, if untreated, death of the host (Cavallaro and Christofori, 2004).

A recent review by Hanahan and Weinberg (2011) proposed that the hallmarks of cancer involve biological capabilities which are enabled by genomic instability and tumour promoting inflammation, during the multistep development of human tumours. These include: (i) **sustaining proliferation signalling** - cancer cells deregulate growth factor ligands which typically bind to receptor tyrosine kinase (RTK) domains. Abnormal RTK activation in human cancers is mediated by four principal mechanisms: autocrine activation, chromosomal translocations, RTK overexpression, or gain-of-function mutations (Lemmon and Schlessinger, 2010). These cells further acquire somatic mutations affecting B-Raf proteins involved in the Raf to mitogen activated protein (MAP)-kinase pathway (Bennasroune *et al.,* 2004; Lemmon and Schlessinger, 2010), subsequently affecting the oncogenic phosphatidylinositol 3-kinase pathway (PI3K/Akt) which allows for survivin mRNA expression, preventing cell death (Favoni *et al.,* 2000; Zhao *et al.,* 2011). Some cancers also acquire a loss of function mutation in the potent tumour suppressor, PTEN, which causes a deregulation of the mammalian target of rapamycin (mTOR)

which further increases PI3K signalling thus sustaining proliferation (Guertin and Sabatini, 2007; Fang *et al.,* 2010; Rodriguez and Huynh-Do, 2012); (ii) **evading growth suppressors** - in contrast to stimulating factors to induce chronic proliferation, cancer cells have to further equivocate processes which negatively control cell proliferation. The mechanisms by which this can be achieved are greatly influenced by the activity of tumour suppressor genes. Mutations in the tumour suppressor genes which encode TP53 protein (tumour protein 53) are frequent in most human cancers. Such mutations render TP53 protein incapable of inducing cell death and inhibiting the progression of cancer cells through the cell cycle; (iii) **resisting cell death** - despite the enormity of DNA damage that may be present in cancer cells or which are induced by chemotherapeutic treatments, programmed cell death is attenuated via genetic mutation in TP53 (Junttila and Evan, 2009); (iv) **enabling replicative immortality** - as mentioned previously progression of normal cells is limited via homeostatic mechanisms, therefore after a certain number of divisions, cells enter a state of senescence in which they are still viable but no longer proliferate; this leads to eventual death within the population. On the contrary, cancer cells are much more resilient and avoid senescence and cell death, displaying infinite replicative capacity. Telomeres which protect the end of chromosomes have been implicated in playing a key role in this immortalisation (Blasco, 2005); (iv) **inducing angiogenesis** - the tumour microenvironment is deprived of nutrients and oxygen, thus in their relentless drive to survive, tumour cells develop new blood vessels from existing ones to satisfy the nourishment required by these demanding population of cells via activation of

vascular endothelial factor (VEGF) (Ferara, 2010; Olive *et al*., 2009); (vi) **invasion and metastasis** - all cancers are known to invade and destroy adjacent and normal tissues. They metastasize via lymphatic channels or blood vessels to other regions of the body. As malignant neoplasms progress, the phenotypic resemblance once shared with the cells in the tissues they originated from, is lost. The loss of E-cadherin, which is a cell adhesion molecule, has been closely associated with this characteristic (Cavallaro and Christofori, 2004); (vii) **reprogramming of energy metabolism** - due to their chronic proliferation, cancer cells have a high glycolytic rate to meet their metabolic demands. Thus, a metabolic switch from mitochondrial oxidative phosphorylation to aerobic glycolysis is required to meet this energy demand in hypoxic conditions (Warburg, 1956b); (viii) **evading immune destruction** - cancer cells evade immune surveillance by disabling components such as cytotoxic T lymphocytes and secreting TGF- β which is an immune-suppressive factor (Yang *et al.*, 2010). The latter two are emerging hallmarks (Figure 1.1.1).

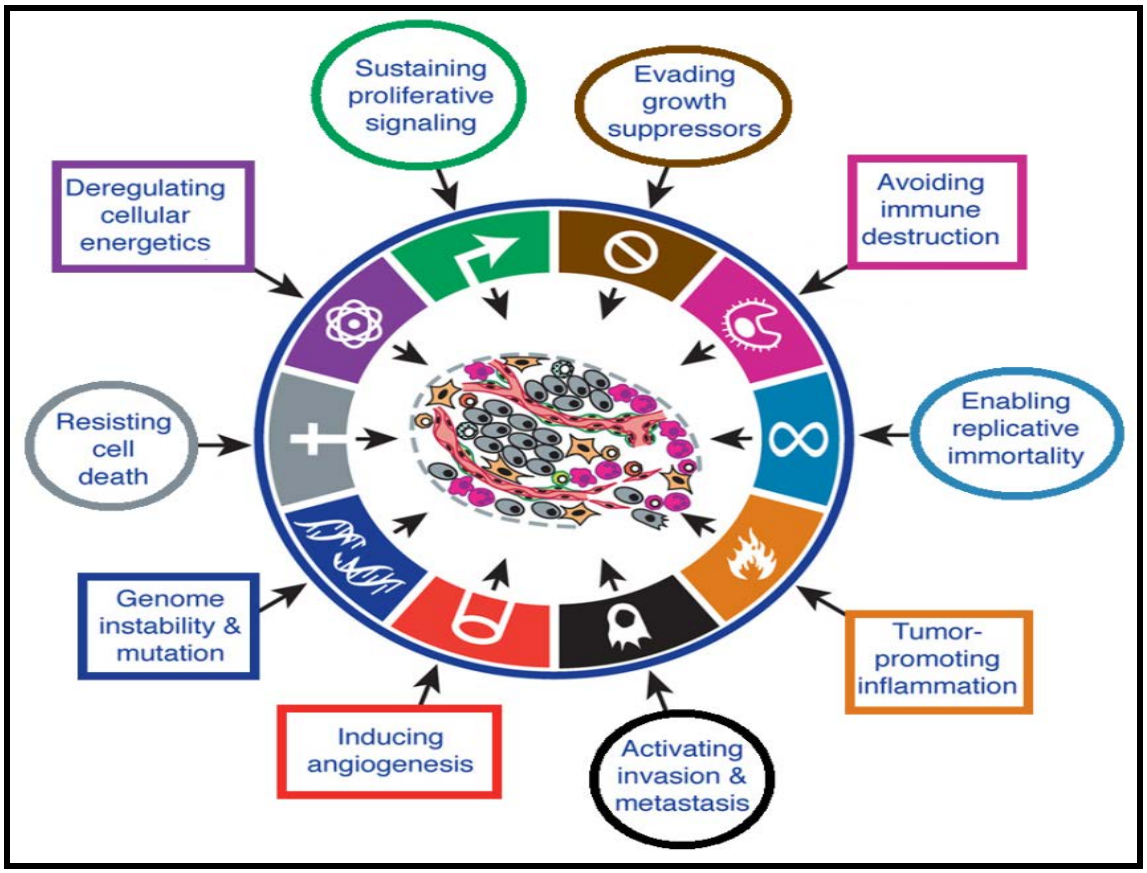

Figure 1.1.1: The Ten Hallmarks of Cancer and Enabling Characteristics. The hallmarks establish an organising principle for elucidating the complexities of neoplastic disease. They include sustaining proliferation, evading growth suppressors, resisting cell death, enabling replicative immortality, inducing angiogenesis, activating invasion and metastasis, reprogramming of energy metabolism and evading immune destruction. Underlying these hallmarks are genome instability, which generates the genetic diversity and mutability to drive tumour progression, and inflammation, which supports multiple hallmark capabilities (Adapted from Hanahan and Weinberg, 2011).

These fundamental hallmarks provide context and perspective, aiding in our understanding of all human cancers. Yet, a major question as to precisely how cancer cells learn to invade and to undergo the metastases that are responsible for 90% of cancer mortality, remains unresolved.

According to the Cancer Association of South Africa (CANSA), one in six South African men and one in seven South African women will get cancer during their lives (Bateman, 2009). In a chapter on lifestyle-induced cancer in South Africa, the

authors found that the highest age-standardised cancer death rates are found in the coloured population (212.5/100 000), followed by the white (198.9), African (126.0) and Asian (121.4) groups. The Western Cape has the highest cancer death rates followed by Gauteng (Bateman, 2009).

1.2: Breast Cancer

Breast cancer is one of the most prevalent cancers affecting 12.4% of South African women. Statistics show a dramatic increase of breast cancer to 15.8% by the year 2015. An estimated 8 000 South African women are diagnosed with breast cancer every year and about 1 600 (20%) will die (Bateman, 2009) (Figure 1.2.1).

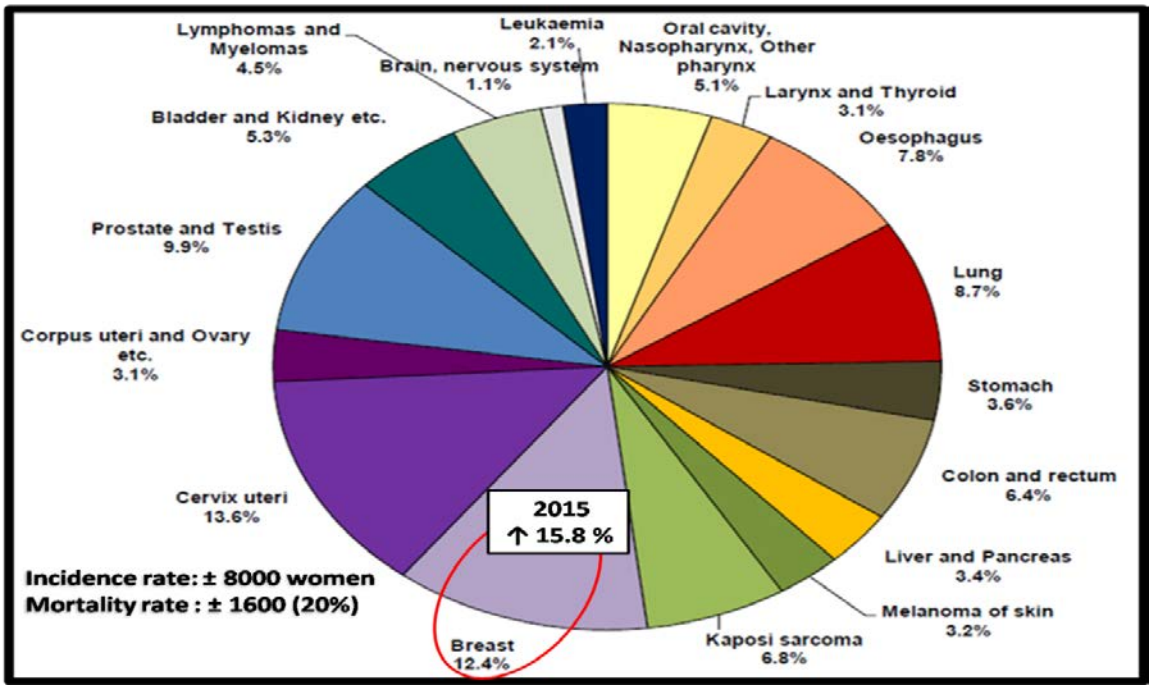

Figure 1.2.1: Cancer incidence in South Africa (2009). Breast cancer accounts for 12.4%, being second most prevalent type of cancer affecting South African women (Adapted from GLOBOCAN, 2008).

Risk factors include high dietary fat intake associated with obesity; duration of exposure to female hormones during early menarche and late menopause; alcohol consumption; reproductive factors involving nulliparity and late age of first pregnancy; chronic use of hormone replacement therapy; exposure to ionising radiation during breast development; and genetic inheritance of breast cancer such as *brca1*, *brca2* or *p53* germline mutations (Richie and Swanson, 2003).

The human breast is composed of stromal and epithelial elements. The stromal elements are comprised of adipose tissue, connective tissue, blood and lymphatic vessels, whereas the epithelial elements are composed of numerous branching ducts, which connect the lobules leading to the nipple-areolar complex. More than 95% of breast cancers originate from the epithelial elements and are classified as adenocarcinomas (Colditz *et al*., 2000; Richie and Swanson, 2003).

It is generally accepted that breast cancer initiates as the premalignant stage of atypical ductal hyperplasia (ADH) and further progresses into two major types, *in situ* carcinomas and invasive carcinomas. The *in situ* carcinomas may arise in either ductal or lobular epithelium, remaining there, posing no invasion of the underlying basement membrane and infiltration of the surrounding stroma of the breast; this constitutes the pre-invasive stage of ductal carcinoma *in situ* (DCIS). In contrast, when the ductal or lobular malignancy extends beyond the basement membrane that constitutes the epithelial border and invades the breast stroma, the malignancy is considered as an invasive (or infiltrating) ductal or lobular carcinoma (IDC) ensuing to a potentially lethal stage. Seventy-five – 80% of invasive cancers

are infiltrating ductal carcinomas, while infiltrating lobular carcinomas make up the second most common type of invasive cancers (Colditz *et al*., 2000).

This linear model of breast cancer progression has been the underlying principle for the use of detection methods such as mammography to diagnose and treat breast cancer at early clinical stages (Ma *et al*., 2003). However, one of the most challenging aspects faced by clinicians is how to accurately grade these tumours as the stages of DCIS and IDC exhibit mitotic activity and cellular differentiation both within a tumour and among individual tumours contributing to heterogeneity.

Existing tumour grading systems, subtype the stages of DCIS and IDC into three tumour grades. Grade I (well differentiated), Grade II (moderately differentiated) and with Grade III (poorly differentiated), being the most malignant resulting in poor prognosis (Schnitt, 2001; Ma *et al*., 2003).

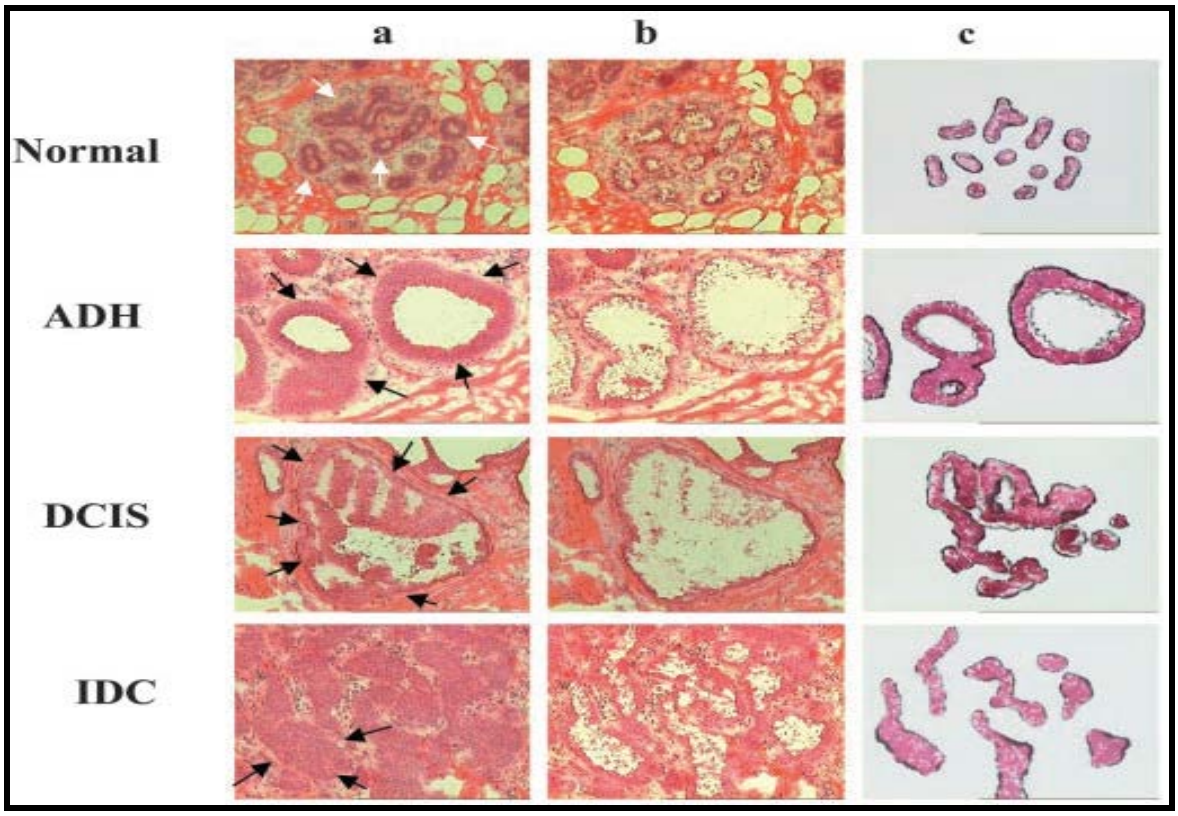

Figure 1.2.2: Phenothypical changes in breast malignancies. Phenotypically normal breast epithelium (white arrows) and phenotypically abnormal epithelium (black arrows) from ADH, DCIS, and IDC from a single breast specimen (case 79) were captured from haematoxylin and eosin stained sections (Ma *et al*., 2003).

As mentioned previously, one of the hallmarks of cancers is resistance to cell death. Breast epithelial cell homeostasis requires the balance of cell proliferation with a type of cell death called apoptosis (Ma *et al*., 2003). Apoptosis is defined as genetically programmed autonomous cell death, and it occurs in healthy breast cells at varying rates during the estrus cycle in response to changes in hormone levels (Ma *et al*., 2003). Apoptosis is also regulated by non-hormonal signals, such as heat, radiation, nutrient deprivation, viral infection, hypoxia and increased intracellular calcium concentration (Ameisen, 2002).

Changes in the genetics of apoptotic regulatory mechanisms may result in an increase in cell numbers, as well as the preservation of genetically altered cells, which begins the process of tumourigenesis (Junttila and Evan, 2009).

1.3: Apoptosis

The term “apoptosis” was first mentioned in an insightful review by Kerr, Wyllie, and Currie in 1972 where they described a tightly regulated, energy-dependent and morphologically distinct form of cell death. Apoptosis is considered as an integral component of significant processes including normal cell turnover, proper development and functioning of the immune system, hormone-dependent atrophy, embryonic development and chemical-induced cell death. Either too much or too little apoptosis has been implicated in many human disorders including neurodegenerative diseases, ischemic damage, autoimmune disorders and many types of cancer (Elmore, 2007).

Morphological changes that occur during apoptosis include highly conserved chromatin, segregated into distinctly defined bodies within an intact nuclear envelope (nuclear pyknosis), cytoplasmic condensation, cells become smaller in size, the cytoplasm is dense and the organelles are more tightly packed (cell shrinkage), followed by nuclear and cellular fragmentation and rapid phagocytosis of apoptotic bodies by adjacent cells (Figure 1.3.1) (Kerr *et al*., 1994; Ameisen, 2002).

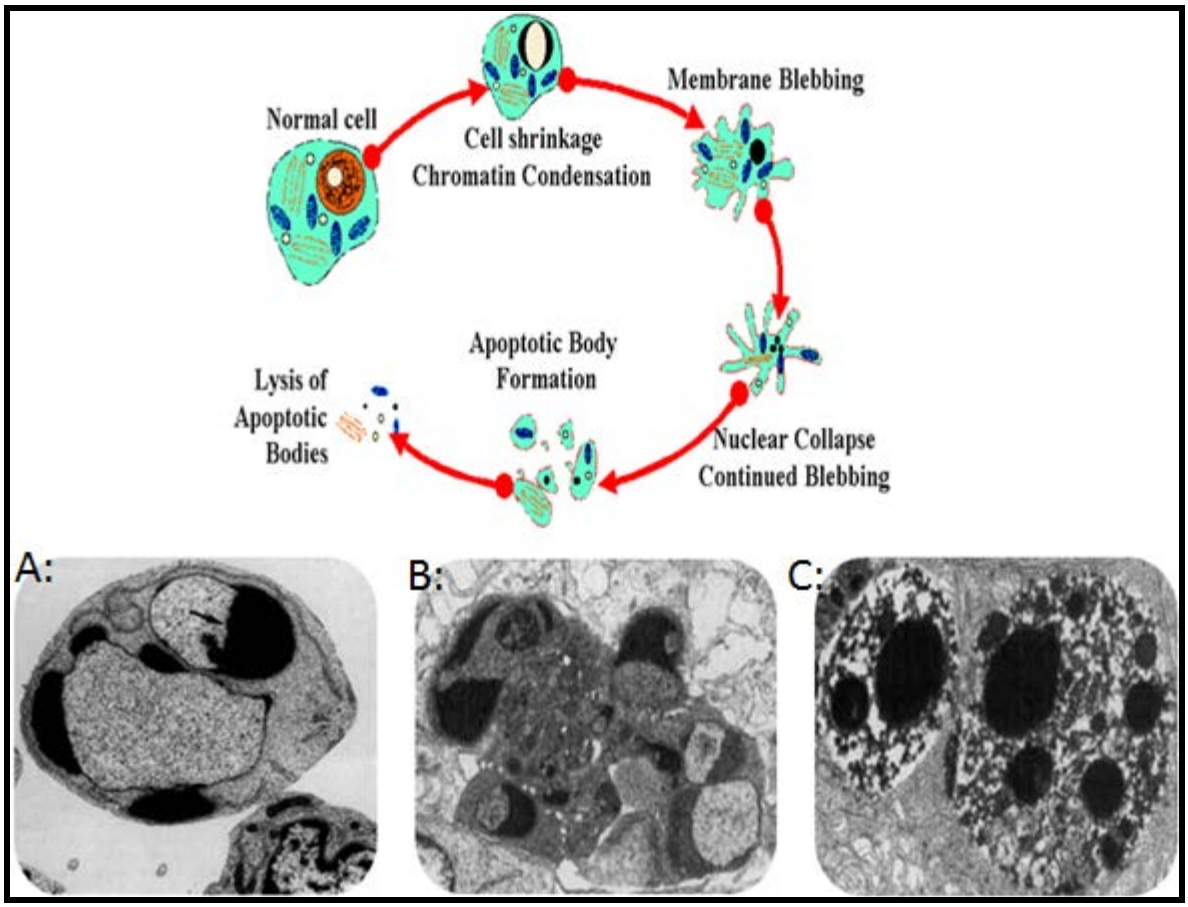

Figure 1.3.1: **Schematic view and electron micrographs of morphological changes during apoptosis.** Electron micrographs depicting: **A- c**ondensed chromatin in membrane-enclosed nuclear fragments and remnants of the nucleolus, **B-** nuclear fragmentation, and budding of cell to form apoptotic bodies and **C-** formation of apoptotic bodies (Adapted from Kerr *et al*., 1994).

Essentially, no inflammatory reaction is associated with the process of apoptosis nor with the removal of apoptotic cells, since: (1) apoptotic cells do not release their cellular constituents into the surrounding interstitial tissue; (2) they are rapidly engulfed and phagocytosed by surrounding cells hence preventing secondary necrosis; and, (3) the engulfing cells do not produce anti-inflammatory cytokines (Savill and Fadok, 2000; Kurosaka *et al*., 2003).

1.3.1: The Caspases

The central executioners of apoptosis consist of proteases from the caspase family (Kerr *et al*., 1994; Elmore, 2007; Salvesan and Reidl, 2008). Thus far, 14 mammalian caspases have been cloned (Budihardjo *et al*., 1999). Caspases, are a subclass of cystein proteases that cleave substrates after aspartic residues (Thornberry and Lazebnik, 1998). Similarly, to proteases, caspases are synthesized and remain in a latent form (zymogens) until proteolysis and activation by other caspases in the cascade occurs.

These pro-enzymes can be classified into 3 classes (Figure 1.3.2). (1) The initiator caspases, have long pro-domains of 90 amino acid residues, containing either a death effector domain (caspase-8 and caspase-10) or a caspase recruitment domain (caspase-2 and caspase-9). Both the death effector domain and the recruitment domain interact with complementary domains on adaptor proteins which aid in auto proteolysis. (2) The executioner or effector caspases contain short pro-domains (caspases 3, 6 and 7). (3) Inflammation caspases are mainly involved in cytokine maturation (caspases 1, 4, 5, 12, and 14) (Grütter, 2000).

Collectively, in a classically formed cascade, initiator caspases (upstream in the cascade) cleave and activate effector caspases (downstream in the cascade) resulting in rapid caspase mobilization and cascade amplification, ultimately culminating in apoptotic cell death by two central pathways: the extrinsic or death

receptor pathway and the intrinsic or mitochondrial pathway (Thornberry and Lazebnik, 1998; Elmore, 2007; Salvesan and Reidl, 2008).

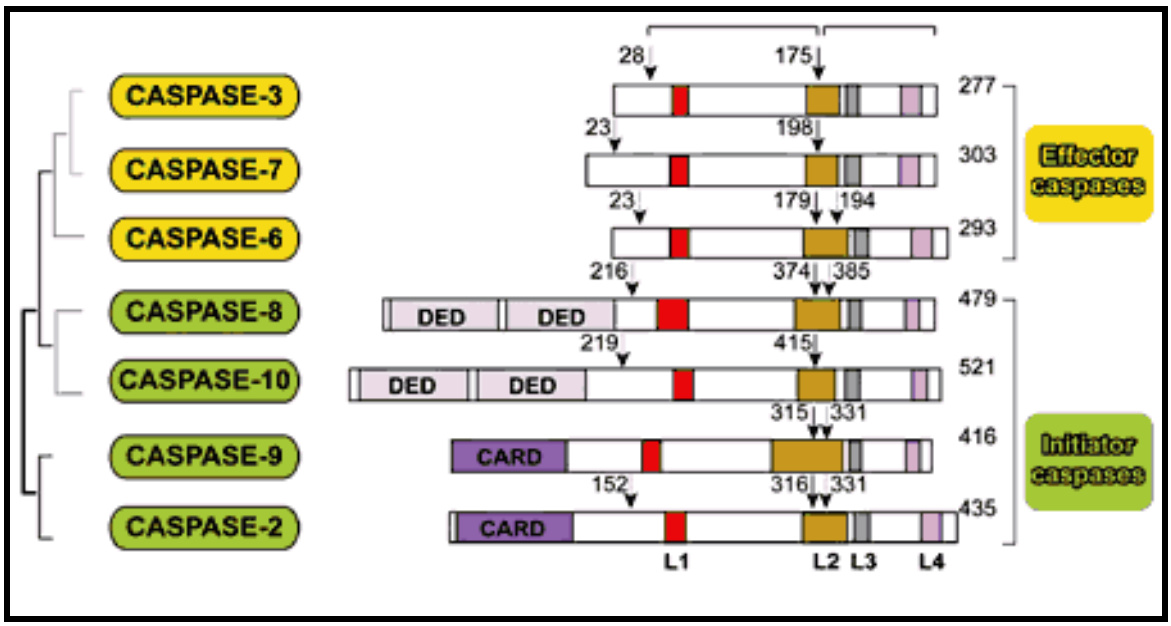

Figure 1.3.2: Schematic representation of effector and initiator caspases and their domains (Petronelli *et al.,* 2005).

1.3.2: The Extrinsic Pathway

The extrinsic or death receptor-mediated pathway is initiated by the binding of ligands of the death receptor super-family [Fas ligand (CD95), tumour necrosis factor-α (TNF-α), TRIAL and Apo-3L] to their associated cell surface receptors. Each of these death receptors contains a cytosolic domain or death domain. Once bound to their respective ligands and with the aid of death domain-mediated protein-protein interactions, intracellular adapter proteins are recruited to the cell membrane, creating a multi-protein complex commonly known as the death-inducing signaling complex (DISC). DISC in turn, activates caspase-8/10 which

activates caspase-3, thereby inducing apoptosis. In Fas signaling, the binding of Fas ligand to the Fas death receptor leads to its association with an adaptor protein known as Fas-associated-death-domain (FADD). FADD contains a death effector domain (DED) which in turn binds to the DED of procaspase-8 forming DISC. DISC subsequently activates caspase-8, resulting in the cleavage and activation of caspase-3 and Bid (BH_3 interacting domain death agonist). Importantly, the activation of procaspase-8 can be inhibited by recruitment of c-FLIP, a protease-deficient caspase homolog widely regarded as an apoptosis inhibitor. In many cell types, activation of the extrinsic pathway also requires the activation of the intrinsic pathway to achieve complete execution of cell death (Kroemer, 2003; Thorburn, 2004).

1.3.3: The Intrinsic / Mitochondrial Pathway

Mitochondria are thought to be the “gatekeepers” of apoptotic machinery as they are the principal organelles involved in mediating most apoptotic pathways in mammalian cells (Kroemer, 2003; Thorburn, 2004). The intrinsic pathway is activated in response to various stress stimuli, including DNA damage, heat, gamma and ultraviolet radiation, actions of onco-proteins and tumour suppressor genes (p53), viruses as well as chemotherapeutic agents (Kroemer, 2003).

The intrinsic pathway involves the bcl-2 family of pro-apoptotic (Bax, Bid, Bak) or anti-apoptotic (Bcl-2, Bcl- X_L) proteins (Figure 1.3.3). Activation of pro-apoptotic factors results in their translocation to the mitochondrial membrane, subsequently

depolarizing voltage-dependent mitochondrial channels, releasing cytochrome *c* (Cyt *c*) and smac/DIABLO which are mediators of apoptosis. There are both positive and negative regulators that interact in this pathway as smac/DIABLO protein prevents the activation of inhibitor of apoptosis (IAP) proteins, subsequently inhibiting caspase-3. The crosstalk between the extrinsic and intrinsic pathways is mediated by Bid. When cleaved and activated by caspase-8, Bid triggers Cyt *c* release from the mitochondria. It is crucial for this process to be tightly regulated, as it decides the fate of every cell in the human body thus, ensuring the existence of mankind. It is well established that apoptosis contributes to cell death in tumours treated with various anticancer agents (Kerr *et al*., 1994; Ameisen, 2002; Simstein *et al*., 2003).

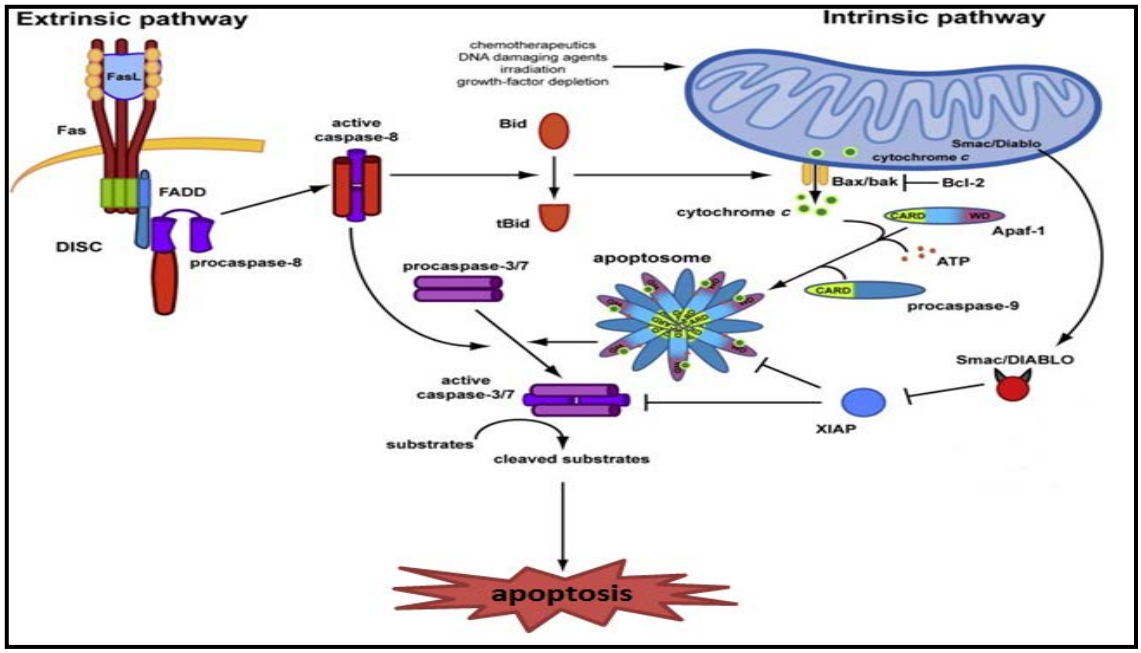

Figure 1.3.3: **Schematic representation of the intrinsic and extrinsic pathways of apoptosis** (Lamkanfi and Dixit, 2010).

Standard treatment, which includes maximal surgical removal of the tumours and post-operative radiation therapy combined with doxorubicin (DXR) chemotherapy, still yields unsatisfactory results. This is mainly due to the high resistance of infiltrative tumour cells to programmed cell death (Verheij, 2000).

1.4: Doxorubicin

First developed in the 1970's, derived from a metabolite of *Streptomyces peucetius* var. *Caesius*, the anthracycline, doxorubicin (DXR) has become a highly effective anti-neoplastic agent used in the treatment of breast cancer and various other cancers (Octavia *et al*., 2012). Several mechanisms have been postulated to describe the apoptotic effects of anthracyclins which mainly involve: free radical

.

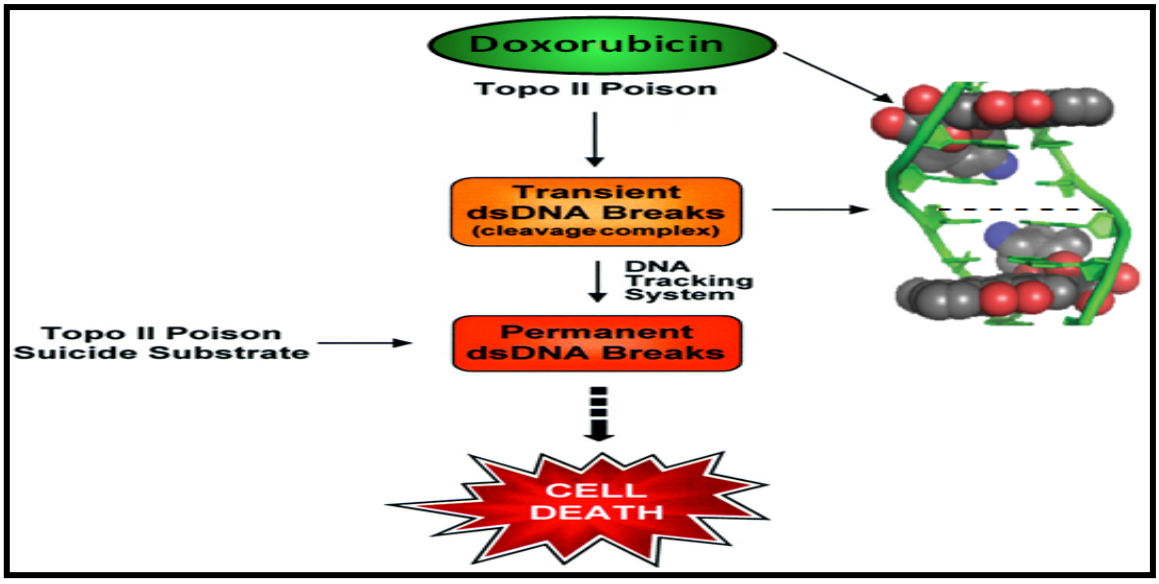

Figure 1.4.1: Doxorubicin intercalates into DNA and stabilises the cleavable complex (Frederick *et al.,* 1990).

formation subsequently leading to DNA and cell membrane damage, disruption of DNA topoisomerase II (TOP2A) and also DNA intercalation, resulting in inhibition of DNA replication, synthesis and strand break related DNA damage (Figure 1.4.1) (Gewirtz, 1999). Chemotherapy using DNA intercalators have proven to be one of the most successful approaches to cancer treatment. Although DNA intercalators are believed to inhibit DNA polymerases and topoisomerases, resulting in the induction of apoptosis in tumour cells, other factors potentially inhibited by the anthracycline antibiotic have been successfully elucidated. One of the major targets of doxorubicin (DXR) was shown to be DNA methyltransferase 1 (DNMT1) which is a primary enzyme responsible for the maintenance of DNA methylation on genomic DNA. Doxorubicin-induced inhibition of DNMT1 resulted in drug-induced apoptosis in human cancer cells indicating that the levels of DNMT1 in tumour cells may affect the effectiveness of doxorubicin in chemotherapy (Yokochi and Robertson, 2004).

Recently, a study conducted by Lee and colleagues (2010) using cDNA microarray analysis, identified 18 genes which mediated DXR- induced cell death; mainly via poly (ADP-ribose) polymerase cleavage (PARP), and activation of caspase-3. Poly (ADP-ribose) polymerase (PARP) is a nuclear enzyme, present abundantly in eukaryotic cells. It is activated in response to DNA strand breakage which is induced by chemotherapeutic agents and various other environmental stresses. When activated, the enzyme increases its catalytic capacity and rapidly binds to damaged DNA; this in turn initiates an energy-consuming cycle by transferring ADP ribose units from NAD to nuclear proteins to induce DNA repair (Munoz-

Gamez *et al*., 2005; Lee *et al*., 2002). Since, this process is ATP-dependent, extensive DNA damage subsequently cleaves PARP resulting in the rapid depletion of the intracellular NAD and ATP pools, slowing the rate of glycolysis and mitochondrial respiration and eventually leading to the proteolytic cleavage of PARP by caspase-3 ultimately resulting in apoptotic cell death (Pacher *et al*., 2002).

In contrast, other genes such as TP53 and CD95 have also been implicated in inducing p53- mediated apoptosis (Lorenzo *et al*., 2002). Furthermore, it was also demonstrated that treatment of the cells with DXR resulted in reactive oxygen species (ROS) generation and a concomitant increase in apoptotic cell death through the mitochondrial death pathway independent of p53 (Luanpitpong *et al*., 2012). Additionally, different doses of doxorubicin activate different regulatory mechanisms to induce either apoptosis or cell death through mitotic catastrophe. Specifically, high dose DXR induced apoptosis through activation of NF-kB, p38, c-Jun N-terminal kinase, and caspases; where low doses of DXR resulted in loss of cell membrane integrity and cell death through mitotic catastrophe (Eom *et al*., 2005).

1.4.1: Side-effects of Doxorubicin Therapy

Chemotherapy using DNA intercalators such as DXR to induce its cancer eradicating properties has proven to be one of the most successful approaches to cancer treatment; however it induces various side- effects such as hematopoietic suppression, nausea, vomiting, extravasation and alopecia (Octavia *et al*., 2012). Yet, the most detrimental side-effect induced by anthracyclines is its cumulative and dose-dependent cardiac toxicity which has been a major concern of oncologists in cancer therapeutic practice for decades (Singal and Iliskovic 1998; Zhang *et al*., 2009). DXR-induced cardiotoxicity may be recognized by symptoms such as asymptomatic electrocardiography (ECG)-changes, pericarditis and either acute or chronic cardiomyopathy.

Occurring during or immediately after a high dose of chemotherapy, acute cardiomyopathy develops into acute tachyarrhythmia and acute heart failure; these effects are however, thought to be reversible and can be clinically controlled (Schimmel *et al*., 2004). Techniques employed by clinicians to detect acute myocardial related injuries directly after a high dose of DXR involves the detection of decreases in ejection fractions as well as elevated plasma concentrations of cardiac troponin I (Tn I). This biomarker is a highly specific indicator of poor cardiac output as well as left ventricular injury (Schimmel *et al*., 2004). In contrast, chronic DXR-induced cardiac toxicity is dependent on the dose of chemotherapy administered to a patient (Arola *et al*., 2000; Zhang *et al*., 2009). Under these

circumstances, patients become predisposed to developing an irreversible form of dilated cardiomyopathy, which may occur years later after receiving the last DXR treatment, manifesting into a poor prognosis. Acute and chronic DXR-induced cardiac toxicity, equally contribute to cardiac dysfunction, cardiomyopathy, ultimately terminating in severe heart failure and death (Wallace, 2003; Zhang *et al*., 2009).

Evidently, cardiotoxicity also occurs at low dose administration as a result of varying susceptibility among patients (Jain, 2000). A study conducted by Lipshultz *et al*. (1995) revealed that gender difference is a key risk factor, as females suffered more severe cardiotoxicity with more depressed contractility thus, indicating a greater susceptibility to the toxic effects of doxorubicin. Age is an additional risk factor as children younger than 4 and elders older than 65 showed greater risk of developing doxorubicin-induced cardiotoxicity. Frequently, patients who are administered a combination of chemotherapeutic drugs, mediastinal radiotherapy and others who have hypertension, diabetes mellitus, liver disease, and a history of previous cardiac disease further correlates with an increased risk of cardiotoxicity (Jain, 2000; Hershman *et al*., 2008). Although, investigations on DXR-induced cardiotoxicity have persisted for decades, a patient's onset of developing symptomatic cardiomyopathy (within or up to 15 years later post chemotherapy) is unpredictable. This strongly indicates that different mechanisms may be involved in doxorubicin-induced cardiomyopathy.

Most studies have implicated free radical-induced oxidative stress (ROS) as a pivotal role player in the induction of cardiomyocyte death in DXR-induced cardiotoxicity (Figure 1.4.2). Due to the fact that DXR is cationic in nature, it remains in the inner mitochondrial membrane space disrupting the electron-transport chain and causing mitochondrial DNA lesions which subsequently generates vast amounts of ROS (Jehle *et al*., 2001). These DNA lesions may also be caused directly by DXR leading to activation of extracellular-regulated kinase (ERK1/2), followed by increased phosphorylation of p53, the latter further up-regulating p53-downstream genes such as Bax. This eventually leads to intrinsic apoptotic cell death (Figure 1.4.2) (Liu *et al*., 2006). In the 1980's, DXR has shown to have a high affinity for iron, forming complexes which lead to lipid peroxidation, reduced levels of antioxidants, sulfhydryl groups and further induction of ROS resulting in cell damage (Doroshow *et al.*, 1980; Wallace, 2003; Xu *et al*., 2005; Neilan *et al*. 2007).

Another study reported that the conversion of DXR to an unstable semiquinone intermediate by an endothelial nitric oxide synthase reductase domain, further increases ROS production (Neilan *et al*. 2007). This generation of ROS, increases intracellular calcium levels which, in turn, further increase ROS production. The calcium and ROS overload triggers mitochondrial permeability transition (MPT), resulting in mitochondrial swelling, loss of membrane potential and outer membrane rupture, ultimately causing apoptosis of cardiomyocytes via activation

of the intrinsic apoptotic pathway, mediated by the release of cytochrome *c* and apoptosis inducing factor (Figure 1.4.2) (Camello-Almaraz *et al*., 2005).

The extrinsic pathway of apoptotic death is also involved in DXR-induced cardiomyocyte apoptosis. Deregulation of transcription factors leads to FAS and subsequent caspase-8 activation, terminating in apoptotic cell death (Figure 1.4.2) (Nakamura *et al*, 2000). Interestingly, the heat-shock family of proteins plays a distinct role in these processes. Heat shock proteins are well recognized for their involvement in inducing anti-apoptotic proteins. However, it has become apparent that ROS activates HSF-1, which produces more Hsp25, which stabilizes p53 and increases the production of pro-apoptotic proteins (Figure 1.4.2) (Vedam *et al*., 2010).

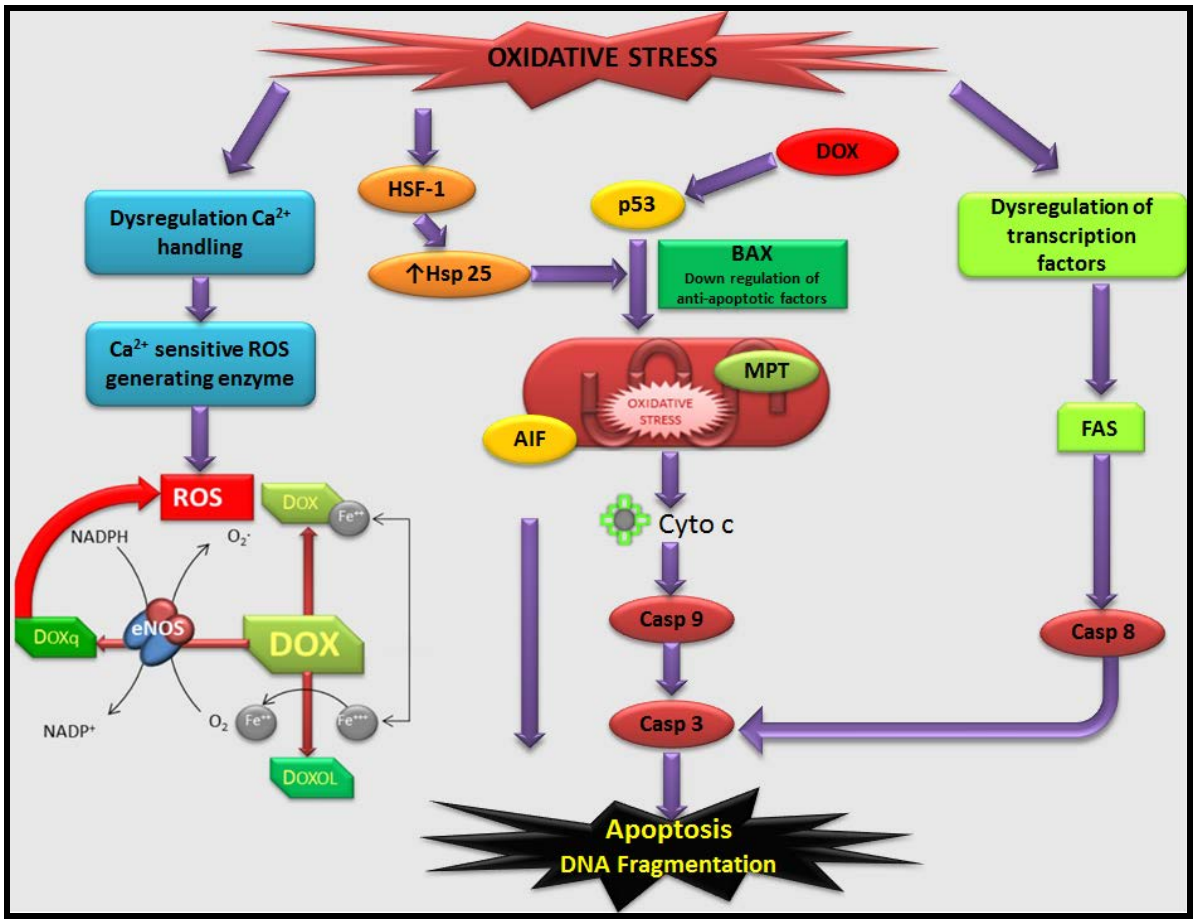

Figure 1.4.2: Interaction between doxorubicin with the various apoptotic pathways in the cardiomyocyte. The left side of the figure shows how doxorubicin begins to generate ROS and the dissociation of the eNOS into monomers. Doxorubicin also enters the mitochondria, causing the release of cytochrome C oxidase, and also prolongs the opening time of calcium channels in the sarcoplasmic reticulum, which activates calcineurin. Akt phosphorylation inhibits Bad activation and is one of the main anti-apoptotic pathways. Oxidative stress activates HSF-1 and produces more Hsp25, which increases the pro-apoptotic proteins. **Abbreviations:** Dox: doxorubicin, Doxol: doxorubicinol, Doxq: doxorubicin semiquinone, ROS: reactive oxygen species, SE: sarcoplasmic reticulum, HSF: heat-shock factor, Hsp: heat-shock protein, CytC: cytochrome C, and Casp3: caspase 3 (Adapted from Octavia *et al*., 2012).

Evidently, researchers have established various mechanisms involved in DXR-induced cardiotoxicity. Unfortunately, much remains to be elucidated in order to effectively implement pharmacological interventions and treatment options

improving prognosis of patients. However, this is not the only challenge that researchers and clinicians are faced with. In addition to the fact that DXR induces damaging effects on the heart, cancer cells are becoming inherently resistant to DXR-induced cell death.

1.5 Chemo-resistance

The resistance of cancer cells to chemotherapy (chemo-resistance) is a multifaceted challenge faced by oncologists and their cancer victims. Initially, patients are susceptible to chemotherapy (chemo-sensitive) and cancer free directly after their course of treatment. However, 50% to 70% of patients relapse within one year as a result of poor surgical outcomes in which whole tumours are not completely resected subsequently leading to the formation of another tumour. In most cases of relapse, the adenocarcinoma cells acquire a chemo-resistant phenotype (Chang, 2011; Castells *et al*., 2012). In breast cancer specifically, chemo-resistance is often associated with the progression of the malignancy from a hormone-dependent, non-metastatic, anti-estrogen-sensitive phenotype to a hormone independent, invasive, metastatic, anti-estrogen-resistant phenotype (Simstein *et al*., 2003).

Literature has shown that the topoisomerase II enzyme, which is mainly targeted by DXR to induce its cancer eradicating properties, is associated with drug resistance via two major routes. Firstly, many cancer cell lines display reduced

expression of the enzyme, and secondly, there are a number of mutations to topoisomerase I/II that prevent or reduce the affinity of drug binding (Mellor and Callaghan, 2008). This type of chemo-resistance highly correlates with genetic alterations within the cancer cells. For example, loss of p53 function as a result of genetic mutations prevents the initiation of apoptosis following chemotherapeutic treatment, thus conferring resistance (Yang *et al*., 2003). Cancer cells are capable of recruiting various DNA repair pathways such as base excision, nucleotide excision, mismatch or direct repair of damage introduced by chemotherapy (Madhusudan and Middleton, 2005).

Furthermore, increased mRNA levels of ERCC1 (excision repair cross-complementing) protein, which plays a significant role in determining success or failure of chemotherapy, were observed in drug-resistant cell lines (Lord *et al*., 2002; Rosell *et al*., 2002). Apart from these genetic mutations, it has become well established that cancer cells also express reduced sensitivity to apoptosis. Clinical data in advanced breast cancer patients revealed that overexpression of the anti-apoptotic Bcl-2/Bcl-x L proteins correlated with chemotherapy resistance (Sjostrom *et al*., 2002). In breast cancer, deregulation of the Akt signaling pathway and amplification of the Akt gene were implicated in promoting cell proliferation and survival and thus chemo-resistance (Nicholson and Anderson, 2002). Other mechanisms involved include, active efflux of the chemotherapeutic agent from the tumour cell; modification of drug targets; changes or mutation in mitotic checkpoint signals; drug sequestration and detoxification of cytotoxic agents (Chang, 2011). A

more recent and evolving concept strongly associates chemo-resistance with the tumour microenvironment as it evidently influences the growth of cancer which have an impact on the outcome of therapy (Meads *et al*., 2009). Interestingly, non-malignant cells in this niche play a supportive role in cancer growth as well (Basak *et al*., 2009). In support of this notion, Meads *et al*. (2009) reported that the tumour microenvironment induces rapid signaling which mediates cancer cell survival and removal of this microenvironment will ameliorate chemo-resistance.

The microenvironment (stroma) consists of endothelial cells, carcinoma-associated fibroblasts, adipocytes, mesenchymal cells, mesenchymal stem cells and cells from the immune and inflammatory systems. These stromal cells communicate with each other, also known as oncologic trogocytosis (Raffi *et al*., 2012). Accumulating evidence shows that the cells residing in this niche could potentially induce chemo-resistance in tumour cells by: (i) cell to cell and cell to matrix interactions which influences cancer cell sensitivity to apoptosis; (ii) local release of soluble factors such as interleukin-6 (IL-6) that promote survival and tumour growth as there is communication via paracrine factors between stromal and tumour cells (Castells *et al*., 2012); (iii) direct cell-cell interactions with tumour cells (Raffi *et al*., 2012; Lis *et al*., 2011; Scherzed *et al*., 2011); iv) the generation of specific niches within the tumour microenvironment which consist of subpopulations of tumour cells that may gain a survival advantage following initial drug exposure, and (v) the conversion of the cancer cells into cancer-initiating cells or cancer stem cells (Teng *et al*., 2011). Additionally, in 1979, Sutherland *et al*. reported a higher

resistance against DXR-induced cell death when cells were organized spherically in culture in comparison to a monolayer.

Although the cross talk between the stromal cells and tumour cells are crucial in developing tumours, cells located in the intra-tumour, avascular regions face other challenges posed by this niche. This specific region is characterized by low nutrients and oxygen (hypoxia), acidic extracellular pH and populations of quiescent cells which subsequently impact on the success of chemotherapy in solid tumours (Izuishi *et al.,* 2000). The rapid rate of tumour growth requires increased levels of energy production through cellular metabolism. However, inadequate vascularisation progressively leads to a tumour hypoxic environment. The hypoxic environment requires that energy demands are satisfied through glycolytic pathways rather than the more efficient oxidative phosphorylation route known as the “Warburg Effect” (Sutherland *et al.,* 1998; Dang and Semenza, 1999).

Additionally, the high interstitial pressure prevents clearance of metabolic end-products such as lactic acid (Dang and Semenza, 1999). Enhanced hypoxia further leads to the up-regulation of growth factors such as platelet-derived growth factor B (PDGF-B), transforming growth factor β (TGF-β), insulin-like growth factor 2 (IGF-2), and epidermal growth factor (EGF) (Tredan *et al*., 2007). Angiogenesis is regarded as the key contributor of metabolites and oxygen found in large tumours thus, allowing for tumour progression (Izuishi *et al.,* 2000). An additional prevailing

mechanism thought to be involved in chemo-resistance is autophagy. A study conducted by Yoon *et al*., (2012) concluded that the induction of autophagy by genotoxic stress is likely to contribute to the sustained survival of breast cancer cells through DNA repair regulated by ataxia telangiectasia mutated (ATM)-mediated activation of DNA-dependent protein kinase catalytic subunit (DNA–PKcs), and PARP. Another study has also implicated autophagy in either sensitising cancer cells to chemotherapeutic agents through 'recycling' damaged cellular contents or intensifying chemotherapy-induced apoptosis (Zhuang *et al*., 2009).

1.6 Autophagy

First described in the 1960's, autophagy is characterised by the development of autophagosomes that engulf bulk cytoplasm, organelles and other cellular components such as proteins before fusing with the lysosome, which results in mass proteolysis (Figure 1.6.1). This has been shown to occur mainly in response to nutrient starvation, hypoxia, ATP depletion or signals prompting cellular remodelling and is mainly controlled via the mTOR signalling cascade. Although it has become widely accepted as a mode of programmed cell death, autophagy (type II cell death) is yet to be definitively defined as such (Amaravadi et al., 2011).The current hypotheses in the literature reveals, that autophagy might more accurately be described as a cell survival mechanism that acts alongside cell death but does not necessarily lead to it.

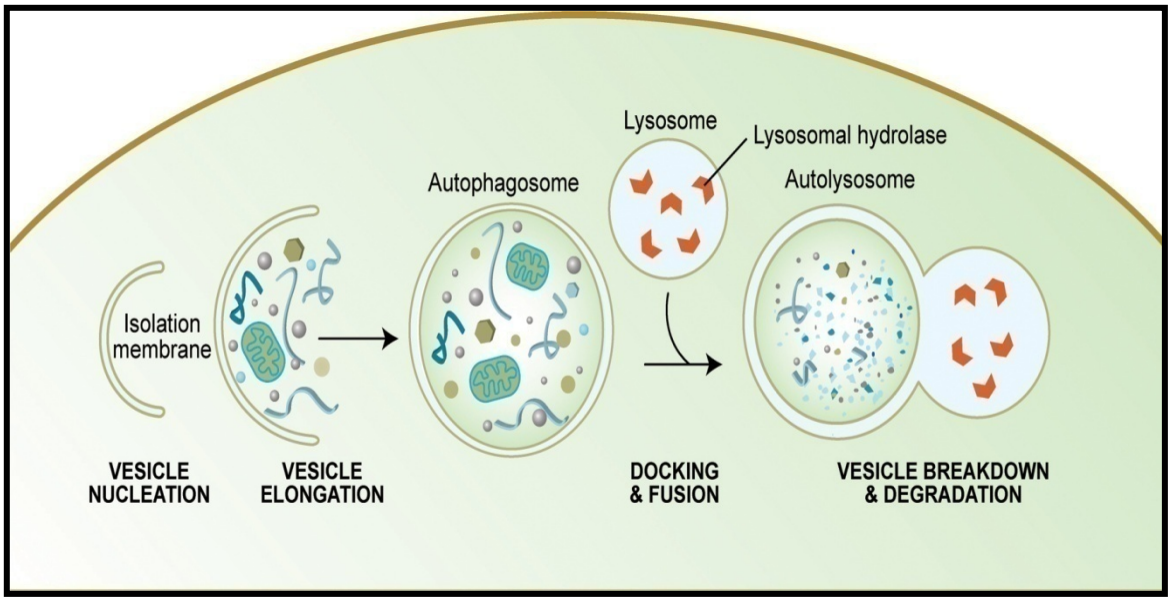

Figure 1.6.1: Schematic diagram of the steps involved in the process of autophagy. Autophagy begins with the formation of the phagophore or isolation membrane (vesicle nucleation step).The expansion of the phagophore into an autophagosome (vesicle elongation). The autophagosome can engulf bulk cytoplasm non-specifically, including entire organelles or targeted cellular constituents specifically. When the outer membrane of the autophagosome fuses with an endosome (forming an amphisome before fusing with the lysosome) or directly with a lysosome (docking and fusion steps), it forms an autophagolysosome. Finally, the sequestered material is degraded inside the autophagolysosome (vesicle breakdown and degradation) and recycled **(**adapted from Meléndez and Levine, 2009).

Although cell death through autophagy has been suggested as a mechanism of tumour suppression (Sun *et al.,* 2009; Liang *et al*., 1999), it still remains a controversial matter whether autophagy leads to tumour formation or suppression. In addition, a recent study by Zhang *et al*., (2009), revealed that hypoxia induces mitochondrial autophagy to prevent an increase in the level of reactive oxygen species and subsequent cell death. Thus, when viewed dynamically, it is becoming apparent that autophagy acts to delay cell death and may only manifest as such due to a failed attempt to keep cells alive. However, this can only occur once autophagy has progressed and persisted beyond the so-called 'point of no return'

(PONR), resulting in apoptosis or possibly even necrosis (Loos and Engelbrecht, 2009; Sun *et al.,* 2009).

There is however, a great lack of knowledge, regarding the progression of autophagy with time in oxygen and nutrient deficient tumour micro-environments. This could be due to autophagy being recognized predominantly as a death mechanism in the cancer environment as well as due to the lack of investigation on autophagy in the different tumour microenvironments.

1.6.1 The role of autophagy in nutrient deprivation

Functional autophagy requires the recruitment of multiple autophagy-related (Atg) gene products. These genes are responsible for regulating the well-orchestrated processes of nucleation, elongation and maturation of the phagophore membranes around the targeted cargo for degradation (autophagosomes), and their subsequent fusion with lysosomes forming autophagolysosomes (Figure 1.6.2) (Yang and Klionsky, 2010). A commonly-associated mechanism by which autophagy is activated in response to nutrient and growth factor deprivation involves the activation of AMP-activated protein kinase (AMPK) and subsequent inhibition of the mammalian target of rapamycin (mTOR). These proteins tightly maintain and regulate the energy status of the cell and have been implicated in playing a role in autophagy in many human cancers (DiPaola *et al*., 2008). AMPK plays a key role in the regulation of energy homeostasis. This kinase is phosphorylated at the Thr172 residue leading to its activation in response to a low

AMP/ATP ratio due to cellular stresses such as starvation. mTOR acts as a sensor for energy and amino acids, balancing the availability of nutrients and cell growth.

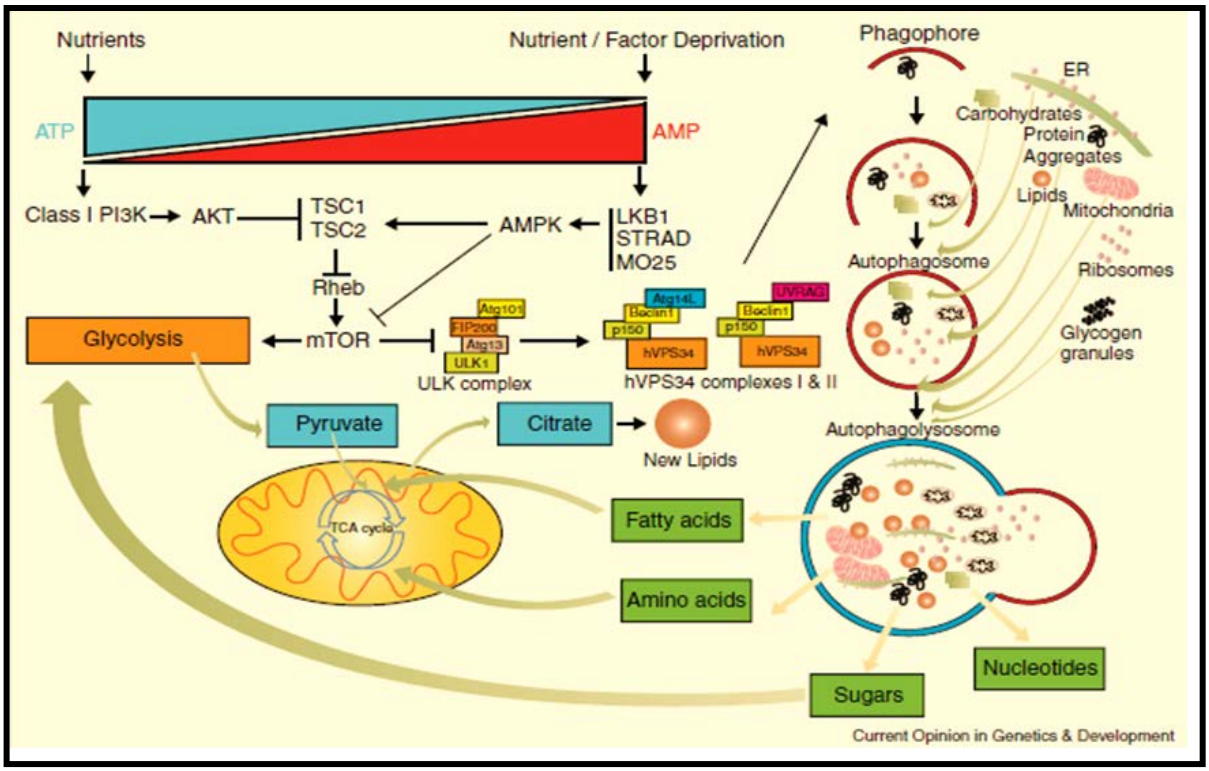

Figure 1.6.2: Regulation of autophagy under nutrient deprivation and its interaction with central carbon metabolism. The major extra-cellular nutrient sensing pathways, controlled by PI3K-I and adenosine monophosphate activated kinase (AMPK) tightly regulate autophagy through mTOR signaling, although other mTOR independent mechanisms exist. Under nutrient-replete conditions autophagy is inhibited by mTOR and inactivation of the ULK1 complex. Metabolic stress relieves this inhibition to activate autophagy, and AMPK is activated. AMPK inhibits mTOR by activating its negative regulator, the tuberous sclerosis protein 2 (TSC2) and inhibiting its positive-regulatory subunit, Raptor. The ULK1 complex activates the vacuolar sorting protein34 (hVPS34)- and Beclin1-containing complexes (complex I and complex II), to initiate phagophore formation. Phagophores nucleate and expand around the cargo encapsulating it and targeting it to lysosomes for degradation. Degradation products of autophagy substrates may re-enter glycolysis and the TCA cycle for anabolic as well as catabolic processes leading to generation of energy and biomass production (Mathew and White, 2011).

When nutrients are available, AMPK is inactive allowing for mTOR activation via phosphorylation at the Ser 2448 position. Activated mTOR binds and inactivates two components of the Unc-51-like kinase (ULK1) complex, ULK1 and Atg13,

which are essential positive regulators of autophagosome formation (Kim *et al*., 2011) (Figure 1.6.2). This leads to the subsequent inhibition of phagophores becoming nucleated, thus inhibiting autophagy (Hasokawa *et al*., 2009; Kim *et al*., 2011). In contrast, when nutrients are limited, AMPK is activated, subsequently inhibiting or reducing mTOR activity and inducing autophagy. This provides a controlled homeostatic system that ensures the necessary integration of growth control signals with nutrient availability and catabolism.

When mTOR activity is inhibited in this scenario, it induces autophagy by dissociating from the ULK1 complex, freeing it to trigger autophagosome nucleation and elongation (Hasokawa *et al*., 2009; Kim *et al*., 2011). The elongation of autophagosome membranes involves microtubule-associated protein 1A/1B-light chain 3 (LC3). LC3 is a soluble protein with a molecular mass of ~17 kDa that is distributed ubiquitously in mammalian tissues and cultured cells. The cytosolic form of LC3 (LC3-I) is conjugated to phosphatidylethanolamine to form LC3-phosphatidylethanolamine conjugate (LC3-II), which is recruited to autophagosomal membranes (Tanida *et al*., 2004). Autophagosomes then fuse with lysosomes to form autolysosomes which are degraded by lysosomal enzymes. Simultaneoulsy, LC3-II in the autolysosomal lumen is degraded (Tanida *et al*., 2004). Thus, lysosomal turnover of the autophagosomal marker LC3-II reflects starvation-induced autophagic activity, and detecting LC3 by western blotting has become a reliable method for monitoring autophagic activity (Mizushima and Yoshimori, 2007). Importantly, although mTOR signaling tightly regulates

autophagy in response to starvation, there are various other mechanisms independent of mTOR, through which autophagy can be regulated (Meijer and Codongo, 2004; Jung *et al*., 2010).

The process of selecting cargo for autophagic degradation involves ubiquitin modifications of targeted proteins and cellular constituents. LC3-II binds p62/SQSTM1, an adapter protein that targets these ubiquitinated protein aggregates which are selected for degradation via autophagy (Pankiv *et al*., 2007). Specifically, p62 contains an ubiquitin-binding domain (UBA domain), a LC3-interacting region (LIR domain). The UBA domain is required for the appropriate localization of p62 within cytoplasmic aggregates such as misfolded and ubiquitinated proteins, referred to as p62 bodies. These p62 bodies then bind to LC3 II on the autophagosomal membranes via the LIR domain and are degraded when autophagosomes fuse with lysomes (Pankiv *et al*., 2007). Thus, p62 plays a key role as an adaptor between the autophagic machinery and the ubiquitinated substrates, regulating cell survival, as the disposal of toxic aggregates is essential for the prevention of cell death in several pathological situations in which p62 is a component of these aggregates (Vadlamudi and Shin, 1998; Pankiv *et al*., 2007). Since, LC3-II (present on the inner and outer membrane of the autophagosome) and p62 are both degraded in the autolysosome during autophagy; the lysosomal-dependent turnover of these proteins, especially p62, has emerged as a valid measure of autophagic flux (Bjorkoy *et al*, 2005). Additionally, the intracellular

accumulation of p62 and an increase in p62 bodies may indicate a defect in autophagic degradation (Komatsu *et al*., 2007; Mathew *et al*., 2009).

In mammals, all cells have internal nutrient stores such as glycogen and lipid droplets for use during starvation. When required, these stores are broken down enzymatically (glycogen phosphorylase and hormone-sensitive lipase). Autophagy plays a pivotal role in providing access to such undedicated nutrient stores, thereby supporting mammalian cells during nutrient deprivation. Evidence of this has been shown with lymphocytes which possess the ability to consume environmental nutrients, depending on growth factor availability. In the absence of such growth factors, energy is maintained through induction of autophagy, with lymphocyte cells shrinking ~50% in size during 3 months as result of self-cannibalizing (Lum *et al*., 2005). An animal study observed that starved pups with defective autophagy died within 24 hours of starvation since both circulating and tissue amino acid levels are reduced, and AMPK is activated in the heart, which showed electrocardiographic changes similar to those observed with severe myocardial infarction (Kuma *et al*., 2004).

In human adult starvation, autophagy also has a central role, increasing within 24 hours in liver, pancreas, kidney, skeletal muscle, and heart; the brain is spared (Mizushima *et al*., 2004). Pharmacological inhibition of autophagy, early in starvation culminates in cardiac dysfunction (Kanamori et al., 2009). After 2 days (48 hours) of starvation, levels of autophagy remain elevated in the both cardiac

and skeletal muscle and return to basal levels in the liver. However, liver mass decreases rapidly indicating a correlation between the failure of biosynthesis to balance basal consumption of autophagy by the liver (Komatsu *et al*., 2005). With the simultaneous decrease in liver mass, breakdown of muscle and adipose tissue feeds the liver, which exports glucose and ketone bodies required by the brain.

In the context of human cancers, it is known that cancer cells alter metabolism to suit their specific growth requirements and express chronic proliferation and thus requiring an increased need for energy and a carbon/nitrogen sources for biomass production. As a major contributor to energy substrates during stressful conditions, autophagy supports cancer cells to meet their enhanced metabolic demands. This may be achieved in the form of lipophagy, in which autophagy provides fatty acids for β-oxidation that generates acetyl-CoA in mitochondria to support the TCA cycle. Additionally, autophagic degradation of pre-existing intracellular proteins forms an abundance of amino acids in cancer cells (Yuneva *et al*., 2007; Rabinowitz and White, 2010). These free amino acids subsequently enter into central carbon metabolism at multiple points that include pyruvate, acetyl-CoA and TCA intermediates such as α-ketoglutarate (α-KG) (from glutamine) and oxaloacetate (from aspartate) (Rabinowitz and White, 2010). Evidently, Guo *et al*. (2011) showed that cancers with *Ras* mutations and malfunctioning autophagic machinery resulted in impaired cell growth, suggesting that targeting autophagy and mitochondrial metabolism are valuable new approaches to treat these aggressive cancers.

The role that autophagy plays in cancer metabolism remains to be entirely elucidated. Not much is known about how autophagy selectively accesses major energy sources such as lipids and carbohydrates, and to what extent do these sources contribute to stress survival. Another interesting and yet unanswered question is how tumours with autophagy defects, and mitochondrial and TCA cycle impairments, sustain tumour growth. Ultimately, how can scientists manipulate the metabolic role of autophagy in tumour progression clinically to ameliorate chemo-resistance? Answers to these imperative questions may translate into beneficial treatment regimens for cancer sufferers.

This lack of knowledge raises areas of concern and questions which require clear answers: What is the specific role of autophagy in tumours and what is the contribution of autophagy to cellular survival during therapy resistance? Whether cell death by autophagy or autophagy itself actually occurs in breast cancer is still largely undetermined, therefore further investigation in this field is required. Another concept that still remains to be explored is the possibility that malignant cells in the advanced stages of the carcinogenesis undergo autophagy as a pro-survival mechanism.

1.7 Starvation

During ancient times, as far as the beliefs of Egyptians, legendary philosophers and doctors of western medicine like Hippocrates and Paracelus believed that therapeutic fasting should be practiced as a method of healing various health conditions. From an infant's refusal to eat due to a common cold to a cancer patients loss of appetite during chemotherapy, it appears that the body's innate response to, or perhaps therapy for combating against disease and infection, is to limit one's nutritional intake. Since, such a phenomenon persists in nature, the concept of controlled nutrient starvation is increasingly becoming an appealing concept worth exploring by physiologists and oncologists.

It is well established that cancer cells have increased glycolytic activity despite the nutritional status of their environment. In contrast, the human body is designed such, that when faced with decreased nutrient intake, the body is capable of mobilizing energy stores to its most vital organs to sustain homeostasis and function. Following digestion of a meal, 3-4 hours later, the body enters a post-absorptive phase in which glycogenolysis occurs. During this process, the pancreas releases the hormone, glucagon, which stimulates the breakdown of glycogen stores in the liver thereby maintaining blood glucose levels. The early starvation phase occurs 24 hours after a meal and whilst glycogenolysis persists, the body activates an additional metabolic pathway to meet its energetic demands namely, gluconeogenesis. During gluconeogenesis adipose tissue is broken down,

and the glycerol back bone of fatty acids and amino acids are used to synthesize glucose. This phase persists until 60 hours of starvation is reached. At this point, all glucose stores have been depleted and thus the body resorts to activate ketogenesis in which the liver directs acetyl-CoA to synthesise ketone bodies. The brain being the most vital organ, adapts to use ketone bodies as its primary fuel through the synthesis of appropriate enzymes. Evidently, this is a well-orchestrated process of adaptation to nutritional deprivation (Hellerstein *et al*., 1997).

In the context of cancer, one of the earliest studies was conducted in 1988 by Raffaghello and colleagues where normal and cancerous yeast cells were starved and then exposed to chemotherapy (unpublished). They found that normal cells survived the toxic dosage, but the cancer cells did not. These findings concluded that normal cells have a 'shield mode' - a kind of protective strategy that allows the organism to be resistant to not just one but various stresses, including starvation. This inspired an animal trial in which tumour bearing mice were starved for 48 hours and then administered a high dose of chemotherapy. This study proved to be successful as 43% of the non-starved mice died, but only one of the starved mice. Once chemotherapy was terminated, a normal diet was resumed and the starved mice regained all the lost weight. With the great success of the animal trial, Raffaghello and colleagues proceeded with a human trial in 2010, in which ten patients starved from 48-140 hours prior to 5-56 hours after chemotherapy reported reduced side-effects of the toxic drug.

1.8 Motivation for this study

Although extensive research has been done on human cancers, the role that starvation plays specifically in breast cancer in response to DXR-induced cell death remains to be elucidated. Additionally, the duration of starvation in the studies conducted by Raffaghello *et al.* (2010) is extensive and some individuals may be unable to sustain such an extensive fast. It is thus imperative to explore this concept under shorter and more tolerable periods of starvation. For the purposes of this study we define starvation as the way in which the body responds to total nutrient deprivation.

We **hypothesise** that short-term starvation will sensitize cancer cells to doxorubicin-induced cell death.

In order to assess the hypothesis, this study was approached by four **aims:**

1. To establish a time point at which MCF12A breast epithelial cells are protected against starvation.
2. To determine the effect of short – term starvation on doxorubicin- induced cell death.
3. To assess autophagy in our experimental model.
4. To assess these aims in an *in vivo* model of tumour bearing mice.

Chapter 2 – Materials and Methods

2.1 Study Design (*In vitro*)

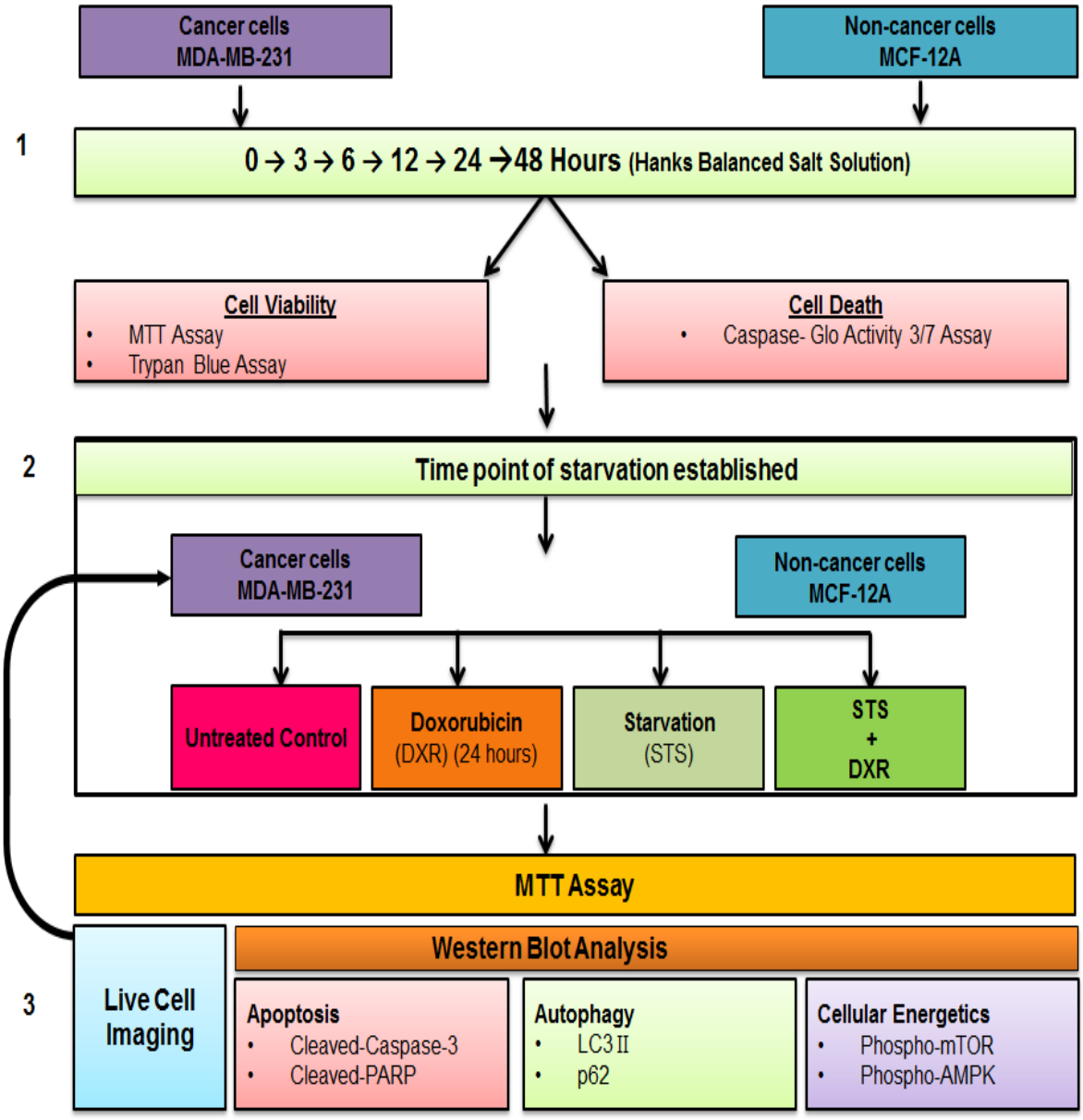

Figure 2.1.1: Study Design: Human breast carcinoma cell line (MDA-MB-231) and human non-tumourigenic mammary epithelial cell line (MCF12A) were subjected to: (1) various hours of starvation. (2) Depending on the results obtained at (1) these cell lines were used to conduct a MTT cell viability assay. (3) Only the cancer cells were further used for western blot analysis.

2.2 Cell culture

Human non-tumourigenic mammary epithelial cell line (MCF12A) was obtained from the University of Cape Town and a human breast carcinoma cell line (MDA-MB-231) was obtained from American Type Culture Collection (Rockville, MD, USA) which were maintained in a monolayer at 37°C and in a 21% O_2, 5% CO_2 humidified air atmosphere of 95%. MDA-MB-231 cells were cultured in Dulbecco's modified Eagle's medium (DMEM) (Sigma Chemical Co., St Louis, MO, USA) supplemented with 10% foetal bovine serum (FBS) (Sigma Chemical Co., St Louis, MO, USA) and 1% penicillin/streptomycin (PenStrep) (Sigma Chemical Co., St Louis, MO, USA). The MCF12A growth medium contained a combination of Dulbecco's modified Eagle's medium (DMEM) and Nutrient Ham's-F12 medium without phenol red (1:1) (Sigma Chemical Co., St Louis, MO, USA) and was supplemented with 10% foetal bovine serum (FBS), 1% PenStrep, 20 ng/ml epidermal growth factor (EGF) (Sigma Chemical Co., St Louis, MO, USA), 100 ng/ml cholera toxin (Sigma Chemical Co., St Louis, MO, USA**),** 10 µg/ml insulin (Coetzenburg Campus Pharmacy) and 500 ng/ml hydrocortisone (Sigma Chemical Co., St Louis, MO, USA). Cells were allowed to proliferate in T75 flasks (75 cm^2 flasks, Greiner Bio One, Germany) over a period of three days with changing of fresh growth medium after every 24 hours. When cultures reached 80% confluency (Figure 2.2.1), they were passaged. Cells were then rinsed with phosphate buffered saline (PBS) and trypsinised (0.25% Trypsin-ethylene-diaminetetra-acetic acid (EDTA) (Invitrogen, Life Technologies) with gentle agitation to ensure

complete detachment, following centrifugation at 200 g for 3 minutes. After cells were counted, cells were seeded at the appropriate density in fresh warm growth medium and plated in either 6 well plates (Greiner Bio One) or T25 flasks (25 cm^2 flasks, Greiner Bio One, Germany).

2.3 Experimental protocol

2.3.1 Treatment

Upon treatment, growth medium was removed and replaced with fresh growth medium. Additionally, cells were washed twice with warm PBS to ensure removal of all debris and non-viable cells. Initially, to induce starvation, cells were incubated for 3, 6, 12, 24 and 48 hours in Hank's Balanced Salt Solution (HBSS) (Sigma Chemical Co., St Louis, MO, USA), in order to establish a time point at which cells respond to starvation. Once a time point of 3 hours was established, four treatment groups were used: (1): control; (2): 5 µM of doxorubicin (DXR) for 24 hours; (3): short-term starvation (3 hours) (STS) and (4): short-term starvation (3 hours) prior to 24 hours treatment with doxorubicin (STS+ DXR). For complete treatment protocol, see Appendix A.

2.4 Cell Viability Analysis

2.4.1 Trypan blue cell exclusion technique

Following the termination of treatment, growth medium was removed and cells were washed with warm PBS, trypsinised and centrifuged. The supernatant was removed and the pellet re-suspended in 1 ml of PBS. From this cell suspension 10 µl was removed and added to 10 µl of a 0.3%Trypan Blue dye (Invitrogen) and gently agitated. Of this solution, 10 µl was added to a two chambered cell counting slide (Invitrogen). An automatic cell counter (Invitrogen) was then employed to count the total number of viable cells. Trypan Blue cell exclusion technique is based upon the unique properties of the chromophores present in this vital dye. The chromophores are negatively charged, thus only interact with cells that have damaged membranes (staining blue). Thus, all cells which are viable exclude the dye. This technique was conducted in triplicate and three independent experiments were performed. Data was expressed as a percentage of the control, which was normalized to 100%. A detailed protocol is provided in appendix A.

2.4.2 MTT Cell Viability Assay

The MTT cell viability assay is based on the principal of MTT (3-(4,5-Dimethylthiazol-2-yl)-2,5-diphenyltetrazolium bromide, a tetrazole) a yellow salt which is reduced to purple formazan crystals by enzymes in the cytoplasm and in the mitochondria of viable cells. This reductive capacity is dependent on active mitochondrial reductase enzymes (dehydrogenases), thus the conversion can be

directly correlated to the number of viable cells when assessed spectrophotometrically. Mitochondrial dehydrogenases of viable cells cleave the tetrazolium ring, yielding purple MTT formazan crystals which are insoluble in aqueous solutions. Acidified solutions such as the Isopropanol/Triton X solution can be used to dissolve the purple crystals.

After the termination of the treatment, the medium was removed from each well of a 6 well plate and 1.5 ml PBS plus 500 µl MTT (0.01 g/ml) solution was added to each well and incubated at 37ºC for 1 hour. After 1 hour incubation period, if cells were detached, the content was transferred to eppendorf tubes and centrifuged for 2 min at 1000 rpm. The supernatant was decanted and 2 ml of hydrogen chloride-isopropanol/Triton (1% HCl in isopropanol; 0.1% Triton X-100; 50:1) solution was added to each pellet and re-suspended. Some cells remained attached, thus the re-suspension was added back to the original plates and 2 ml HCl-isopropanol/Triton X solution was added to each well, covered with silver foil and gently agitated at 37ºC for 5 minutes to dissolve the purple crystals formed. The content of each well was then transferred to a 2 ml cuvette. The optical density (OD) was determined spectrophotometrically (Cecil-CE 2021-2000 Series, Lasec) at a wavelength of 540 nm, using HCl-isopropanol/Triton X solution as the blank. All values obtained from treated groups were expressed as a percentage of the control values. A detailed protocol is provided in appendix A.

2.4.3 Caspase-Glo®3/7 Assay

The Caspase-Glo® 3/7 assay kit (Promega, G8091) provides a reagent containing a luminogenic caspase-3/7 substrate, which is optimized for caspase and luciferase activity. Addition of the reagent to cells results in caspase mediated cleavage of the substrate, followed by the release of amino-luciferin (a substrate for luciferase) which generates a luminescent signal. Luminescence is proportional to the amount of caspase activity present in the sample. MDA-MB-231 and MCF-12A cells were grown and treated, as previously stated, in 96-well luminometer white plates. Caspase-3/7 reagent was added to each well (100 µl) and incubated for 1 hour at room temperature. Immediately after incubation, luminescence was measured using a luminometer (GLOMAX 96 microplate Luminometer, Promega). A detailed protocol is provided in appendix A.

.

2.5 Western Blots

2.5.1 Protein extraction and cell lysate preparation

Cells were washed thoroughly with PBS after which T25 flasks were placed on ice. This was followed by the addition of 2 ml of ice cold radio-immunoprecipitation (RIPA) buffer, pH 7.4, containing (in mM): tri-(hydroxylmethyl)-aminomethane (TRIS)-HCl 50, NP-40 1%, Na-Deoxycholate 0.25%, EDTA (Ethylenediamine-tetra-acetic acid) 1, sodium fluoride (NaF) 1, soybean trypsin inhibitor (SBTI) 4 µg/ml, phenyl-methyl-sulphonyl fluoride (PMSF) 1, Benzamidine 1, leupeptin 1 µg/ml and

Triton X-100. Whilst remaining on ice, cells were scraped free from flasks and transferred to eppendorf tubes placed on ice. Cells were then sonicated (Ultrasonic Liquid Processor, Qsonica) for ± 20 seconds to ensure the release of proteins and centrifuged (5900 g at 4ºC for 10 min) to remove nuclei and cellular debris. Lysates were either stored at -80˚C or protein content was quantified using Bradford protein determination method (Bradford, 1976), followed by immediate preparation of cell lysates. Laemmli sample buffer containing (in M): 33.3 ml TRIS 0.5, pH 6.8, 10%SDS, 2.5 ml glycerol, 0.2 ml 0.5% bromophenol blue in deionized water was used to prepare cell lysates. A combination of 850 µl sample buffer and 150 µl mercaptoethanol was vortexed and the appropriate amounts according to calculations were accurately aliquoted to each protein sample (20 µg). Samples were boiled for 5 min at 95˚C before being spun shortly in a microcentrifuge.

2.5.2 Sodium-dodecyl-sulphate-polyacrylamide gel electrophoresis (SDS-PAGE) and Western blot analysis

Total protein lysates (20 µg) were loaded and separated using gradient gels (4% - 15%) sodium-dodecyl-sulphate poly-acrylamide gel electrophoresis(SDS-PAGE) and a 4% stacking gel (Bio-Rad Mini-Protean ® TGX ™ Precast Gels). A pre-stained protein marker ladder (peqGOLD, PEQLAB Biotechnologie GMBH, Germany) was loaded in the first lane on each gel for determination of molecular weights of specific bands. Proteins were separated on gels at 150 V (constant) and 400 mA for 60 minutes (Mini- PROTEAN Tetra Tank, Bio-Rad, USA). Following, SDS- PAGE, proteins were transferred to a polyvinylidine fluoride (PVDF)

membrane (Bio-Rad Trans-Blot Turbo Transfer packs) using the Bio-Rad electro-transfer system (Bio-Rad Trans- Blot Transfer System) for 12 minutes at 150V and 1.5 A. Non-specific binding sites were blocked with 5% fat-free milk in TRIS-buffered saline-Tween (TBS-T) and membranes were incubated overnight with the primary antibodies (cleaved-caspase-3, cleaved- PARP, p62/SQSTM1, LC-3, phosphor-AMPK-α, phopho-mTOR and β-Actin). Membranes were then washed with TBS-T (3 x 5 min) and the primary antibody was conjugated by the addition of a diluted horseradish peroxidase-labelled secondary antibody (Amersham LIFE SCIENCE) for 1 hour at room temperature. Thereafter, membranes were thoroughly washed before being exposed to ECL (chemi-luminescent reagent) for 1 minute. Bands were then detected using the Bio-Rad Chemi-Doc system. Exposed bands were visualised and quantified using densitometry software (Quantity1). All bands were expressed as optical density readings relative to a control present on the same blot.

In this study, western blot procedure was performed in the following manner. Cells were treated as previously described and at the end of treatment, harvested. Three independent experiments were performed (n=3). Each experiment consists of the four experimental groups and samples were loaded on the gel as follows: lane 1: protein ladder, lane 2: control, lane 3: doxorubicin, lane 4 starvation and lane 5: doxorubicin + starvation. Twelve well gradient gels (4-15%) were used throughout the study. We used western blot analysis to examine the following proteins: cleaved caspase-3 (17-19 kDa) and cleaved-PARP (89 kDa); LC3 I and II (16-18

kDa) and p62 (62 kDa) as well as phospho-AMPK (62 kDa) and phospho-mTOR (289 kDa). The membranes were cut or stripped to visualise all proteins mentioned above for each experiment. Thereafter the membranes were probed with β-actin to ensure equal loading of proteins. Membranes were then washed with TBS-T (3 x 5 min) and the primary antibody was conjugated by the addition of a diluted horseradish peroxidase-labelled secondary antibody (Amersham LIFE SCIENCE) for 1 hour at room temperature. Thereafter, membranes were thoroughly washed before being exposed to ECL (chemi-luminescent reagent) for 1 minute. Bands were then detected using the Bio-Rad Chemi-Doc system. Exposed bands were visualised and quantified using densitometry software (Quantity1). Each experimental group on a membrane was normalised to its corresponding β-actin band. Thereafter, the averages of all experimental groups (control, doxorubicin, starvation and dox+starvation) (n=3) were normalised to the control which was set as one.

2.6 Live Cell Imaging

This technique offers a dynamic approach to monitor over time the various morphological changes, localisation and distribution of organelles within cells after treatment. For Live Cell Imaging, MDA-MB-231 cells were seeded in 8-chamber dishes with a density of $2x10^4$ cells and maintained at 37°C and in a 21% O_2, 5% CO_2 humidified air atmosphere of 95%, in growth medium. Once confluent, cells were treated as previously described and stained accordingly. Image acquisition

was performed on an Olympus Cell^R system attached to an IX 81 inverted fluorescence microscope equipped with an F-view-II cooled CCD camera (Soft Imaging Systems). Using a Xenon-Arc burner (Olympus Biosystems GMBH) as light source, images were acquired, using GFP excitation and emission settings, as well as the UGB triple band pass emission filter cube.

2.6.1 GFP- LC3 Transfection

LC3 (microtubule- associated protein 1 light chain 3) is recruited to the autophagosomal membrane, in response to nutrient starvation during autophagy (Mizushimi, 2004). Thus, the green fluorescent protein (GFP) - tagged microtubule-associated protein 1 light chain 3 (LC3)-expressing cells may be used to demonstrate the induction of autophagy. GFP- LC3 transfected cells produce a scattered pattern of distribution under control conditions, in comparison to a punctuate pattern of GFP-LC3 expression (GFP-LC3 dots) when induced by autophagy (Kanzawa *et al*., 2004). Prior to transfection, media was removed and cells were washed with warm PBS. Transfection was performed using 800 ng of plasmid DNA concentration for LC3 which was prepared with 50 µl serum free media by the addition of a solution containing 200 µl serum free media and 12 µl of lipofectamin. After vortexing for 20 minutes at room temperature this reagent mixture was added to each chamber (Kindly provided by Dr B. Loos, University of Stellenbosch, South Africa). Lipofectamin is a chemical transfection agent. This is a process of transient transfection as only few cells may take up the plasmid construct and thus express the protein in a non-stable fashion. Therefore, cells do

not express the protein for long periods of time as the plasmid is released during cell cycle progression or after a few divisions.

2.6.2 Fluorescent Staining: Morphological Analysis of Cell Death and Mitochondria

To assess cell death, cells were stained with Hoechst 33342 (in a 1:200 dilution in PBS) (Sigma, B2261). Hoechst intercalates with DNA of all cells however; apoptotic cells are characterised by nuclear fragmentation (karyorrhexis) and nuclear condensation (pyknosis) (Kerr, 1994) and exhibit a greater intensity of the fluorescent signal emitted. Hoechst was added onto the cells at a final concentration of 50 µg/ml, and incubated for 10 min. Cells were classified according to their nuclear signal: (i) normal nuclei with blue chromatin, showing organization with a distribution of heterochromatin and euchromatin and (ii) cells displaying bright blue and substantially condensed or fragmented nuclei indicative of apoptosis. Together with Hoechst 33342, the cell-permeant, MitoTracker ® Red (Molecular Probes, M-7512) was added directly to the cells at a final concentration of 25 nM. This fluorescent probe contains a mildly thiol-reactive chloro-methyl moiety specific for mitochondrial labelling and maybe used to visualise localisation and morphology of mitochondria. Staining mitochondria only in viable cells, its accumulation is dependent upon membrane potential. Using the Olympus Cell^R Soft Imaging Systems, images of three random selected fields of view were acquired immediately thereafter, using 572 excitation and UBG emission filters.

2.7 Statistical analysis

Values are expressed as mean ± standard error of the mean (SEM). Data were analysed using a one-way analysis of variance (ANOVA) with Bonferroni's Multiple Comparison as a post-hoc test. $P<0.05$ was considered as statistically significant.

2.8 Study Design (*In vivo*)

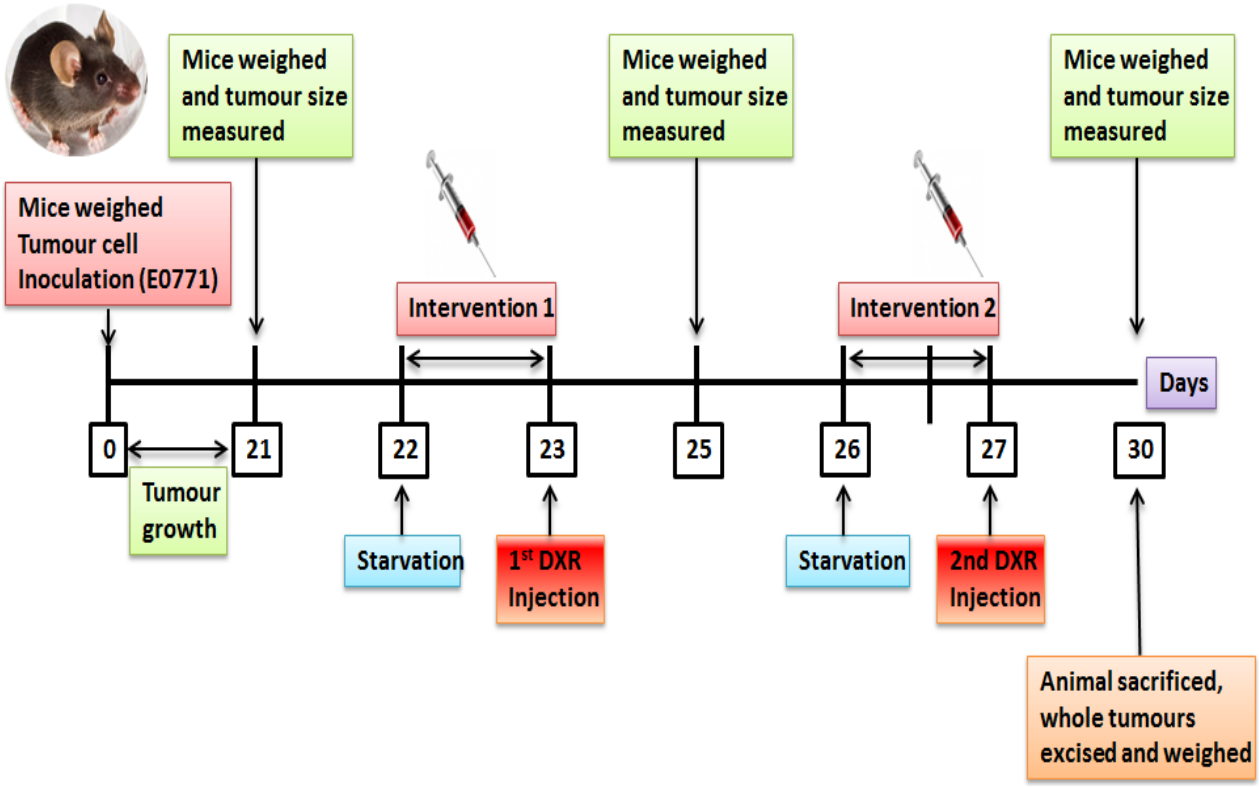

Figure 2.8.1: *In vivo* experimental protocol. Tumours were allowed to grow for 21 days and mice were subjected thereafter to the above treatment protocol.

2.9 Cell culture of E0771 mouse mammary cancer cells

Experiments were conducted using the murine metastatic mammary adenocarcinoma cell line E0771 provided by Fengzhi Li (Rosswel Park Cancer Institute, Buffalo, New York, USA). Cells were cultured in Dulbecco's modified Eagle's medium (DMEM) (Sigma Chemical Co., St Louis, MO, USA) supplemented with 10% foetal bovine serum (FBS) (Sigma Chemical Co., St Louis, MO, USA) and 1% penicillin/streptomycin (PenStrep) (Sigma Chemical Co., St Louis, MO, USA). Cells were allowed to proliferate in T75 flasks (75 cm^2 flasks, Greiner Bio One, Germany) over a period of two days with changing of fresh growth medium after every 24 hours. When cultures reached 80% confluence (Figure 2.9.1), they were split equally into 3 other T75 flasks in order to yield a sufficient amount of cells for inoculation. Splitting was achieved by rinsing cells with warm, sterile phosphate buffered saline (PBS) and trypsinising the cells (0.25% Trypsin – ethylene diaminetetra-acetic acid (EDTA) (Invitrogen, Life Technologies) with occasional gentle agitation to ensure complete detachment, following centrifugation at 200 g for 3 minutes. Experiments were conducted using exponentially growing cells.

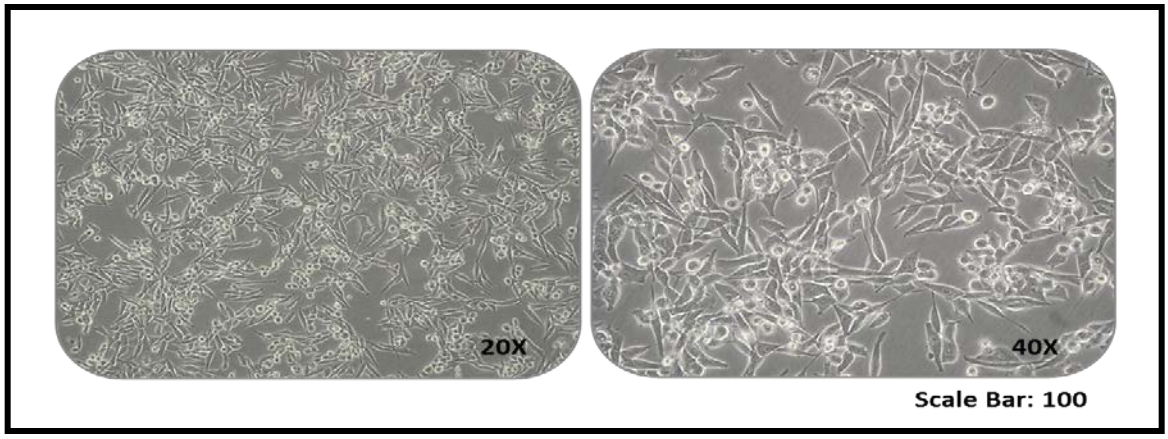

Figure 2.9.1: Breast cancer mouse cell line E0771, showed at 80% confluence, under 20X and 40X magnification.

2.10 Animal Protocols and tumour establishment

All animal protocols were carried out according to the guideline for the care and use of laboratory animals implemented at Stellenbosch University. Institutional and international ethical guidelines were applied with respect to the handling of the experimental animals. Six week old C57BL6 mice (Stellenbosch University animal facility) were used for the purposes of this study. Mice were maintained on a standard diet and tap water *ad libitum* before being subjected to the experimental protocol. The protocol used was adapted from Ewens *et al* (2006). Mice were inoculated subcutaneously on the left pad of the fourth mammary gland with 200 µl of $2.5x10^5$ E0771 cells suspended in Hanks Balanced Salt Solution, using a 23-gauge needle. Mice were weighed and inoculated with E0771 cell suspensions on day 0 and small tumours were evident by days 11-14. Tumours were allowed to grow further until day 21, when medium to large size tumours were visible. Tumour sizes were monitored every second day by taking measurements in two

perpendicular dimensions parallel to the ventricular surface of the mice using a digital calliper (tumour volume = length x width). The body weight was monitored twice weekly. On day 20, mice were distributed among four groups which included a Control group, DXR treated group, Starvation group and a combination group of prior starvation following DXR treatment (Figure 2.10.1). Additionally, mice in each group were labelled by ear clipping procedure. Administration of treatment occurred on the days indicated in Figure 2.10.1. The Doxorubicin group received a total of two injections (5 mg/kg, intra-peritoneal) as described by Zhu *et al* (2009) for 1 week. Briefly, 5 mg/kg doxorubicin was administered at 2 day intervals with an accumulative dose of 10 mg/kg. The Starvation group was subjected to 24 hours of starvation (removal of standard chow diet). For the Starvation and DXR, mice were subjected to 24 hours of starvation before receiving a 5 mg/kg DXR injection. Upon termination of the experimental protocol, mice were killed and tumours excised. The tumours appeared to be homogenous by macroscopic examination and were vascularised with no apparent hypoxic regions. Therefore, the whole tumour was excised and cut into three equal parts. Samples were placed in eppendorf tubes and exposed to liquid nitrogen before being placed in a -80 freezer for future experimental analysis. Prior to protein extraction, samples were submitted to further tissue homogenization and sonification protocols (see appendix A).

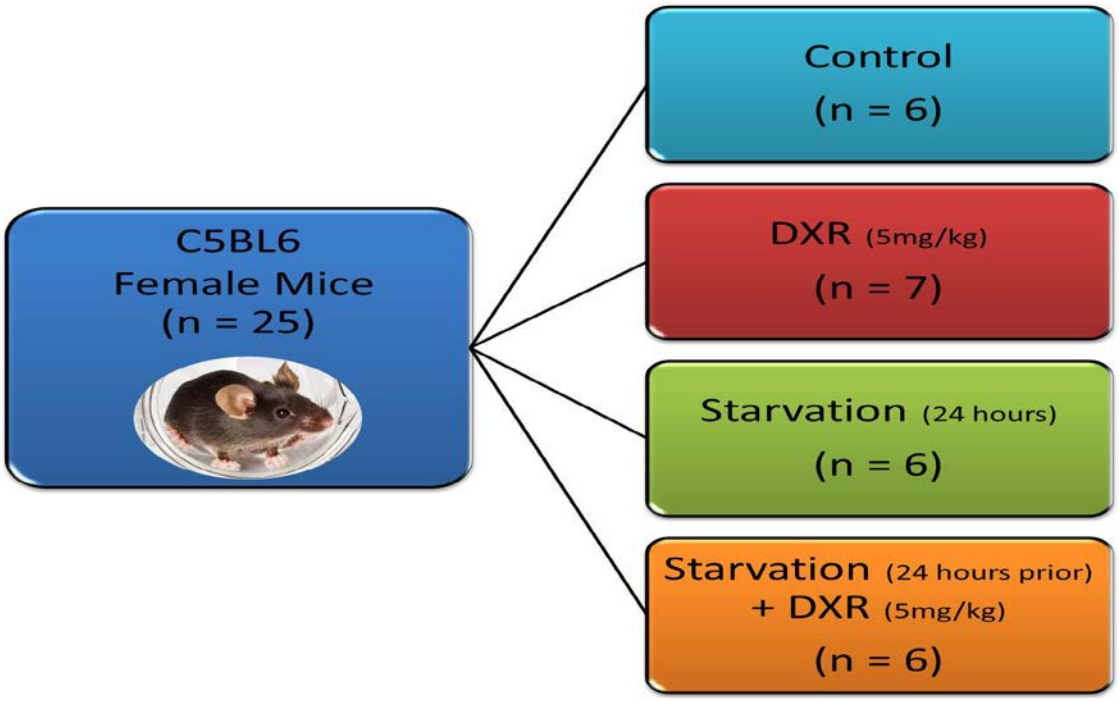

Figure 2.10.1: *In vivo* experimental groups utilised for the entire duration of this study.

2.11 Western Blots

2.11.1 Protein extraction and sample preparation

Proteins in tumours were extracted with 1000 µl of ice cold radioimmunoprecipitation (RIPA) buffer, pH 7.4, containing (in mM): tri-(hydroxylmethyl)-aminomethane (TRIS)-HCl 50, NP-40 1%, Na-Deoxycholate 0.25%, EDTA (Ethylenediamine-tetra-acetic acid) 1, sodium fluoride (NaF) 1, soybean trypsin inhibitor (SBTI) 4 µg/ml, phenyl-methyl-sulphonyl fluoride (PMSF) 1, Benzamidine 1, leupeptin 1µg/ml and Triton X-100. Tumour tissue samples were then sonicated (Ultrasonic Liquid Processor, Qsonica) for ± 5 mins to ensure the release of proteins and centrifuged (5900 g at 4ºC for 10 min) to remove nuclei and cellular debris. Samples were either stored at -80˚C or protein content was quantified using Bradford protein determination method (Bradford, 1976), followed

by immediate preparation of tissues samples. Laemmli sample buffer containing: 33.3 ml TRIS 0.5, pH 6.8, 10% SDS, 2.5 ml glycerol, 0.2 ml 0.5% bromophenol blue in deionized water was used to prepare cell samples. A combination of 850 µl sample buffer and 150 µl mercaptoethanol was vortexed and the appropriate amounts according to calculations were accurately aliquoted to each protein sample (20 µg). Samples were boiled for 5 min at 95˚C before being spun for 5 mins in a microcentrifuge.

2.11.2 Sodium-dodecyl-sulphate-polyacrylamide gel electrophoresis (SDS-PAGE) and Western blot analysis

Total protein lysates (20 µg) were loaded and separated using gradient gels (4% - 15%) sodium-dodecyl-sulphate-poly-acrylamide gel electrophoresis(SDS-PAGE) and a 4% stacking gel (Bio-Rad Mini-Protean ® TGX ™ Precast Gels). A pre-stained protein marker ladder (peqGOLD, PEQLAB Biotechnologie GMBH, Germany) was loaded in the first lane on each gel for determination of molecular weights of specific bands. Gels were run at 150 V (constant) and 400 mA for 60 minutes (Mini- PROTEAN Tetra Tank, Bio-Rad, USA). Following, SDS- PAGE, proteins were transferred to polyvinylidine fluoride (PVDF) membrane (Bio-Rad Trans-Blot Turbo Transfer packs) using the Bio-Rad electro-transfer system (Bio-Rad Trans- Blot Transfer System) for 12 minutes at 150V and 1.5 A. Non-specific binding sites were blocked with 5% fat-free milk in TRIS-buffered saline-Tween (TBS-T) and membranes were incubated overnight with the primary antibodies (cleaved-caspase-3, cleaved-PARP, p62/SQSTM1, LC-3, phosphor-AMPK-α,

phospho-mTOR and β-Actin). In this part of the study, western blot procedure was performed in the following manner: Animals were treated as previously described and at the end of the treatment; tissue was obtained as previously described. Although there were initially at least six animals per group, some animals died before the termination of the experiment. These tumours were not used for western blotting, however, at least three animals remained in each group and their tumours were analysed. The samples were loaded on the gel as follows: lane 1: protein ladder, lane 2: control, lane 3: doxorubicin, lane 4 starvation and lane 5: doxorubicin + starvation. Fifteen well gradient gels (4-15%) were used throughout this part of the study. We used western blot analysis to examine the following proteins; cleaved caspase-3 (17-19 kDa) and cleaved-PARP (89 kDa); LC3 I and II (16-18 kDa) and p62 (62 kDa) as well as phospho-AMPK (62 kDa) and phospho-mTOR (289 kDa). The membranes were cut or stripped to visualise all proteins mentioned above for each experiment. Thereafter the membranes were probed with β-actin to ensure equal loading of proteins. Membranes were then washed with TBS-T (3 x 5 min) and the primary antibody was conjugated by the addition of a diluted horseradish peroxidase-labelled secondary antibody (Amersham LIFE SCIENCE) for 1 hour at room temperature. Thereafter, membranes were thoroughly washed before being exposed to ECL (chemi-luminescent reagent) for 1 minute. Bands were detected using the Bio-Rad Chemi-Doc system. Exposed bands were visualised and quantified using densitometry software (Quantity1). All bands were expressed as optical density readings relative to a control present on the same blot. Membranes were then washed with TBS-T (3 x 5 min) and the

primary antibody was conjugated by the addition of a diluted horseradish peroxidase-labelled secondary antibody (Amersham LIFE SCIENCE) for 1 hour at room temperature. Thereafter, membranes were thoroughly washed before being exposed to ECL (chemi-luminescent reagent) for 1 minute. Bands were then detected using the Bio-Rad Chemi-Doc system. Exposed bands were visualised and quantified using densitometry software (Quantity1). Each experimental group on a membrane was normalised to its corresponding β-actin band. Thereafter, the averages of all experimental groups (control, doxorubicin, starvation and dox+starvation) (n=3) were normalised to the control which was set as one.

2.12 Statistical analysis

Values are expressed as mean ± standard error of the mean (SEM). Data were analysed using a one-way analysis of variance (ANOVA) with Bonferroni's Multiple Comparison as a post-hoc test. $P<0.05$ was considered as statistically significant.

Chapter 3 - Results

IN VITRO

3.1 The effect of various hours of starvation on cell viability and cell death

To establish a time point at which MCF12A breast epithelial cells are protected against starvation. Both cells lines were subjected to 0, 3, 6, 12, 24 and 48 hours of starvation in Hanks Balanced Salt Solution and cell viability was assessed using the MTT assay and the trypan blue assay. This was followed by a Caspase-Glo 3/7 assay to determine if programmed cell death was involved during short-term starvation.

MDAMB231 cells showed a significant decrease in cell viability following 48 hours of incubation in nutrient deprived media (HBSS) when compared to the control (9.364 ± 2.126% vs 100%, $p < 0.0001$) (Figure 3.1.1 A). In contrast to this observation, the viability of MCF12A cells significantly decreased following 6, 24 and 48 hours of starvation when compared to the control. However, no significant changes in cell viability were observed following 3 and 12 hours of starvation when compared to the control (Figure 3.1.1 B).

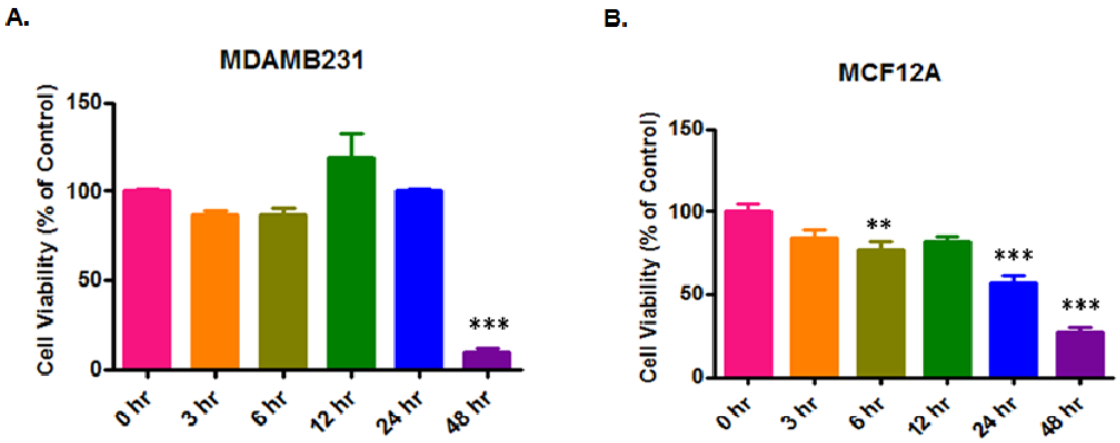

Figure 3.1.1: The effect of various hours of starvation on the viability of MDAMB231 breast cancer cells (Bar graph A) and MCF12A non-tumourigenic breast epithelial cells (Bar graph B). MDAMB231 and MCF12A cells were incubated in Hanks Balanced Salt Solution for 0 (Control), 3, 6, 12, 24 and 48 hours. Cell viability was assessed using the MTT Assay. Values are expressed as percentage of the control and presented as means ± SEM (n=3), **A:** ***p < 0.0001 vs 0 hrs. **B:** **p < 0.001 vs 0 hrs, ***p<0.0001 vs 0 hrs. Abbreviations- **hr:** hours.

MDAMB231 cells showed a significant decrease in cell viability following 48 hours of incubation in nutrient deprived media when compared to the control (5.889 ± 1.852% vs 100%, p < 0.0001) (Figure 3.1.2 A). The viability of MCF12A cells demonstrated no significant changes following 3 hours of starvation in comparison to the control, however viability decreased following 6, 12, 24 and 48 hours of nutrient deprivation (Figure 3.1.2 B).

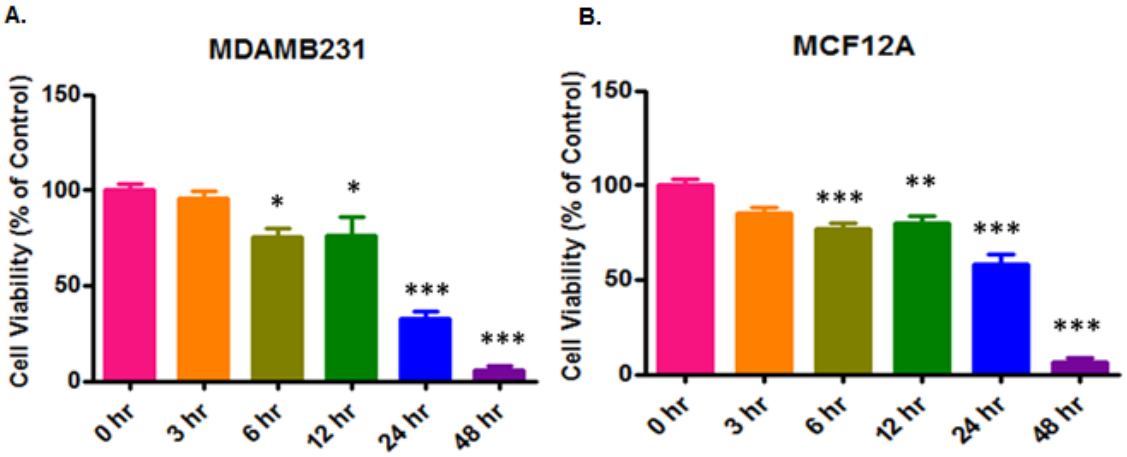

Figure 3.1.2: The effect of various hours of starvation on the viability of MDAMB231 breast cancer cells (Bar graph A) and MCF12A non-tumourigenic breast epithelial cells (Bar graph B). MDAMB231 and MCF12A cells were incubated in Hanks Balanced Salt Solution for 0 (Control), 3, 6, 12, 24 and 48 hours. Cell viability was assessed using the trypan blue assay. Values are expressed as percentage of the control and presented as means ± SEM (n=3), **A**: *p < 0.05 vs 0 hrs, ***p < 0.0001 vs 0 hrs. **B:** **p < 0.001 vs 0 hrs, ***p<0.0001 vs 0 hrs. Abbreviations- **hr:** hours.

MDAMB231 cells displayed a significant increase in caspase 3/7 activity in response to 48 hours of starvation when compared to the control (8.346 ± 1.620 fold vs 1.000 ± 0.000 fold, $p < 0.0001$) (Figure 3.1.3 A). MCF12A cells showed no significant changes in caspase 3/7 activity following 3 hours of starvation. However, a significant decrease in caspase3/7 activity was detected when cells were starved for 12 hours when compared to the control (0.169 ± 0.039 fold vs 1.000 ± 0.013 fold, $p < 0.0001$) (Figure 3.1.3 B).

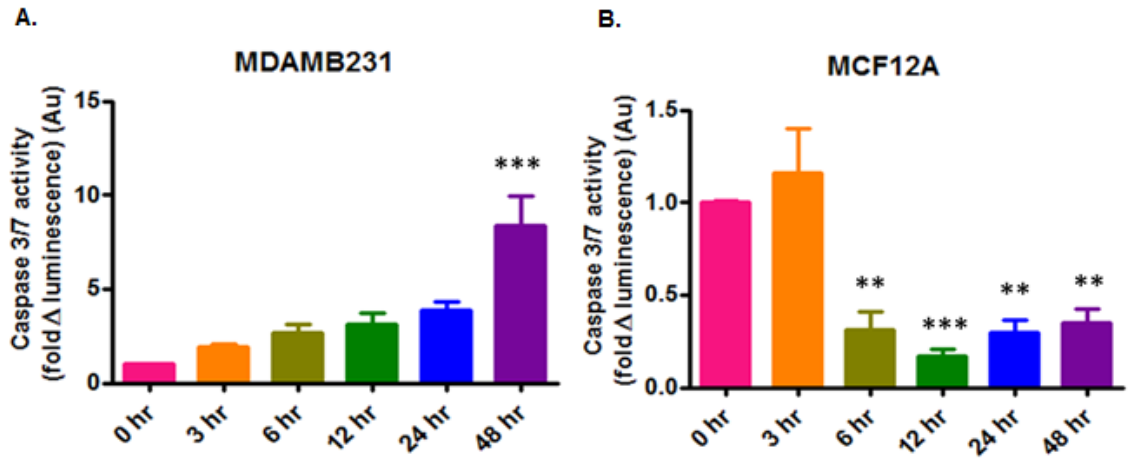

Figure 3.1.3: The effect of various hours of starvation on programmed cell death in MDAMB231 breast cancer cells (Bar graph A) and MCF12A non- tumourigenic breast epithelial cells (Bar graph B).Programmed cell death was assessed using the Caspase-Glo® 3/7 Assay. Caspase 3/7 activity was taken to be proportionate to the produced luminescence intensity per sample. Results represent the fold change in luminescence and presented as means ± SEM (n=3), **A:** *p < 0.0001 vs 0 hrs. **B:** **p < 0.001 vs 0 hrs, ***p < 0.0001 vs 0 hrs. Abbreviations- **hr:**hours; **AU:** Arbitrary Units.

3.2 The effect of short-term starvation on doxorubicin-induced cell death

Based on the results obtained in our preliminary study, 3 hours of starvation was chosen for future *in vitro* experiments since no significant changes in cell viability or increase in apoptosis occurred at this time-point in the normal MCF12A breast epithelial cells. The following four treatment groups were used in this study: (1): control; (2): 5 µM of doxorubicin (DXR) for 24 hours; (3): short-term starvation (3 hours) (STS) and (4): short- term starvation (3 hours) prior to 24 hours treatment with doxorubicin (STS+ DXR).

The MTT Assay was first used to assess cell viability in both MDAMB231 cancer cells and MCF12A breast epithelial cells. MDAMB231 cells starved for 3 hours and treated with DXR for 24 hours showed a significant decrease in cell

viability when compared to the DXR treated group only (59.91 ± 4.208% vs 71.16 ± 2.490%, $p < 0.05$) (Figure 3.2.1A). In contrast, MCF12A cells starved for 3 hours and treated with DXR for 24 hours were protected by starvation as the cell viability significantly increased when compared to the DXR treated group only (93.36 ± 5.406% vs 73.55 ± 7.197%, $p < 0.05$) (Figure 3.2.1 B).

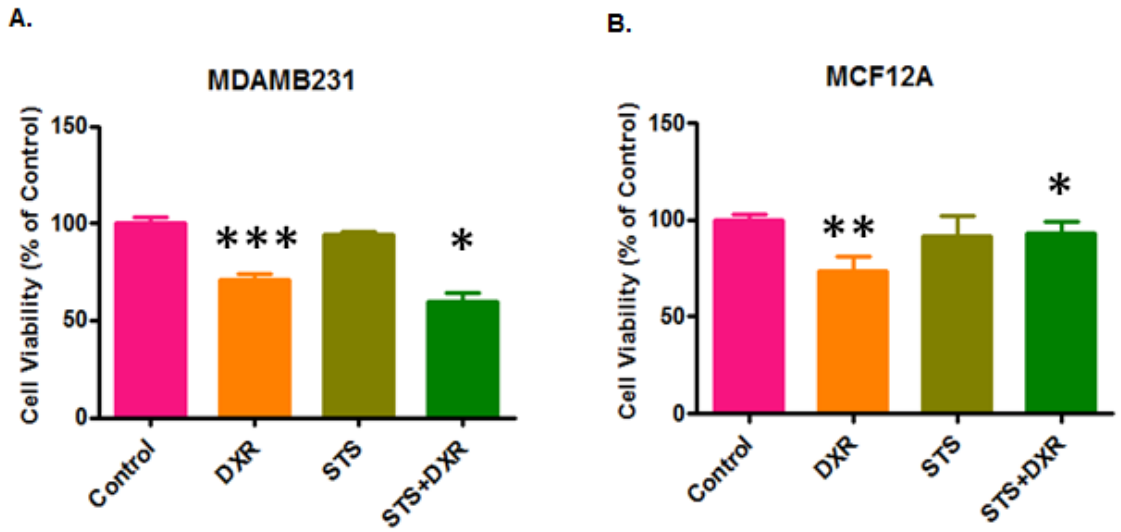

Figure 3.2.1: The effect of short-term starvation on doxorubicin-induced cell death. MDAMB231 breast cancer cells (Bar graph A) and MCF12A non-tumourigenic breast epithelial cells (Bar graph B) were subjected to the following conditions: (1) control; (2) 5 µM DXR; (3) 3 hours starvation and (4) starvation with DXR. Cell viability was assessed using MTT Assay. Values are expressed as percentage of the control and presented as means ± SEM (n=3), **A:** ***$p < 0.0001$ vs control, *$p < 0.05$ vs DXR. **B:** **$p < 0.001$ vs control, *$p < 0.05$ vs DXR. Abbreviations- **DXR:** Doxorubicin; **STS:** Short-term starvation.

To provide further insight into programmed cell death and the mechanisms that are involved, MDAMB231 breast cancer cells were analysed using recognized markers for programmed cell death, namely cleaved caspase-3 and cleaved-PARP. The presence of these markers was quantified using western blot analysis to indicate the response of the treated groups to apoptotic stimuli. MDAMB231 cells showed a significant increase in caspase-3 cleavage in response to DXR when compared to the control (2.376 ± 0.1022 fold vs 1.000 ± 0.000 fold, $p < 0.0001$). A further increase in caspase-3 cleavage was observed

with STS+DXR when compared to the DXR treated group (2.376 ± 0.1022 fold vs 1.991 ± 0.0794 fold, $p < 0.05$) (Figure 3.2.2 A). Confirming this increase in apoptotic activity, PARP cleavage was significantly increased in response to STS+DXR in comparison to the DXR (1.939 ± 0.201 fold vs 0.236 ± 0.089 fold, $p < 0.05$) (Figure 3.2.2 B).

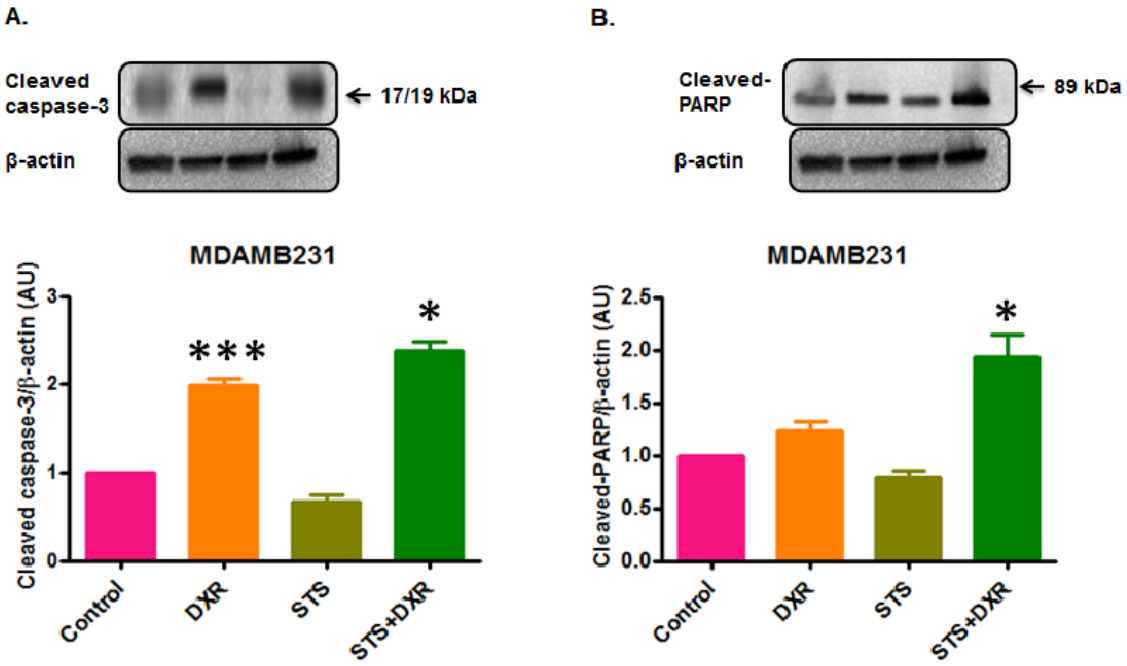

Figure 3.2.2: The effect of short-term starvation on doxorubicin-induced apoptotic cell death. MDAMB231 breast cancer cells were subjected to the following conditions: (1) control; (2) 5 μM DXR; (3) 3 hours starvation and (4) starvation with DXR. Apoptotic cell death was measured using western blot analysis. Bar graphs show: A) Cleaved caspase-3 and B) Cleaved-PARP protein levels (normalized to β-actin vs control). Values are expressed as means ± SEM (n=3), **A:** ***p < 0.0001 vs control,*p < 0.05 vs DXR. **B:** *p < 0.05 vs DXR. Abbreviations- **DXR:** Doxorubicin; **STS:** Short-term starvation; **AU:** Arbitrary Units. A representative blot is shown.

3.3 The effect of short-term starvation and doxorubicin treatment on autophagic activity

LC3 and p62/SQSTM1 as markers of autophagic activity were assessed by western blotting. LC3 II examination revealed high basal levels of autophagy in the control group. This significantly decreased with DXR treatment (0.634 ±

0.0147 fold vs 1.000 ± 0.000 fold, $p < 0.001$) and STS (0.248 ± 0.090 fold vs 1.000 ± 0.000 fold, $p < 0.0001$) when compared to the control. A further decrease was observed with STS+DXR (0.128 ± 0.003 fold vs 0.634 ± 0.0147 fold, $p < 0.0001$) when compared to the DXR (Figure 3.3.1 A).

p62, a poly-ubiquitin protein degraded by autophagy is inversely proportional to the extent of autophagic activity. However, the presence of DXR significantly decreased p62 (0.519 ± 0.443 fold vs 1.000 ± 0.000 fold, $p < 0.001$) when compared to the control. A significant increase was observed with STS+DXR (2.524 ± 0.131 fold vs 0.519 ± 0.443 fold, $p < 0.0001$) when compared to DXR treatment only (Figure 3.3.1 B).

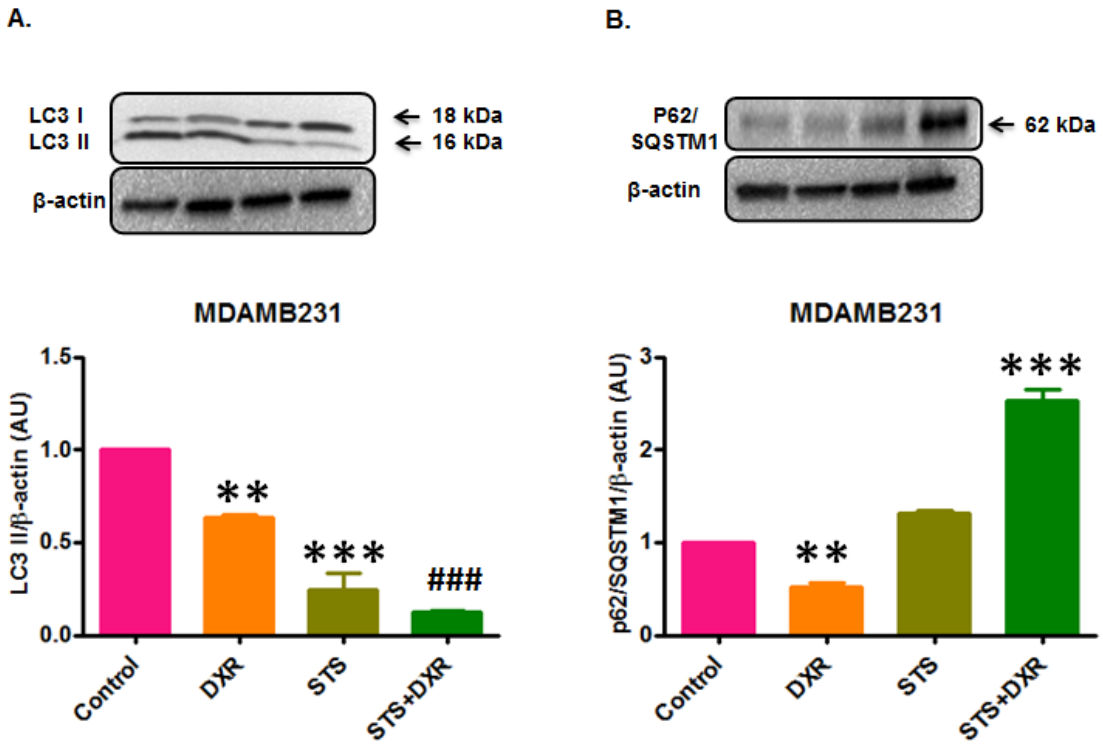

Figure 3.3.1: The effect of short-term starvation and doxorubicin treatment on autophagic activity. MDAMB231 breast cancer cells were subjected to the following conditions: (1) control; (2) 5 µM DXR; (3) 3 hours starvation and (4) starvation with DXR. Autophagic activity was measured using western blot analysis. Bar graphs show: A) LC3 II and B) p62/SQSTM1 protein levels (normalized to β-actin vs control). Values are expressed as means ± SEM (n=3), **A:** $^{**}p < 0.001$ vs control, $^{***}p < 0.0001$ vs control $^{\#\#\#}p < 0.0001$ vs DXR. **B:** $^{**}p < 0.001$ vs control, $^{***}p < 0.0001$ vs DXR. Abbreviations- **DXR:** Doxorubicin; **STS:** Short-term starvation; **AU:** Arbitrary Units. A representative blot is shown.

3.4 The effect of short-term starvation and doxorubicin treatment on p-AMPK (oxygen sensor) and p-mTOR (energy sensor)

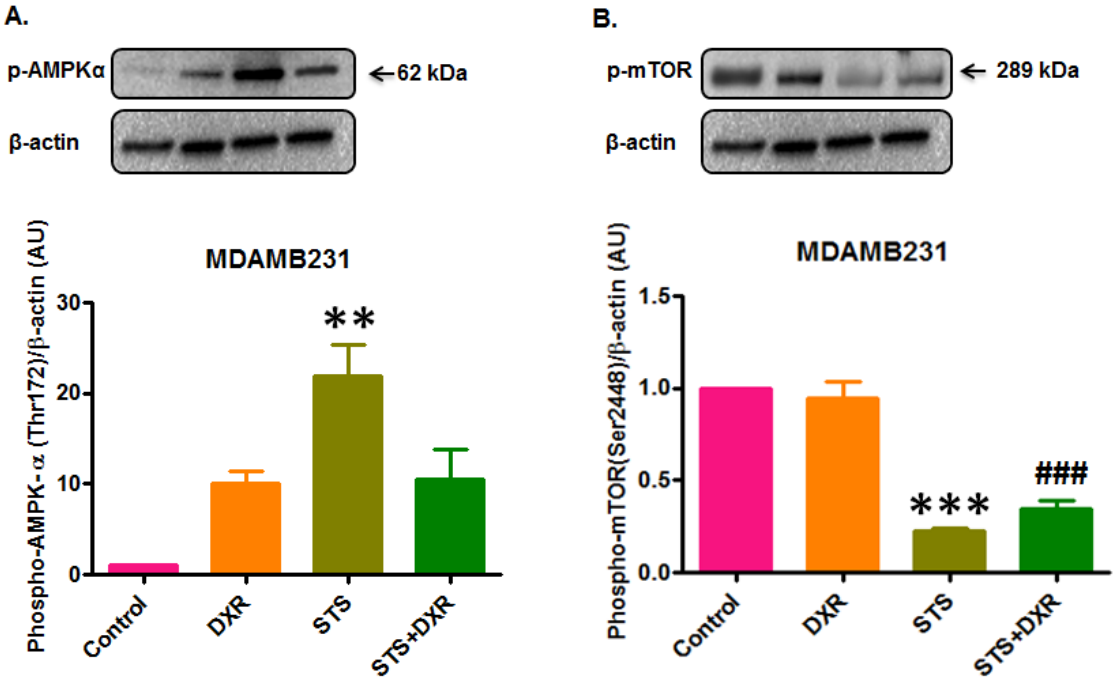

Figure 3.4.1: The effect of short-term starvation and doxorubicin treatment on p-AMPK and p-mTOR. MDAMB231 breast cancer cells were subjected to the following conditions: (1) control; (2) 5 μM DXR; (3) 3 hours starvation and (4) starvation with DXR. Markers for AMPK and mTOR were measured using western blot analysis. Bar graphs show: A) p-AMPK and B) p-mTOR protein levels (normalized to β-actin vs control). Values are expressed as means ± SEM (n=3), **A:** **p < 0.0001 vs control. **B:** ***p < 0.0001 vs control, $^{###}$p < 0.0001 vs DXR. Abbreviations- **DXR:** Doxorubicin; **STS:** Short-term starvation; **AU:** Arbitrary Units. A representative blot is shown.

Phospho-AMPK-α (p-AMPK) and phospho-mTOR (p-mTOR) as an oxygen and energy sensor respectively, were assessed by western blotting. AMPK phosphorylation was significantly higher in the STS treated group when compared to the control (21.90 ± 3.530 fold vs 1.000 ± 0.000 fold, p < 0.001) (Figure 3.4.1 A). STS also increased p-mTOR activity significantly when compared to the control (0.226 ± 0.021 fold vs 1.000 ± 0.000 fold, p < 0.0001). Furthermore, p-mTOR activity with STS+DXR significantly decreased (0.349 ±

0.043 fold vs 0.946 ± 0.091 fold, $p < 0.0001$) when compared to DXR (Figure 3.4.1B). In addition, to visually confirm apoptotic and autophagic activity as well as mitochondrial membrane integrity, MDAMB231 cells were transfected with GFP-LC3 and stained with Hoechst 3422 and MitoTracker Red and visualized using Live Cell Imaging.

Mitochondrial integrity was maintained when cells were starved for 3 hours and in the control. However, when cells were treated with DXR, this induced severe damage to the mitochondrial membranes. GFP- LC3 transfected cells produce a scattered pattern of distribution of autophagic vacuoles under control conditions (Figure 3.42), in comparison to a punctuate pattern of GFP-LC3 expression (GFP-LC3 dots) when induced by autophagy (Kanzawa *et al*., 2004) as visualized in the STS and STS+DXR treated groups.

Additionally, Hoechst binds to DNA of all cells however; apoptotic cells are characterized by nuclear fragmentation and nuclear condensation (Kerr, 1994) and exhibit a greater intensity of the dye as observed in the DXR, STS and STS+DXR groups. Observations are indicated by yellow arrows in Figure 3.42.

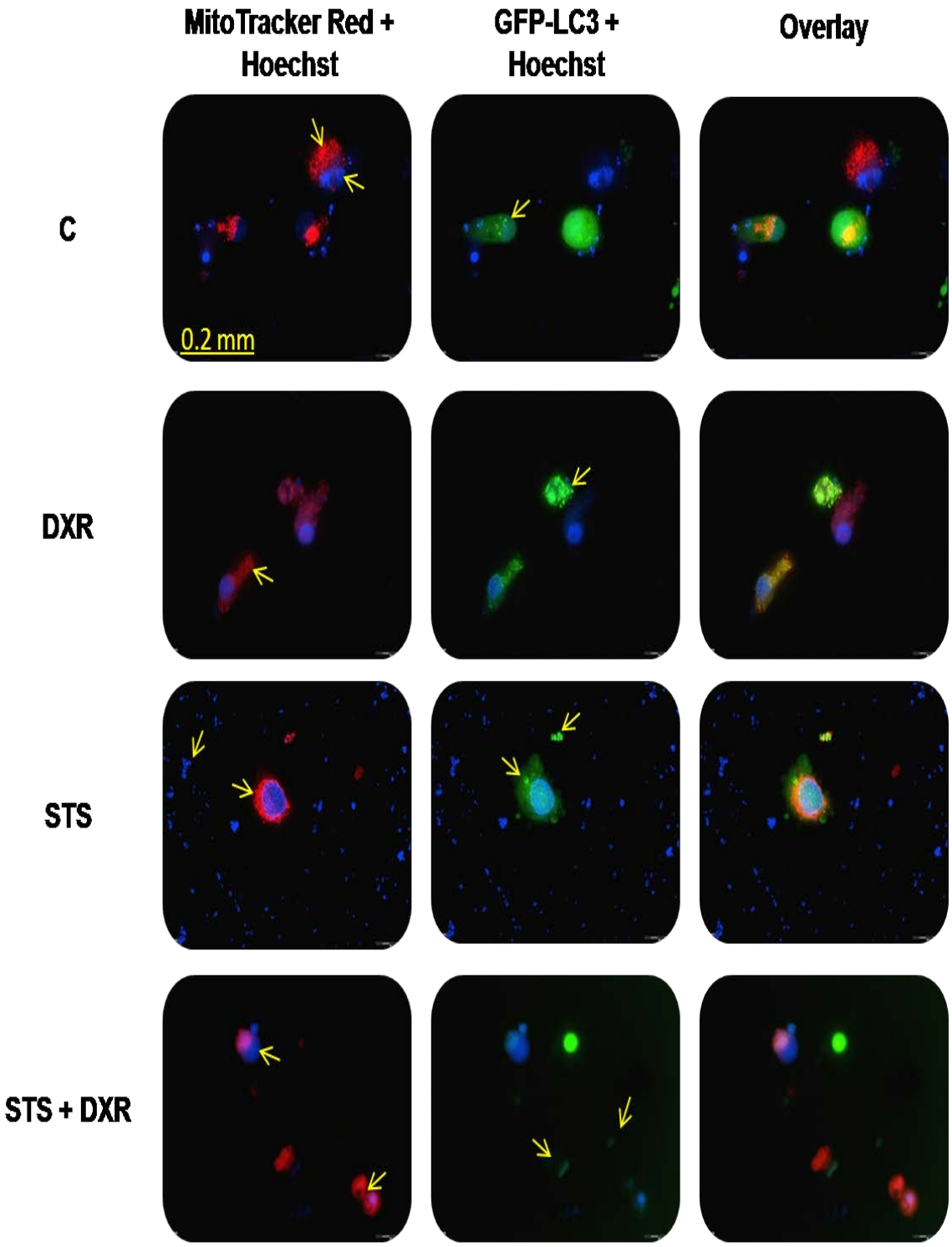

Figure: 3.4.2: Effects of various treatment regimens on mitochondrial integrity, apoptotic cell death and formation of autophagic vacuoles. MDAMB231 cells were transfected with GFP-LC3 and stained with Hoechst 33342 and MitoTracker Red and visualized using Live Cell Imaging. Yellow Arrows indicate: presence of autophagic vacuoles (green), changes in mitochondrial integrity (red) and DNA fragmentation and membrane blebbing (blue) in the various groups. Abbreviations- **C:** Control; **DXR:** Doxorubicin; **STS:** Short-term starvation.

In vivo

3.5 The effect of various treatments on tumour growth

In the *in vivo* section of this study, C57BL6 tumour-bearing mice were distributed among four groups which included a Control group, DXR treated group, 24 hour starvation group and a combination group of 24 hours starvation prior to DXR treatment. Tumour size was measured every second day as described previously. Due to difficulty in accessibility of the tumour to obtain parameters of length and width in all tumours, no SEM or multiple comparisons were performed, hence the obtained values merely represent averages between groups. The following trends were however observed; a decrease in tumour volume was observed in the DXR-group when compared to the control. A similar response was observed in the combination of starvation and DXR and in the starvation group (at a slower rate) where tumour volume also decreased when compared to the DXR treated group.

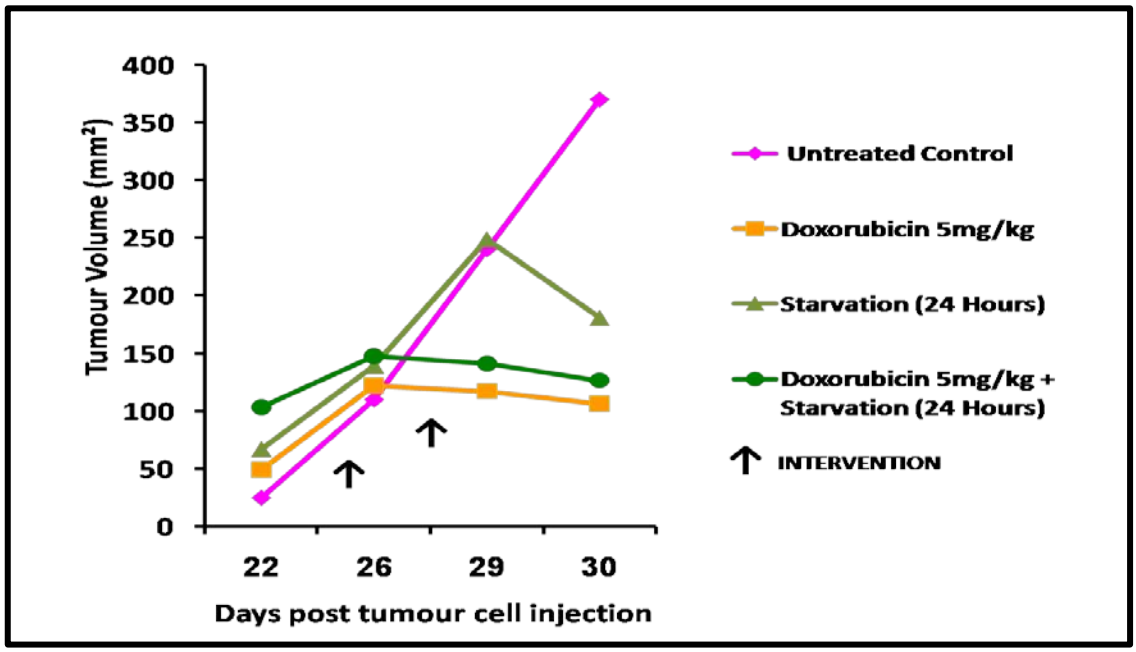

Figure 3.5.1: The effect of different treatment regimens on tumour growth. Tumour size was assessed immediately after the occurrence of tumours (± 21 days after tumour cell inoculation) and throughout the study. Day 30 represents the last day tumour size was assessed before prior to intervention treatment was conducted. Animals were either treated with DXR (5 mg/kg) or starved for 24 hours or a combination of prior starvation following DXR treatment.

3.6 The effect of short-term starvation on doxorubicin-induced cell death in tumour bearing mice

To provide further insight into programmed cell death and the mechanisms that are involved, tumour tissue from the various treated groups were analysed utilizing cleaved caspase-3 and cleaved-PARP as markers for apoptotic cell death. The presence of these markers in the above mentioned groups were quantified using western blot analysis. Tumour tissue analysis revealed a significant increase in caspase-3 cleavage in response to DXR (9.367 ± 0.626 fold vs 1.000 ± 0.000 fold, $p < 0.0001$) and a significant decrease with STS (3.831 ± 0.025 fold vs 1.000 ± 0.000 fold, $p < 0.001$) when compared to the control. Additionally, treatment with STS+DXR significantly decreased when compared to DXR (6.916 ± 0.165 fold vs 9.367 ± 0.626 fold, $p < 0.0001$) (Figure: 3.6.1A). Subsequently, PARP cleavage was significantly increased in response to DXR treatment when compared to the control (17.61 ± 1.572 fold vs 1.000 ± 0.000 fold, $p < 0.001$) and significantly decreased with STS+DXR when compared to DXR (10.84 ± 0.490 fold vs 17.61 ± 1.572 fold, $p < 0.0001$) (Figure 3.6.1 B).

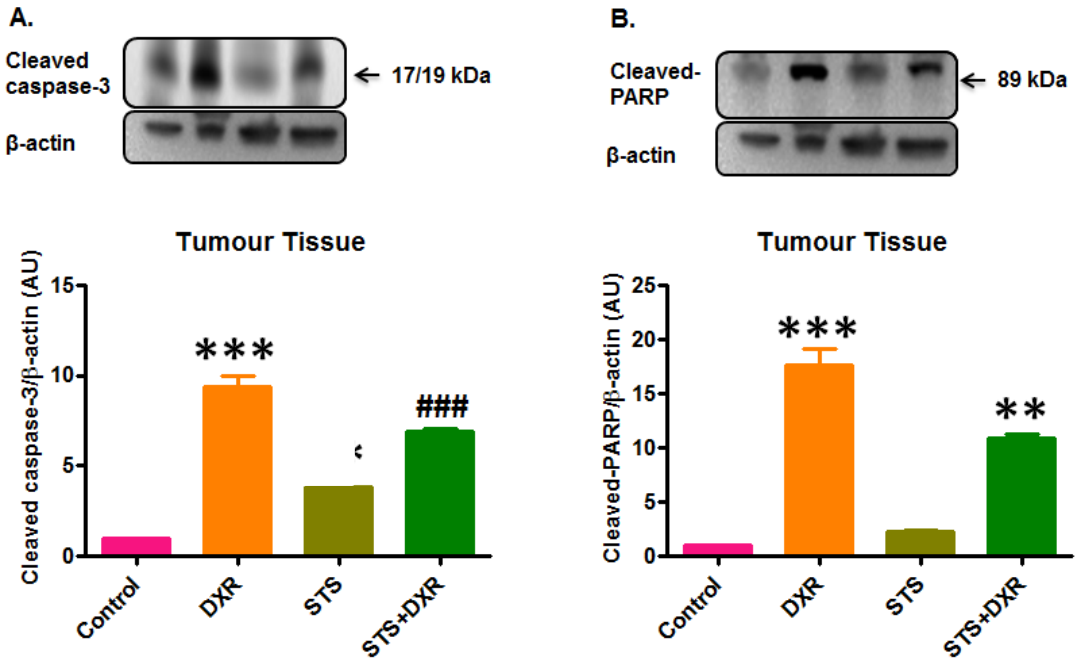

Figure 3.6.1: The effect of short-term starvation on doxorubicin-induced apoptotic cell death. Animals were either treated with DXR (5 mg/kg) or starved for 24 hours or a combination of prior starvation following DXR treatment. Apoptotic cell death was measured using western blot analysis. Bar graphs show: A) cleaved caspase-3 and B) cleaved-PARP protein levels (normalized to β-actin vs control). Values are expressed as means ± SEM (n=3), **A:** $^{***}p < 0.0001$ vs control, $^{**}p < 0.001$ vs control, $^{###}p < 0.0001$ vs DXR. **B:** $^{***}p < 0.0001$ vs control,$^{**}p < 0.001$ vs DXR. Abbreviations- **DXR:** Doxorubicin; **STS:** Short-term starvation; **AU:** Arbitrary Units. A representative blot is shown.

3.7 The effect of short-term starvation and doxorubicin treatment on autophagic activity in tumour bearing mice

LC3 and p62/SQSTM1 as markers of autophagic activity were assessed by western blotting. LC3 II examination was significantly higher in the DXR treated group when compared to the control (3.243 ± 0.378 fold vs 1.000 ± 0.000, $p < 0.0001$) (Figure 3.7.1A). Since, p62/SQSTM1 is inversely proportional to the extent of autophagic activity, the presence of DXR significantly decreased p62 when compared to control (0.329 ± 0.040 fold vs 1.000 ± 0.000 fold, $p < 0.001$). In contrast, STS+DXR significantly increased p62 expression in comparison to

the DXR treated group (0.822 ± 0.119 fold vs 0.329 ± 0.040 fold, $p < 0.05$) (Figure 3.7.1B).

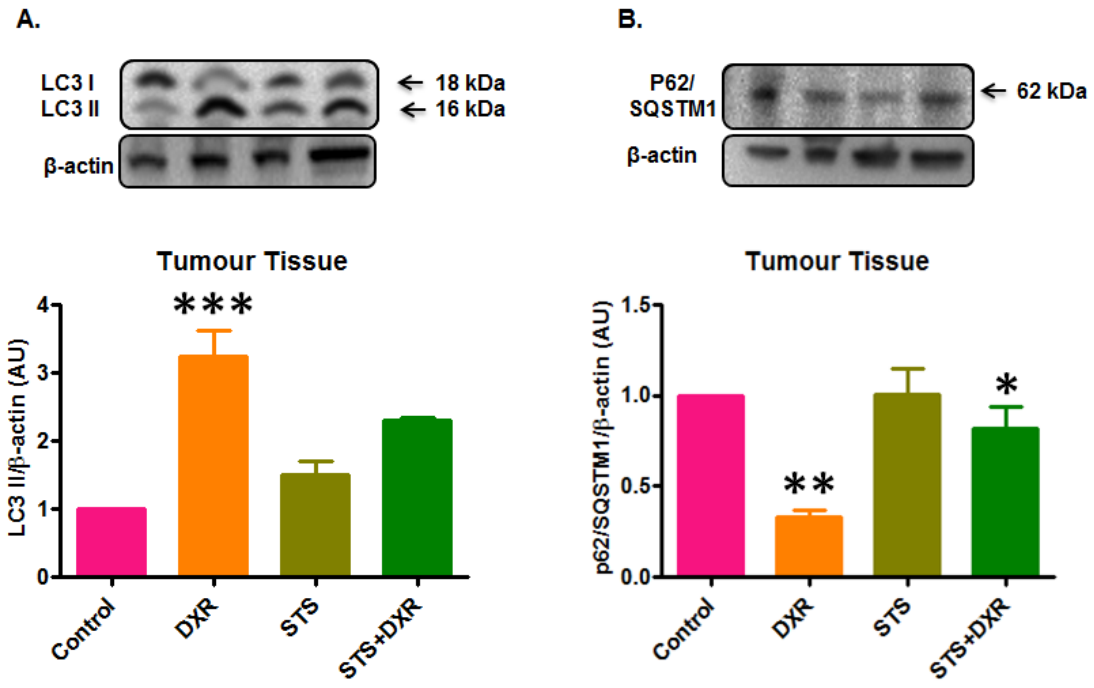

Figure 3.7.1: The effect of short-term starvation and doxorubicin treatment on autophagic activity. Animals were either treated with DXR (5 mg/kg) or starved for 24 hours or a combination of prior starvation following DXR treatment. Apoptotic cell death was measured using western blot analysis. Bar graphs show: A) LC3 II and B) p2/SQSTM1 protein levels (normalized to β-actin vs control). Values are expressed as means ± SEM (n=3), **A:** $^{***}p < 0.0001$ vs control. **B:** $^{**}p < 0.001$ vs control $^{*}p < 0.05$ vs DXR. Abbreviations- **DXR:** Doxorubicin; **STS:** Short-term starvation; **AU:** Arbitrary Units. A representative blot is shown.

3.8 The effect of short-term starvation and doxorubicin treatment on p-AMPK (oxygen sensor) and p-mTOR (energy sensor) in tumour bearing mice

Phospho-AMPK-α (p-AMPK) and phospho-mTOR (p-MTOR) as markers of oxygen and energy sensing respectively, were assessed by western blotting. Phospho-AMPK-α was significantly higher in the DXR treated group when

compared to the control (7.052 ± 0.494 fold vs 1.000 ± 0.000 fold, $p < 0.0001$) (Figure 3.8.1 A). Phospho-mTOR activity significantly decreased with DXR (0.409 ± 0.013 fold vs 1.000 ± 0.000 fold, $p < 0.0001$) and significantly increased with STS (1.234 ± 0.044 fold vs 1.000 ± 0.000 fold, $p < 0.001$) when compared to the control. The combined treatment of STS+DXR significantly increased p-mTOR when compared to DXR (1.140 ± 0.025 fold vs 0.409 ± 0.013 fold, $p < 0.0001$) (Figure 3.8.1 B).

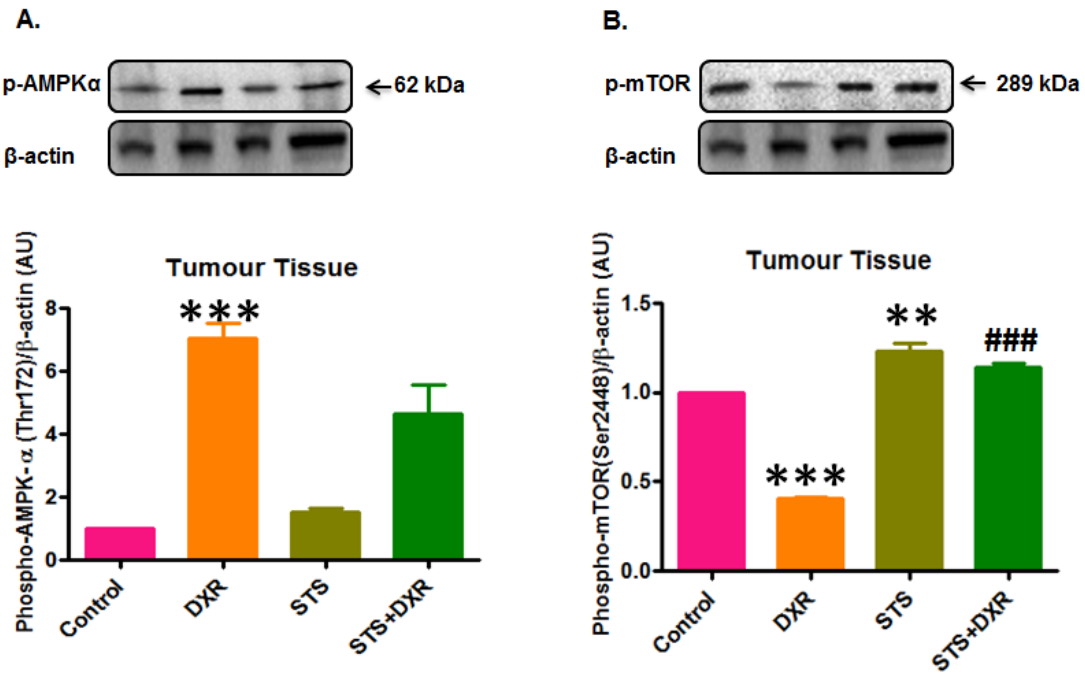

Figure 3.8.1: The effect of short-term starvation and doxorubicin treatment on cellular AMPK and mTOR phosphorylation. Animals were either treated with DXR (5 mg/kg) or starved for 24 hours or a combination of prior starvation following DXR treatment. Apoptotic cell death was measured using western blot analysis. Bar graphs show: A) p-AMPK and B) p-mTOR protein levels (normalized to β-actin vs control). Values are expressed as means ± SEM (n=3), **A:** ***$p < 0.0001$ vs control DXR. **B:** ***$p < 0.0001$ vs control, **$p < 0.001$ vs control, $^{###}p < 0.0001$ vs DXR. Abbreviations- **DXR:** Doxorubicin; **STS:** Short-term starvation; **AU:** Arbitrary Units. A representative blot is shown.

Chapter 4 - Discussion

4.1 Introduction

Breast cancer is a major contributor to the mortality of women worldwide. The essence of this neoplastic disease lies in the ability of cancer cells to sustain chronic cell proliferation which allows for progression to malignancy. Owing to the conceptual progress made in the last decade, it has become established that this phenomena corresponds to adjustments of energy metabolism in order to fuel cell growth and division. This has led to one of the emerging hallmarks of cancer, namely the reprogramming of energy metabolism (Hanahan and Weinberg, 2011).

Targeting metabolism is an attractive new paradigm for investigation because of the increased metabolic fragility of cancer. The understanding and development of clinically available therapies capable of modulating metabolism is thus critical. Most studies that have been conducted focused on either omitting or decreasing glucose, fatty acids and amino acids from the microenvironment of tumors. However, recent clinical and pre-clinical studies investigating complete nutrient deprivation for extended periods of time during cancer treatment showed promising results (Raffaghello *et al*., 2008). However, more studies need to be conducted to clearly demonstrate the beneficial effects of shorter and more endurable periods of starvation. Thus, we aimed: Firstly, to establish a time point at which MCF12A breast epithelial cells are protected against starvation; secondly, to determine the

effect of short-term starvation on doxorubicin-induced cell death; thirdly, to assess the activity of autophagy, AMPK and mTOR in our experimental conditions and finally, to assess these aims using an *in vivo* model.

4.2 *In vitro* study

4.2.1 The effect of various hours of starvation on cell viability and cell death

Our results demonstrated that MCF12A cells maintained cell viability following 3 hours of starvation, however cell viability significantly decreased and cell death significantly increased following 6 hours of starvation, persisting till 48 hours (Figure 3.1.1B, Figure 3.1.2 B and Figure 3.1.3 B, respectively). In contrast, MDAMB231 remain viable until 24 hours of starvation after which a significant decrease in cell viability and an increase in cell death occurred at 48 hours (Figure 3.1.1 A, Figure 3.1.2 A and Figure 3.1.3 A, respectively). These findings clearly demonstrate the resilient nature of breast cancer cells to total nutrient deprivation in comparison to normal breast epithelial cells. The normal breast epithelial cells showed no significant decreases in cell viability or significant increases in cell death following 3 hours of starvation. This time point was therefore chosen for further *in vitro* experimental analysis in this study as we aimed to establish a time frame at which the non-cancerous breast epithelial cells were not adversely affected by the starvation treatment.

4.2.2 The effect of short-term starvation on doxorubicin-induced cell death

In our study, a concentration of 5 μM of doxorubicin induced ±40% cell death in the MDAMB231 cells (cancer cells) and ±30% cell death in the normal MCF12A cells. In a clinical setting doxorubicin is administered intravenously over a brief period of time at a dose of 60 - 75 mg/m^2 with plasma concentrations peaking at a range between 5 and 15 μM. Since ± 75% of doxorubicin is bound by plasma proteins, the peak concentration of free doxorubicin available to induce its apoptotic effects is between 1.25 and 3.75 μM (Liu, 2008). Previous work done in our group demonstrated a significant decrease in cell viability in the MDAMB231 cells treated with 5 μM of doxorubicin for 24 hours (data not shown) (Thomas, PhD thesis, 2012) (Available: http://scholar.sun.ac.za/mark peter thomas). Since, 5 μM of doxorubicin is within the clinically accepted dose range of 0.1 - 5 μM *in vitro* (Liu, 2008), this was the reasoning for using this specific concentration in our study.

In our study, results were further validated by western blot analysis of apoptotic markers as a significant increase in cleaved caspase-3 in MDAMB231 cells were observed when treated with doxorubicin compared with the control group (Figure 3.2.2 A). Our results are in accordance with another study where doxorubicin-induced apoptosis induced poly (ADP-ribose) polymerase cleavage (PARP) and activation of caspase-3 (Lee *et al*., 2002). However, despite its wide-spread clinical use, doxorubicin, as with most chemotherapeutic drugs, is highly toxic and detrimental to healthy viable tissue in the body. Thus, urgent treatment modification is required to attenuate doxorubicin toxicity in normal cells.

The results obtained from the MTT assay, clearly demonstrated that the combined treatment of starvation and doxorubicin protected normal MCF12A breast epithelial cells against doxorubicin-induced cytotoxicity. Furthermore, it also sensitized MDAMB231 to doxorubicin-induced cell death (Figure 3.2.1 A & Figure 3.2.2 A and B). These results confirm the findings of other studies which demonstrated that low-serum media protected normal glial cells but not glioma and neuroblastoma cancer cell lines against the toxicity of the chemotherapeutic drug, cyclophosphamide (Raffaghello *et al.*, 2008).

In addition, it was also reported that patients who starved 48 - 140 hours pre-chemotherapy and 5 - 56 hours post-chemotherapy experienced reduced toxic side-effects (Raffaghello *et al.*, 2010). Some of these side-effects included decreased headache, nausea, vomiting, abdominal cramps, hair loss and short-term memory loss. It is known that cancer cells have a high metabolic demand that allows them to sustain high proliferation rates. Thus, this concept of using starvation as a method of sensitization aims to further exploit this fact, leaving cancer cells more vulnerable to the cytotoxic effects of chemotherapy.

Images obtained during live cell imaging, revealed distinct observable morphological changes which occurred as cancer cells progressed through apoptosis. The highest degree of cell death occurred in the group subjected to starvation and doxorubicin treatment of 24 hours, in which distinct nuclear fragmentation and nuclear condensation was clearly observed (Figure 3.4.2)

confirming the results discussed above and further substantiating that short-term starvation sensitizes cancer cells to doxorubicin- induced cell death.

4.2.3 The effect of short-term starvation and doxorubicin treatment on autophagic activity

Our results demonstrated high basal autophagic activity under control conditions (Figure 3.3.1 A). The MDAMB231 cells utilised in our study is an aggressive cancer cell line which possesses *ras*-mutations. Our results is thus in agreement with the finding that activated *Ras* promotes tumourigenesis but also up-regulates basal autophagy which is essential for maintaining mitochondrial metabolism, cellular viability and cell growth both *in vitro* and *in vivo* (Guo *et al*., 2011).

Interestingly, doxorubicin only and starvation only significantly decreased this high basal level of autophagy when compared to the control group. Furthermore, the combination group of doxorubicin plus starvation further attenuated the autophagic response when compared to the doxorubicin group. These results are confirmed with a significant increase in accumulation of p62 which was observed in the combined group compared with the doxorubicin only group (Figure 3.3.1 B). This was also associated with an increase in apoptosis in our results. Our results confirmed those by Qadir and co-workers (2008) who have demonstrated that siRNA of Beclin-1, ATG5 and ATG7 (genes associated with autophagy) which attenuates the autophagic response by causing defects in autophagic degradation, resulted in increased apoptosis when cells were exposed to the

chemotherapeutical drug, tamoxifen. Tiwari and co-workers (2008) have also shown that the silencing of ATG proteins sensitized cancer cells to radio- and chemotherapy.

On the other hand, it is well known that autophagy plays a critical role in maintaining cellular homeostasis during cellular stresses such as chemotherapy and nutrient or growth factor depletion, and thus represents a pro-survival pathway (Denis and Codogno, 2003; Pouyssegur *et al*., 2006). This fact is supported by studies which showed that chemotherapy agents such as doxorubicin induced an increased autophagic response in cancer cells (Lambert *et al.*, 2008; Manov *et al.*, 2011). Additionally, studies which deprived cancer cells of amino acids or glucose reported elevated levels of autophagy (Liang *et al*., 1999; DiPaola *et al*., 2008). A more recent study revealed that *ras*-mutated cancer cells subjected to total nutrient deprivation for 3 hours displayed elevated levels of autophagy (Guo *et al*., 2011). These conflicting results may be due to different cell models, different chemotherapeutic agents and concentrations utilized as well as duration of treatment regimes employed. Additionally, it has been previously demonstrated in our group that during amino acid starvation, autophagy displays a bi-phasic response (Thomas, PhD thesis, 2012) (Available: http://scholar.sun.ac.za/mark peter thomas). This observation indicates that autophagic activity fluctuates between time points thus, in order to characterise the role of autophagy in this study, it is imperative to assess autophagic activity at various time points. Furthermore, this observation possibly suggests that the initial peak in autophagic

activity in these cells is used as a survival mechanism during nutrient deprivation, whereas the second peak may potentially be detrimental to cancer cells since autophagy is often associated with other forms of cell death such as apoptosis (Kobayashi et al., 2010). Since, dying cells are observed to contain autophagosomes, it is unclear whether autophagy promotes cell death or is up-regulated in an effort to prevent cell death (Gozuacik and Komchi, 2007).The role of autophagy in tumourigenesis therefore remains to be clearly elucidated, as some studies indicate that autophagy plays a role in tumour progression and others confirm that it contributes to cell death.

4.2.4 The effect of short-term starvation and doxorubicin treatment on p-AMPK (oxygen sensor) and p-mTOR (energy sensor)

The results obtained from western blot analysis performed on MDAMB231 cells showed a significant increase in p-AMPK in response to 3 hours of starvation as expected, as it is well known that this kinase is activated in response to a low AMP/ATP ratio due to cellular stresses such as starvation (Figure 3.8.1 A). The activation of p-AMPK coincided with a significant decrease of p-mTOR (Figure 3.8.1 B). Interestingly, this elevated p-AMPK and attenuated p-mTOR levels in the starvation group were not associated with increased autophagy or apoptotic cell death. As such a response usually corresponds with an up-regulation of autophagy, our results contradict this fact as autophagy significantly decreased in response to starvation. It might be that if the starvation period was extended, that increased autophagy would have been observed in our model. These results

confirm the fact that cancer cells possess the innate ability to evade the earliest forms of cell death by adapting to declining ATP levels through the activation of AMPK (Buzzai *et al*., 2005) which reduces mTOR activity thus resulting in a decrease in protein synthesis.

Various cancers, including human breast cancers possess a mutation in the tumour suppressor phosphatase and tensin homologue deleted from chromosome 10 (PTEN) (Meric-Bernstam and Gonzalez-Angulo, 2009). A subsequent loss of PTEN was shown to lead to a constitutive activation of mTOR following doxorubicin treatment in prostate cancer cells conferring resistance to doxorubicin-induced cell death (Grunwald et al., 2002). However, doxorubicin treatment only in our study showed no significant changes in p-mTOR expression. However, starvation with doxorubicin treatment induced a significant decrease in p-mTOR which was unexpected, since it is generally believed that inhibition of mTOR is associated with an increase in autophagy which was not observed in our results. The attenuation of mTOR in the combination treatment group in our experimental model might thus be associated with an inhibition of protein synthesis which could subsequently reduce growth and cellular proliferation of cancer cells (Figure 3.8.1 B).

4.3 *In vivo* study

4.3.1 The effect of short-term starvation on doxorubicin-induced cell death and autophagy, p-AMPK (oxygen sensor) and p-mTOR (energy sensor) in tumour bearing mice.

Although no significant changes were observed in tumour volumes between the various treated groups (Figure 3.5.1) for reasons indicated before, significant changes were obtained on a molecular level. In contrast to the results obtained from the *in vitro* experiment, in which short-term starvation sensitized breast cancer cells to doxorubicin-induced cell death, the *in vivo* analysis revealed a significant decrease in cell death in the combination group (starvation and doxorubicin treatment) in comparison to mice which were treated with doxorubicin only. Although the combination treatment did induce a significant increase in apoptosis compared to the control group, it was significantly lower when compared to the doxorubicin only group. Raffaghello and co-workers (2008), on the other hand, did observe a decrease in tumour volume and an increase in apoptosis in a study in when mice were starved for 48 hours prior to chemotherapeutic treatment with etoposide (Raffaghello *et al.*, 2008). These conflicting results might be due to different chemotherapeutic agents and differences in the periods of starvation.

Contrary to the *in vitro* results, doxorubicin caused a significant increase in p-AMPK and a decrease in p-mTOR activation with a subsequent increase in

autophagy which was confirmed by the elevated LC3 II levels and attenuated p62 levels in our model. These results are confirmed by others who reported the same cellular mechanism via which autophagic activity is upregulated in the treatment group (Singh and Cuervo, 2011).

Interestingly, the starvation group and the combination group showed a significant increase in p-mTOR. This might be indicative of increased protein synthesis to counteract the effect of starvation in this model. This may further indicate that mechanisms other than autophagy were up-regulated to provide nutrients. Such mechanisms in an *in vivo* setting may involve interplay of hormones which affect molecular responses such as the body's innate response to up-regulate both gluconeogenesis and glycogenolysis to provide substrates for energy during 24 hours of starvation, hence compensating for this bioenergetics compromise. Thus, for future *in vivo* studies more time points should be considered as a part of preliminary experimentation.

Additionally, since tumours are heterogeneous masses composed of metastatic cells and stromal cells which are both vital for the proliferation and survival of malignancies, protection of tumourigenic or non-tumourigenic cells during chemotherapy or starvation could directly confer a survival advantage onto treated cancers. Hence, it would be important to identify the various cell types which comprise biological tumours before experimental procedures are conducted and then to take into consideration how these cell types may affect the response of

cancer cells to treatment in an experimental setting. Future studies that employ *in-vivo* whole animal imaging techniques as well as cell sorting will contribute to address these challenges.

Chapter 5 – Final Conclusions

The remarkable success of the few cell culture and animal models as well as from a recent clinical trial which exploits the concept of starvation has gained much attention and shows great promise. However, if short-term starvation could prove to be safer and reproducible, then this form of differential therapy would be much easily translated into a clinical setting to improve the quality of life and perhaps even reduce or prevent some of the detrimental side-effects of patients receiving conventional chemotherapy.

In the *in vitro* model of our study, we have established that short-term starvation has the potential to sensitize breast cancer cells to doxorubicin-induced cell death. Additionally, it appears that this therapy combination aids in protecting breast epithelial cells against the toxic effects of doxorubicin. However, translation of these results in our in *vivo* study is worth further exploration by examining these effects under various time-points in order to achieve this desired effect. Conclusively, short-term starvation during chemotherapy is a realistic avenue for adjuvant therapy but there is a need for further investigation.

No studies to date have investigated autophagy in the context of short-term starvation therapy during anticancer treatment regimens. Cancer cells are known to innately up-regulate autophagy to meet their metabolic demands. This was confirmed in the MDAMB231 cell line utilised in our study which demonstrated high basal autophagic activity. Although starvation induced a rapid increase in p-AMPK

levels and the subsequent inhibition of p-mTOR, no changes in autophagy was observed. These results confirm the fact that cancer cells possess the innate ability to evade the earliest forms of cell death by adapting to declining ATP levels through the activation of p-AMPK. What was interesting and probably of clinical value, is the fact that cell death increased and autophagy decreased when cells were starved and treated with DXR. Since, autophagy is associated with chemo-resistance and there is an urgent demand for autophagic inhibitors which can be utilized clinically; short-term starvation with chemotherapy may serve as a safe and novel approach to inhibit autophagy for future therapeutic benefits. However, to identify the precise role that autophagy is playing in this study, autophagic inhibitors and inducers as well as additional time points should be utilized as it has been previously demonstrated in our group that autophagy during amino acid starvation demonstrated a bi-phasic response (Thomas, PhD thesis, 2012).

As the interest in modification of autophagy for therapeutic benefit ensues and novel strategies such as starvation during high-dose chemotherapy are explored, it is crucial that future studies undertaken are aimed at developing methods to determine how various cancers respond to autophagy during treatment and if increases in autophagy confers a survival advantage. Furthermore, it is imperative to identify the underlying mechanisms influencing the beneficial effects of short-term starvation, prior to being translated into a clinical setting.

Chapter 6 - Limitations and Future directions

One of the major challenges faced by biological scientists is the inability to directly translate *in vitro* protocols to an *in vivo* setting. This is greatly attributed to the fact that most *in vitro* work is done on monolayer cell culture models. This is an imprecise representation of biological tumours which are three-dimensional in nature and highly heterogeneous containing not only tumourigenic cells but a network of non-tumourigenic cell types as well. A step towards ameliorating this concern would be to introduce the growth of 3-dimensional spheroid cultures *in vitro*, thereby providing a more relevant representation of tumour structure and functional dynamics.

In the context of inducing starvation in an *in vivo* model, it is imperative to consider the innate responses of a physiological system in maintaining homeostasis during periods of starvation. Such a response would be to up-regulate gluconeogenesis and glycogenolysis to provide substrates for energy production which could affect the results of *in vivo* experimentation. Additionally, since cancer cells form a dynamic relationship with the tumour microenvironment, other factors such as hypoxia, changes in hormonal levels and genetic alterations may influence the response to starvation further. These parameters are controlled in an *in vitro* setting but are challenging to control in an *in vivo* model thus contributing to the complexity of extrapolating molecular relationships.

Another significant issue in oncology is tumour heterogeneity. Since tumors are masses composed of metastatic cells and stromal cells which are both vital for the proliferation and survival of malignant cells, protection of tumourigenic or non-tumourigenic cells during chemotherapy or starvation could directly confer a survival advantage onto treated cancers.

In the context of clinical trials, oncologist would have to extensively examine patients before introducing starvation into their chemotherapeutic regimen thus, varying among patients depending on the extent of tumour progression and their individual health status. This may be limiting, as such a protocol may not be suitable for all cancer patients.

Breast cancer represents a multitude of different diseases with intra-tumoural and inter-tumoural genetic and epigenetic alterations. In the future, it will be paramount to understand how these defects originate during disease progression and to identify the key mechanisms underlying chemotherapy resistance before being exploited clinically, for therapeutic benefit. As we realize the complexity resulting from the plethora of factors which manifests this multifaceted disease, conducting clinical trials to assess novel agents in combination with chemotherapy and other modalities such as dietary modification is becoming an increasingly important trend.

Since this study focused primarily on mechanisms induced by cancer cells in response to short-term starvation, the same experiments should be performed on the MCF12A breast epithelial cell line to further complement our study. Additionally, to elucidate the exact role played by autophagy in this scenario, autophagic inhibitors

and inducers should be utilised as well as additional time points in both *in vitro* and *in vivo* should be considered as autophagy is known to display a rhythmic response to starvation.

Despite the molecular mechanisms of autophagy identified in an *in vitro* setting, there continues to be a lack of physiological relevant *in vivo* information on the role of autophagy in neoplastic disease progression. By employing the use of green fluorescent protein-LC3 expressing transgenic mice, we can further investigate and characterise the *in vivo* effects of starvation and chemotherapy on the stimulation and control of autophagy in a variety of tissues.

As cancer is being increasingly characterised as a metabolic disease, an interesting approach to this study would be to further characterise the metabolic profiles of both MCF12A cells and MDAMB231 cells in response to short-term starvation. Thus, amino acids, fatty acids, glucose and ATP should be analysed. Since, cancer cells have high glycolytic activity; it would be of value to distinguish between the different molecular mechanisms involved when a cancer cell is starved as opposed to a non-starved cancer cell. This would aid in a comprehensive understanding of how cancer cells respond to starvation and may also reveal a selection of biomarkers which may be manipulated for therapeutical benefit.

Investigating mitochondrial fate during starvation would be an exciting avenue worth exploring. Changes in mitochondrial mass and morphology as well as characterising the role of mitochondria during autophagy can be further analysed. Future research may also determine if other organelles such as the endoplasmic reticulum and

peroxisomes are also affected in their shape or activity during autophagy under a nutrient deprived scenario.

Chapter 7 – References

Abdulkadir IR, Lizhi Lu, Dwain I, Black KL and Yu JS. A therapeutic dose of doxorubicin activates ubiquitin-proteasome system-mediated proteolysis by acting on both the ubiquitination apparatus and proteasome. *Am J Physiol Heart Circ Physiol* 295(6): H2541–H2550, 2008.

Amaravadi RK, Lippincott-Schwartz J, Yin X-M, Weiss W-A, Takebe N, Timmer W, DiPaola RS, Lotze MT and White E. Principles and current strategies for targeting autophagy for cancer treatment. *Clin Cancer Res* 17(4): 654-666, 2011.

Amaravadi RV and Thompson CB. The roles of therapy-induced autophagy and necrosis in cancer treatment. *Clin Cancer Res* 13: 7271-7279, 2007.

Ameisen JC. On the origin, evolution, and nature of programmed cell. *Cell Death Differ* 9(2): 367-393, 2002.

Arola OJ, Saraste A, Pulkki K, Kallajoki M, Parvinen M and Voipio-Pulkki L-M. Acute Doxorubicin Cardiotoxicity Involves Cardiomyocyte Apoptosis Cancer Res 60: 1789–1792, 2000.

Basak GW and Carrier E. The search for multiple myeloma stem cells: the long and winding road. *Biol Blood Marrow Transplant.* 16(5): 587-594, 2009.

Basak GW, Srivastava AS, Malhotra R and Carrier E. Multiple myeloma bone marrow niche. *Curr Pharm Biotechnol* 3: 345-346, 2009.

Bateman C. Breast Cancer breakthrough in gene profiling. *SAMJ* 99: 11: 780-782, 2009.

Bennasroune A, Gardin A, Aunis D, Crémel G and Hubert P. Tyrosine kinase receptors as attractive targets of cancer therapy. *Crit Rev Oncol Hematol* 50: 23-28, 2004.

Bjorkoy G, Lamark T, Brech A, Outzen H, Perander M, Overvatn A, Stenmark H and Johansen T. p62/SQSTM1 forms protein aggregates degraded by autophagy and has a protective effect on huntingtin-induced cell death. *J Cell Biol* 171: 603-614, 2005.

Blasco MA. Telomeres and human disease: ageing, cancer and beyond. *Nat Rev Genet* 6: 611-622, 2005.

Bradford MM. A rapid and sensitive method for quantitation of microgram quantities of protein utilizing the principle of protein-dye binding. *Annals of Biochemistry*. 71: 248-254, 1976.

Budihardjo I , Oliver H , Lutter M , Luo X and Wang, X. Biochemical pathways of caspase activation during apoptosis. *Annual review of cell and developmental biology*, 15 :1 :269-290, 1999.

Buzzai M, Bauer DE, DeBerardinis JRG, Hatzivassiliou RJ, Elstrom GRL and Thompson CB. The glucose dependence of Akt-transformed cells can be reversed by pharmacologic activation of fatty acid β-oxidation. *Oncogene* 24(26): 4165-4173, 2005.

Camello-Almaraz MC, Pozo MJ, Murphy MP and Camello PJ. Mitochondrial production of oxidants is necessary for physiological calcium oscillations. *J Cell Physiol 206*: 2: 487-494, 2005.

Carew JS, Nawrocki ST and Cleveland JL Modulating Autophagy for Therapeutic Benefit. *Autophagy* 3(5): 464-467, 2007.

Castells M, Thibault B, Delord JP and Couderc B. Implication of tumor microenvironment in chemoresistance: tumor-associated stromal cells protect tumor cells from cell death. *Int J Mol Sci* 13(8): 9545-9571, 2012.

Cavallaro U and Christofori G. Cell adhesion and signalling by cadherins and Ig-CAMs in cancer. *Nature Reviews Cancer* 4: 118-132, 2004.

Chang A. Chemotherapy, chemoresistance and the changing treatment landscape for NSCLC. Lung Cancer 71: 3-10, 2011.

Colditz GA and Rosner BA. Cumulative risk of Breast cancer to Age 70 years according to risk factor status: Data from the Nurses Health study. *AMJ Epidemiol* 10: 950-964, 2000.

Coleman RE and Holen ING. Chemotherapy for breast cancer. *Mol Cancer Ther* 8(1): 2821–2832, 2009.

Dang CV and Semenza GL. Oncogenic alterations of metabolism. *Trends Biochem Sci.* 24(2): 68-72, 1999.

Denis E and Codogno P. Autophagy: a barrier or an adaptive response to cancer. *Biochim Biophys Acta* 1603: 113-128, 2003.

DiPaola RS, Dvorzhinski D, Thalasila A, Garikapaty V, Doram D, May M, Bray K, Mathews R, Beaudoin B, Karp C, Stein M, Foran DJ and White E. Therapeutic starvation and autophagy in prostate cancer: a new paradigm for targeting metabolism in cancer therapy. *The Prostate* 68(16): 1743-1752, 2008.

Doroshow JH, Locker GY and Meyers CE. Enzymatic defences of the mouse heart against reactive oxygen metabolites. *J Clin Invest* 65:128-135, 1980.

Elmore S. Apoptosis: A Review of Programmed Cell Death. *Toxicol Pathol* 35: 495, 2007.

Eom YW, Mi AK, Seok SP, Goo MJ, Kwon HJ, Sohn S, Kim W-H, Yoon G, and Choi KS. Two distinct modes of cell death induced by doxorubicin: apoptosis and cell death through mitotic catastrophe accompanied by senescence-like phenotype. *Oncogene* 24(30): 4765-4777, 2005.

Evan GI and Vousden KH. Proliferation, cell cycle and apoptosis in cancer. *Nature* 411: 342-348, 2001.

Ewens A, Luo L, Berleth E, Alderfer J, Wollman R, Hafeez BB, Kanter P, Mihich E and Ehrke MJ. Doxorubicin plus interleukin-2 chemoimmunotherapy against breast cancer in mice. *Cancer Res 66*: 10: 5419-5426, 2006.

Fang M, Shen Z, Huang S, Zhao L, Chen S, Mak TW and Wang X. The ER UDPase ENTPD5 promotes protein N-glycosylation, the Warburg effect, and proliferation in the PTEN pathway. *Cell* 143: 711-724, 2010.

Favoni RE and de Cupisa A. The role of polypeptide growth factors in human carcinomas: New targets for a novel pharmacological approach. *Pharmacol Rev* 52: 2: 179-206, 2000.

Ferrara N. Pathways mediating VEGF-independent tumor angiogenesis. *Cytokine Growth Factor Rev* 21: 21-26, 2010.

Fontana L, Partridge L and Longo VD. Extending healthy life span-from yeast to humans. *Science 328*: 5976: 321-326, 2010.

Frederick CA, Williams LD, Ughetto G, van der Marel GA, van Boom JH, Rich A and Wang AH. Structural comparison of anticancer drug-DNA complexes: adriamycin and daunomycin. *J Biochem* 29: 2538-2549, 1990.

Fulda S and Debatin KM. Extrinsic versus intrinsic apoptosis pathways in anticancer chemotherapy. *Oncogene* 25: 4798-4811, 2006.

Gewirtz DA. A critical evaluation of the mechanisms of action proposed for the antitumor effects of the anthracycline antibiotics adriamycin and daunorubicin. *Biochem Pharmacol* 57: 727-74, 1999.

GLOBOCAN 2008, International Agency for Research on Cancer

Gozuacik D and Komchi A. Autophagy and cell death. *Curr Top Dev Biol.* 78: 217-245, 2007.

Grünwald V, DeGraffenried L, Russel D, Friedrichs WE, Ray RB and Hidalgo M. Inhibitors of mTOR reverse doxorubicin resistance conferred by PTEN status in prostate cancer cells. *Cancer Res* 62(21): 6141-6145, 2002.

Grütter MG. Caspases: key players in programmed cell death. *Curr Opin Struct Biol* 10(6): 649-655, 2000.

Guertin DA and Sabatini DM. Defining the role of mTOR in cancer. *Cancer Cell* 12: 9-22, 2007.

Guo YJ, Chen H-Y, Mathew R, Fan J, Strohecker AM, Karsli-Uzunbas G, Kamphorst JJ, Chen G, Lemons JMS, Karantza V, Coller HA, DiPaola RS, Gelinas CS, Rabinowitz JD and White E. Activated Ras requires autophagy to maintain oxidative metabolism and tumorigenesis *Genes Dev.* 25: 460-470, 2011.

Hanahan D and Weinberg RA. Hallmarks of Cancer: The Next Generation. death: a timeline of four billion years. *Cell Death Differ* 9: 367-393, 2002.

Hanahan D and Weinberg RA. Hallmarks of cancer: the next generation. *Cell* 144: 5: 646-74, 2011.

Hassan MSU, Ansari J, Spooner, Hussain SA, Ottewell PD, Woodward JK, Lefley and Evans CA. Anticancer mechanisms of doxorubicin and zoledronic acid in breast cancer tumor growth in bone. *Oncol Rep* 24: 1121-1131, 2010.

Hellerstein MK, Neese RA, Linfoot P, Christiansen M, Turner S and Letscher A. Hepatic Gluconeogenic Fluxes and Glycogen Turnover during Fasting in Humans-A Stable Isotope Study. *J Clin Invest* 100(5): 1305-1319, 1997.

Hershman Dawn L., et al. Doxorubicin, cardiac risk factors, and cardiac toxicity in elderly patients with diffuse B-cell non-Hodgkin's lymphoma. *J Clin Oncol* 26(19): 3159-3165, 2008.

Izuishi K, Kato K, Ogura T, Kinoshita T, Esumi H. Remarkable tolerance of tumor cells to nutrient deprivation: possible new biochemical target for cancer therapy. *Cancer Res* 60(21): 6201-6207, 2000.

Jain D. Cardiotoxicity of doxorubicin and other anthracycline derivatives. *J Nucl Cardiol* 7(1): 53-62, 2000.

Jehle R, Schlame M, Büttner C, Frey B, Sinha P and Rüstow B. Platelet-activating factor (PAF)-acetylhydrolase and PAF-like compounds in the lung: Effects of hyperoxia. *BBA-Mol Cell Biol Lipids*, *1532*: 1 60-66, 2001.

Jin S and White Eileen. Role of Autophagy in Cancer: Management of Metabolic Stress.*Autophagy* 3: 1: 28-31, 2007.

Jung CH, Ro SH, Cao J, Otto NM and Kim DH: mTOR regulation of autophagy. *FEBS Lett* 584:1287-1295, 2010.

Junttila MR and Evan GI. p53 - a Jack of all trades but master of none. *Nat Rev Cancer* 9: 821-829, 2009.

Kanamori H, Takemura G, Maruyama R, Goto K, Tsujimoto A, Ogino A, Li L, Kawamura I, Takeyama T, Kawaguchi T, Nagashima K, Fujiwara T, Fujiwara H, Seishima M and Minatoguchi S. Functional Significance and Morphological Characterization of Starvation-Induced Autophagy in the Adult Heart. *Am J Pathol* 174: 5: 1705–1714, 2009.

Kanzawa T, Germano IM, Komata T, Ito H, Kondo Y, Kondo S. Role of autophagy in temozolomide-induced cytotoxicity for malignant glioma cells. *Cell Death Differ*. 4: 448-57, 2004.

Kerr JFR, Winterford CM and Harmon BV. Apoptosis: Its Significance in Cancer and Cancer Therapy. Cancer 73: 8, 1994.

Kerr JF, Wyllie AH, Currie AR. Apoptosis: a basic biological phenomenon with wide-ranging implications in tissue kinetics. *Br J Cancer* 26: 239-257, 1972.

Kim J, Kundu M, Viollet B and Guan KL. AMPK and mTOR regulate autophagy through direct phosphorylation of Ulk1. *Nat Cel Biol* 13:2, 2011.

Kobayashi S, Volden P, Timm D, Mao K, Xu X and Liang Q. Transcription factor GATA4 inhibits doxorubicin-induced autophagy. *J Biol Chem* 285: 793-804, 2010.

Komatsu M, Waguri S, Ueno T, Iwata J, Murata S, Tanida I, Ezaki J, Mizushima N, Ohsumi Y, Uchiyama Y, Kominami E, Tanaka K and Chiba T. Impairment of starvation-induced and constitutive autophagy in Atg7-deficient mice. *J Cell Biol* 169: 425-434, 2005.

Kroemer G. Mitochondrial control of apoptosis: An introduction. *Biochem Biophys Res Commun* 304: 433-435, 2003.

Kuma A, Hatano M, Matsui M, Yamamoto A, Nakaya H, Yoshimori T, Ohsumi Y, Tokuhisa T and Mizushima N. The role of autophagy during the early neonatal starvation period*. Nature* 432: 1032-1036, 2004.

Kurosaka K, Takahashi M, Watanabe N and Kobayashi Y. Silent cleanup of very early apoptotic cells by macrophages. *J Immunol* 171: 4672-4679, 2003.

Lambert LA, Qiao N, Hunt KK, Lambert DH, Mills GB, Meijer L and Keyomarsi K. Autophagy: a novel mechanism of synergistic cytotoxicity between doxorubicin and roscovitine in a sarcoma model. *Cancer Res.* 68: 19: 7966-7974, 2008.

Lamkanfi M and Dixit VM. Inflammasomes and their roles in health and disease *Annu Rev Cell Dev Biol* 28:137-161, 2010.

Lee C, Safdie FM, Raffaghello L, Wei M, Madia F, Parrella E, Hwang D, Cohen P, Bianchi G and Longo VD. Reduced levels of IGF-I mediate differential protection of normal and cancer

cells in response to fasting and improve chemotherapeutic index. *Cancer Res* 70: 4: 1564-1572, 2010.

Lee S, Baek M, Kim H-Y, Ha J-H, Jeoung D-II, Muller M, Wilder S, Bannasch D, Israeli D, Lehlbach K, Li-Weber M, Friedman SL, Galle PR, Stremmel W, Oren M, Krammer PH p53 activates the CD95 gene in response to DNA damage by anticancer drugs. *J. Exp. Med*. 188: 2033–2045, 1988.

Lee S, Baek M, Kim H-Y, Ha J-H and Jeoung D-IL. Mechanism of doxorubicin-induced cell death and expression profile analysis*. Biotech. Letters* 24: 1147-1151, 2002.

Lemmon MA and Schlessinger J. Cell signaling by receptor tyrosine kinases*. Cell* 141: 1117-1134, 2010.

Liang XH, Jackson S, Seaman M, Brown K, Kempkes B, Hibshoosh H and Levine B. Induction of autophagy and inhibition of tumourigenesis by beclin-1. *Nature* 6762: 672-676, 1999.

Lipshultz SE, Colan SD, Gelber RD et al. Late cardiac effects of doxorubicin therapy for acute lymphoblastic leukemia in childhood. *N Engl J Med* 324: 808-815, 1991.

Lipshultz SE, Stuart RL, Mone SM, Goorin AM, Sallan SE, Sanders SP, Orav JE, Gelber R and Colan SD. Female sex and higher drug dose as risk factors for late cardiotoxic effects of doxorubicin therapy for childhood cancer. *New England Journal of Medicine* 332: 26: 1738-1744, 1995.

Lis R, Touboul C, Mirshahi P, Ali F, Mathew S, *et al.* Tumor associated mesenchymal stem cells protects ovarian cancer cells from hyperthermia through CXCL12. *Int J Cancer* 128: 715–725, 2011.

Lis R, Touboul C, Raynaud CM, Malek JA, Suhre K, et al. Mesenchymal Cell Interaction with Ovarian Cancer Cells Triggers Pro-Metastatic Properties. *PLoS ONE* 7(5): e38340, 2012.

Liu G, Yuan X, Zeng Z, Tunici P, NG Hiushan, Abdukkadir IR, Lu L, Hiushan NG. Analysis of gene expression and chemoresistance of CD133+ cancer stem cells in glioblastoma. Mol Cancer 5: 67, 2006.

Liu L, Zhang J, Su X and Mason RP. In vitro and In vivo Assessment of CdTe and CdHgTe Toxicity and Clearance. *J Biomed Nanotechnol.* 4: 4: 524-528, 2008.

Lord RV, Brabender J, Gandara D, Alberola V, Camps C, Domine M, Cardenal F, Sanchez JM, Gumerlock PH, Taron M, Sanchez JJ, Danenburg KD, Danenbeg PV and Rosell, R. Low ERCC1 expression correlates with prolonged survival after cisplatin plus gemcitabine chemotherapy in non-small cell lung cancer. *Clin Cancer Res* 8(7)*:* 2286-2291, 2002.

Lorenzo E, Ruiz-ruiz C; Quesada A; Hernandez G; Rodriguez A; Lopez-rivas and Redondo J. Doxorubicin induces apoptosis and CD95 gene expression in human primary endothelial cells through a p53-dependent mechanism. *J Biol Chem* 277*:* 10883-10892, 2002.

Loos B, Lochner A and Engelbrecht A-M. Autophagy in heart disease: A strong hypothesis for an untouched metabolic reserve. *Med hypothesis*, 2011: Jul77 (1): 52-57. [1.150]

Luanpitpong S, Chanvorachote P, Nimmannit U, Leonard SS, Stehlik C, Wang L and Rojanasakul Y. Mitochondrial superoxide mediates doxorubicin-induced keratinocyte apoptosis through oxidative modification of ERK and Bcl-2 ubiquitination. *Biochem Pharm* 83: 1643–1654, 2012.

Lum JJ, DeBerardinis RJ and Thompson CB. Autophagy in metazoans: cell survival in the land of plenty. *Nat Rev Mol Cell Biol* 6:439-448, 2005.

Ma X-J, Salunga R, Tuggle JT, Gaudet J, Enright E, McQuary P, Payette T, Pistone M, Stecker K, Zhang BM, Zhou Y-X, Varnholt H, Smith B, Gadd M, Chatfield E, Kessler J, Baer TM, Erlander MG and Sgroi DC. Gene expression profiles of human breast cancer progression. *PNAS* 100(10): 5974-5979, 2003.

Madhusudan S and Middleton MR. The emerging role of DNA repair proteins as predictive, prognostic and therapeutic targets in cancer. *Cancer Treat Rev 31*(8), 603-617, 2005.

Manov I, Pollak Y, Broneshter R and Iancu TC. Inhibition of doxorubicin-induced autophagy in hepatocellular carcinoma Hep3B cells by sorafenib-the role of extracellular signal-regulated kinase counteraction. *FEBS J 278*: 18: 3494-3507, 2011.

Mathew R, Karp CM, Beaudoin B, Vuong N, Chen G, Chen HY, Bray K, Reddy A, Bhanot G, Gelinas C, Dipaola RS, Karantza-Wadsworth V and White E. Autophagy suppresses tumorigenesis through elimination of p62. *Cell* 137: 1062-1075, 2009.

Mathew R, Karantza-Wadsworth V and White E. Assessing metabolic stress and autophagy status in epithelial tumors. *Methods Enzymol* 453: 53-81, 2009.

Mathew R and White E. Autophagy in tumorigenesis and energy metabolism: friend by day, foe by night. *Curr Opin Genetics Dev* 21: 1: 113-119, 2011.

Meads M.B., Gatenby R.A and Dalton W.S. Environment-mediated drug resistance: A major contributor to minimal residual disease. *Nat. Rev. Cancer* 9: 665–674, 2009.

Meads MB, Gatenby RA and Dalton WS. Environment-mediated drug resistance: a major contributor to minimal residual disease. *Nat Rev Cancer* 9(9): 665-674, 2009.

Meijer AJ and Codogno P. Regulation and the role of autophagy in mammalian cells. *Int J Biochem Cell Biol 12*: 2445-2456, 2004.

Meléndez A and Levine B. Autophagy in *C. elegans*. Wormbook.1.147.1, 2009.

Mellor HR and Callaghan R. Resistance to chemotherapy in cancer: A Complex and integrated cellular response. *Pharmacol* 81: 275-300, 2008.

Meric-Bernstam F and Gonzalez-Angulo AM. Targeting the mTOR signaling network for cancer therapy. *J Clin Oncol 27*: 13: 2278-2287, 2009.

Michels KB and Ekbom A. Caloric restriction and incidence of breast cancer. *JAMA* 291(10): 1226-1230, 2004.

Mizushima N, Yamamoto A, Matsui M, Yoshimori T and Ohsumi Y. In vivo analysis of autophagy in response to nutrient starvation using transgenic mice expressing a fluorescent autophagosome marker. *Mol Biol Cell* 15:3: 1101-1111, 2004.

Mizushima N and Yoshimori T. How to Interpret LC3 Immunoblotting. *Autophagy* 3:6, 542-545, 2007.

Muller I, Niethammer D and Bruchelt G. Anthracycline-derived chemotherapeutics in apoptosis and free radical cytotoxicity. *Int J Mol Med* 491-494, 1998.

Nakamura T, Ueda Y, Juan Y, Katsuda S, Takahashi H and Koh, E. Fas-mediated apoptosis in adriamycin-induced cardiomyopathy in rats: In vivo study. *Circulation* 102 : 572-578, 2000.

Neilan TG, Blake SL, Ichinose F et al. Disruption of nitric oxide synthase 3 protects against the cardiac injury, dysfunction, and mortality induced by doxorubicin. *Circulation* 116: 506-514, 2007.

Octavia Y, Tocchetti CG, Gabrielson KL, Janssens S, Crijns HJ and L Moens. Doxorubicin-induced cardiomyopathy: From molecular mechanisms to therapeutic strategies. *J Mol Cell Cardiol* 52: 6: 1213-1225, 2012.

Olive KP, Jacobetz MA, Davidson CJ, Gopinathan A, McIntyre D, Honess D, Madhu B, Goldgraben MA, Caldwell ME and Allard D. Inhibition of Hedgehog signaling enhances delivery of chemotherapy in a mouse model of pancreatic cancer. *Science* 324: 457-1461, 2009.

Pacher P, Liaudet L, Bai P, Virag L, Mabley JG, Hask´O G and Szab´O C. Activation Of Poly(ADP-Ribose) Polymerase contributes to development of doxorubicin-induced heart failure. *J Pharmacol and Exp Therap* 300: 862-867, 2002.

Panaretakis T, Pokrovskaja K, Shoshan MC, and Grander D. Activation of Bak, Bax, and BH3-only proteins in the apoptotic response to doxorubicin. *J Biol Chem* 277: 44317-44326, 2002.

Pankiv S, Hoyvarde Clausen T, Lamerk T, Brech A, Bruun, J.A, Outzen H, Overvatn, A, Bjorkkoy G and Johansen T. p62/SQSTMI1 binds directly to Atg8/LC3 to facilitate degradation of ubiquitinated protein aggregates by autophagy. *J Biol Chem* 282: 24131-24145, 2007.

Papandreou I, Lim AL, Laderoute K, and Denko NC. Hypoxia signals autophagy in tumor cells via AMPK activity, independent of HIF-1, BNIP3, and BNIP3L. *Cell Death and Differ* 15: 1572-1581, 2008.

Petronelli A, Riccioni R, Pasquini L, Petrucci E and Testa U. Apoptosis-based therapies for hematological malignancies. *Drugs of the Future 30*: 7: 707-723, 2005.

Pouysségur J, Dayan F, and Mazure NM. Hypoxia signalling in cancer and approaches to enforce tumour regression. *Nature* 441: 437-443, 2006.

Qadir MA, Kwok B, Dragowska WH, To KH, Le D, Bally MB and Gorski SM. Macroautophagy inhibition sensitizes tamoxifen-resistant breast cancer cells and enhances mitochondrial depolarization. *Breast Cancer Res Treat* 112(3): 389-403, 2008.

Rabinowitz JD and White E. Autophagy and Metabolism. *Science* 330: 1344, 2010.

Raffaghello L, Lee C, Safdie FM, Wei M, Madia F, Bianchi G and Longo VD. Starvation-dependent differential stress resistance protects normal but not cancer cells against high-dose chemotherapy. *Proc Natl Acad Sci* 105 (2) 4: 8215-8220, 2008.

Nicholson KM and Anderson NG**.** The protein kinase B/Akt signalling pathway in human malignancy. *Cell Signal.*14:5:381-395, 2002.

Raffaghello L, Safdie F, Bianchi G, Dorff T, Fontana L and Longo VD. Fasting and differential chemotherapy protection in patients. *Cell Cycle* 9(22): 4474-4476, 2010.

Rafii A, Mirshahi P, Poupot M, Faussat AM, Simon A, Ducros E, Mery E, Couderc B., Lis R, Capdet J, *et al*. Oncologic trogocytosis of an original stromal cells induces chemoresistance of ovarian tumours. *PLoS. One* 12: e3894, 2012.

Richie JC and Swanson JO. Breast Cancer: A review of the literature. *J Insur Med* 35(2): 85-101, 2003.

Rodriguez S and Huynh-Do U. The role of PTEN in tumour angiogenesis. *J Oncol* 141:236, 2012.

Rosell R, Lord RV, Taron M and Reguart N. DNA repair and cisplatin resistance in non-small-cell lung cancer. *Lung Cancer* 38(3): 217-227, 2002.

Sachdeva UM and Thompson CB. Diurnal rhythms of autophagy: implications for cell biology and human disease. *Autophagy* 4: 5: 581-589, 2008.

Salvesen GS and Riedl SJ. Caspase mechanisms. *Adv Exp Med Biol.*: 615:13-23, 2008.

Savill J and Fadok V. Corpse clearance defines the meaning of cell death. *Nature* 407: 6805: 784-788, 2000.

Scherzed A, Hackenberg S, Froelich K, Kessler M, Koehler C, Hagen R, Radeloff A, Friehs G and Kleinsasser N. BMSC enhance the survival of paclitaxel treated squamous cell carcinoma cells in vitro. *Cancer Biol. Ther.* 3: 349-357, 2011.

Schimmel KJM, Richel DJ, van den Brink RBA and Guchelaar, H-J. Cardiotoxicity of cytotoxic drugs. *Cancer Treat. Rev.* 30: 181-191, 2008.

Schimmel KJ, Richel DJ, van den Brink RB and Guchelaar HJ. Cardiotoxicity of cytotoxic drugs. *Cancer Treat Rev.* 2:181-91, 2004.

Schnitt SJ. Traditional and newer pathological factors. *JNCI Monographs* 30: 22-26, 2001.

Shuch B, Riggs SB, LaRochelle JC, Kabbinavar FF, Avakian R, Pantuck AJ, Patard JJ and Belldegrun AS. *BJU Int.* 6: 692-696, 2008.

Simstein R, Burow M, Parker A, Weldon C and Beckman B. Apoptosis, chemoresistance, and breast cancer: insights from the MCF-7 cell model system. *Exp Biol Med* 228: 9: 995-1003, 2003.

Simstein R, Burow M, Parker A, Weldon C and Beckman B. Apoptosis, Chemoresistance, and Breast Cancer: Insights From the MCF-7 Cell Model System. *Exp Biol Med* 228: 995-1003, 2003.

Singal PK and Iliskovic N. Doxorubicin-Induced Cardiomyopathy. *N Engl J Med* 339: 900-905, 1998.

Singh R and Cuervo AM. Autophagy in the cellular energetic balance. *Cell Metab* 13: 5: 495-504, 2011.

Singletary K and Milner J. Diet, autophagy, and cancer: a review. *Cancer Epidemiology Biomarkers & Prevention* 17(7): 1596-1610, 2011.

Sjöström, J., Collan, J., Von Boguslawski K, Franssila K, Bengtsson NO, Mjaaland I and Blomqvist C. C-erbB-2 expression does not predict response to docetaxel or sequential methotrexate and 5-fluorouracil in advanced breast cancer. *European Journal of Cancer* 38: 4: 535-542, 2002.

Sun Q, Fan W and Zhong Q. Regulation of Beclin 1 in autophagy. *Autophagy* 5: 713-716, 2009.

Sutherland R.M, Eddy H.A, Bareham B, Reich K and Vanantwerp D. Resistance to adriamycin in multicellular spheroids. *Int J Radiat Oncol Biol Phys* 8: 1225-1230, 1979.

Sutherland RM. Tumor hypoxia and gene expression--implications for malignant progression and therapy. *Acta Oncol.* 37: 6: 567-74, 1998.

Suwei Wang, Eugene A. Konorev, Srigiridhar Kotamraju, Joy Joseph, Shasi Kalivendi, and B. Kalyanaraman Doxorubicin Induces Apoptosis in Normal and Tumor Cells via Distinctly Different Mechanisms. *J Biol Chem* 279: 24: 25535–25543, 2004.

Tanida I, Ueno T and Kominami E. Human light chain 3/MAP1LC3B is cleaved at its carboxyl-terminal Met121 to expose Gly 120 for lipidation and targeting to autophagosomal membranes. *J. Biol. Chem.* 36: 2503-2518, 2004.

Teng IW, Hou PC, Lee KD, Chu PY, Yeh KT, Jin VX, Tseng MJ, Tsai SJ, Chang YS, Wu CS, *et al.* Targeted methylation of two tumor suppressor genes is sufficient to transform mesenchymal stem cells into cancer stem/initiating cells. *Cancer Res* 13: 4653-4663, 2011.

Thomas MP. Differential tolerance of a cancer and a non-cancer cell line to amino acid deprivation: mechanistic insight and clinical potential. Unpublished doctoral dissertation, 2012. University of Stellenbosch. (Available: http://scholar.sun.ac.za/mark peter thomas).

Thorburn A. Death receptor-induced cell killing. *Cell Signal* 16:139-144, 2004.

Thornberry NA and Lazebnik Y. Caspases: enemies within. Science: 5381: 1312-1316, 1998.

Tiwari M, Bajpai VK, Sahasrabuddhe AA, Kumar A, Sinha RA, Behari S, Godbole MM. Inhibition of N-(4-hydroxyphenyl)retinamide-induced autophagy at a lower dose enhances cell death in malignant glioma cells. *Carcinogenesis* 29: 3: 600-609, 2008.

Tredan O, Galmarini CM, Patel K and Tannock IF. Drug resistance and the solid tumor microenvironment. *J. Natl. Cancer Inst 19*: 1441-1454, 2007.

Vadlamudi RK and Shin J. Genomic structure and promoter analysis of the p62 gene encoding a non-proteasomal multiubiquitin chain binding protein. *FEBS Lett* 435:138-142, 1998.

Vedam K, Nishijima Y, Druhan LJ, Khan M, Moldovan NI, Zweier JL and Ilangovan. Role of heat shock factor-1 activation in the doxorubicin-induced heart failure in mice. *AMJ of Physiology-Heart and Circulatory Physiology* 298(6): H1832-H1841, 2010.

Verheij M and Bartelink H. Radiation-induced apoptosis. *Cell Tissue Res* 310: 133-142, 2000.

Wallace KB. Doxorubicin-induced cardiac mitochondrionopathy. *Pharmacol Toxicol* 93:105-115, 2003.

Warburg O. On respiratory impairment in cancer cells. *Science* 124: 269-270, 1956b.

White E and DiPaola RS. The double-edged sword of autophagy modulation in cancer. *Clin Cancer Res* 15: 17: 5308-5316, 2009.

White E, Martin V, Liu J-L ,Klein SR, Piya S, Gomez-Manzano C, Fueyo J and Jiang Hong. Autophagy regulation in cancer development and therapy *Am J Cancer Res* 1: 3: 362-372, 2011.

Xu WS, Perez G, Ngo L, Gui CY, Marks PA. Induction of polyploidy by histone deacetylase inhibitor: a pathway for antitumor effects. *Cancer Res* 65: 7832–7839, 2005.

Yang HY, Wen YY, Chen CH, Lozano G and Lee MH. 14-3-3 sigma positively regulates p53 and suppresses tumor growth. *Mol Cell Biol* 20: 7096-107, 2003.

Yang L, Pang Y.and Moses HL. TGF-beta and immune cells: an important regulatory axis in the tumor microenvironment and progression. *Trends Immunol.* 31: 220-227, 2010.

Yang Z and Klionsky DJ. An overview of the molecular mechanism of autophagy. *Curr Top Microbiol Immunol* 335:1-32, 2009.

Yanxiang J, Guo, Chen H-Y, Mathew R, Fan J, Strohecker AM, Karsli-Uzunbas G, Kamphorst JJ, Chen G, Lemons JMS, Karantza V, Coller HA, DiPaola RS, Gelinas C,

Rabinowitz JD and White E. Activated Ras requires autophagy to maintain oxidative metabolism and tumorigenesis. *Genes Dev* 25: 460-470, 2011.

Yokochi, Tomoki and Robertson KD. Doxorubicin inhibits DNMT1, resulting in conditional apoptosis. *Mol Pharm* 66(6): 1415-1420, 2004.

Yoon J-H, Ahn SG, Lee HB, Jung SH, Ohd SH. Role of autophagy in chemoresistance: Regulation of the ATM-mediated DNA-damage signaling pathway through activation of DNA–PKCs and PARP-1. *Biochem Pharmacol* 83: 747-757, 2012.

Yuneva M, Zamboni N, Oefner P, Sachidanandam R and Lazebnik Y. Deficiency in glutamine but not glucose induces MYC-dependent apoptosis in human cells. *J Cell Biol* 178(1): 93-105, 2007.

Zhang XD, Wang Y, Wang Y, Zhang X, Han R, Wu JC, Liang ZQ, Gu ZL, Han F, Fukunaga K and Qin ZH. p53 mediates mitochondria dysfunction-triggered autophagy activation and cell death in rat striatum. *Autophagy* 5(3): 339-350, 2009 (A).

Zhang Y, Shi W, Li, Y-J and Wei L. Cardiomyocyte death in doxorubicin-induced cardiotoxicity. *Archivum Immunologiae et Therapia Experimentalis* 57: 435-445, 2009 (B).

Zhao X, Ogunwobi OO and Liu C. Survivin inhibition is critical for bcl-2 inhibitor-induced apoptosis in hepatocellular carcinoma cells. *PLoS ONE* 6: 8: e21980, 2011.

Zhu W, Soonpaa MH, Chen H, Shen W, Patne RM, Liechty EA, Caldwell RL, Shou W and Field LJ. Acute doxorubicin cardiotoxicity is associated with p53-induced inhibition of the mammalian target of rapamycin pathway. *Circulation* 119: 99-106, 2009.

Zhuang W, Qin Z and Liang Z. The role of autophagy in sensitizing malignant glioma cells to radiation therapy. *Acta Biochim Biophys* 41:341-351, 2009.

Appendices

Appendix A

Protocol 1: Cell culture

- Before experimental work in the laminar flow began, hands were thoroughly washed and sprayed with 70% ethanol and gloves were worn and sprayed with 70% ethanol once again to ensure sterility.
- T75 flasks containing E0771 breast cancer mouse cells, that were approximately 60-70% confluent were split into 6-well plates of ± 150 000 cells per well of containing 2 ml of media or ± 300 000 cells per T25 flask containing 4 ml of media for experimental procedures.
- Cells were washed with warm PBS (see Appendix B) to remove growth medium (see Appendix B) completely and dead cells.
- Cells were trypsinised using trypsin (3 ml) to release the adherent cells.
- The flask was then placed in an incubator, set at a low shaking speed for 3-mins at 37ºC. Cells were then viewed under a microscope to ensure detachment; if cells were not loosened the flask was gently tapped.
- Once the cells were loosened, warm growth medium (Double the amount of trypsin added = 6ml) was added to the flask to neutralise the trypsin. This was done to prevent the trypsin from killing the cells.
- This solution (growth medium, trypsin and cells) were then transferred to a 15 ml falcon tube and centrifuged at 1500 rpm for 3 minutes.
- The supernatant (trypsin+ growth medium) was removed and the pellet (cells) was re-suspended with 3 ml fresh growth medium using a pipette.

- To determine the average number of cells , 20 µl of the cell suspension was pipette onto a haemocytometer (see protocol 2)
- The number of cells per millilitre was calculated (see protocol 2)

Protocol 2: Cell counting using a haemocytometer.

- The haemocytometer was first cleaned by wiping with 70 % ethanol and then a moistened with breathe on the surface to allow for the coverslip to attach tightly.
- The re-suspended cell suspension (20 µl) was then pipette, 10 µl onto side A and 10 µl onto side B on the haemocytometer, using a micropipette.
- Through capillary action the cell suspension filled both counting grids (side A and B) (see diagram below)
- The total number of cells was counted by counting areas 1 to 8 in both counting grids. The average number of cells was then calculated and multiplied by 10 000 to get the number of cells per millilitre of the original cell suspension.

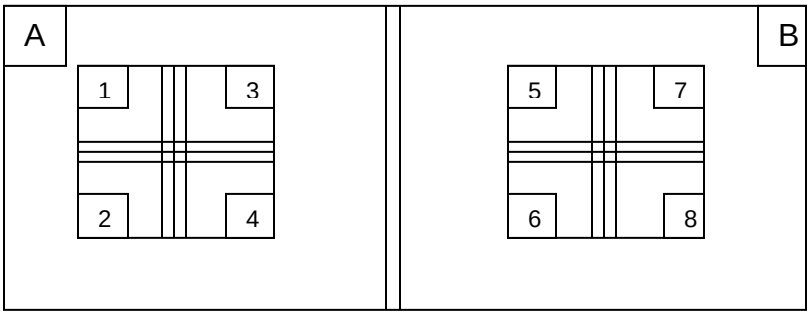

Protocol 3: Cell Harvesting

- This process removes the cells from the plastic substrate and breaks cell-to-cell bonds as gently as possible

- The old medium was discarded either by careful decanting or with a sterile pipette and the monolayer of cells was washed quickly with ice cold PBS. This wash step was repeated three times to remove all traces of FBS.

- The wash medium was decanted and then 250 µl (6-well plates) or 1000 µl (25 cm2 flask) of RIPA buffer (see appendix G) was added to each well other 6-well plate and flasks and placed on ice for 3-5 min

- The plates or flasks were swirled to make sure that the surface area was covered with the buffer

- After the time period had lapsed, the cells were scraped from the surface of each well and flask using a sterile cell scraper

- The buffer containing the cells was then pipetted into already chilled eppendorf tubes and stored at -80 °C until further experiments were carried out.

Protocol 4.1: Extraction of proteins from cell samples

- Work on ice at all times to avoid the denaturing of proteins
- Thawed cell samples (from protocol 3) were placed in chilled test tubes and sonicated. This process ruptures the cell walls in order to release proteins
- The metal piece of the sonicator was rinsed before and after use with distilled water
- After sonicating the cells, the cell solution was transferred into a chilled eppendorf tube and centrifuged at 4 ºC and $8x10^3$ rpm for 10 min.

Protocol 4.2: Extraction of proteins from tissue samples

- Work on ice at all times to avoid the denaturing of proteins
- Thawed cell samples were first cut into smaller pieces before being placed in chilled test tubes containing 1000 µl of RIPA buffer and sonicated. This process ruptures the cell walls in order to release proteins
- The metal piece of the sonicator was rinsed before and after use with distilled water
- After sonicating the contents of the tubes were transferred to eppendorf tubes that were placed on ice.

Protocol 5: Protein determination with Bradford reagent

Bradford Reagent: (5x concentrated)

Dilute 500 mg of Coomasie Brillant Blue G in 250 ml 95 % ethanol

Ass 500 ml of Phosphoric acid ad mix thoroughly

Make up to 1 L with dH_2O

Filer and store a 4˚C

Bradford Working Solution

Dilute stock in 1:5 ratios with dH_2O

Filter using 2filter paper at the same time

Solution should be light brown color

Bradford quantification

- Thaw a 1mg/ml BSA stock solution
- Thaw protein sample if it in -80˚C freezer – Keep on ice at all times
- Make up working solution of 100 ul BSA: 400 µ dH_2O. Vortex mixture
- Make 7 eppendorf tubes for the standards as well as tubes for samples to be tested
- Now add BSA water to marked Eppendorf tubes as follows
- Work on ice at all times to avoid the denaturing of proteins
- For protein determination, make a 1:5 dilution of the Bradford reagent using distilled water.

- This solution needs to be filtered twice using 2 pieces of filter paper. The Bradford reagent is light sensitive therefore remember to use foil or work in the dark room when filtering
- Once the Bradford reagent has been made, a standard curve needs to be made in 7 different eppendorf tubes as follows:

Blank	**0 µl BSA**	**100 µl dH_2O**
2 µg protein	10 µl BSA	90 µl dH_2O
4 µg protein	20 µl BSA	80 µl dH_2O
8 µg protein	40 µl BSA	60 µl dH_2O
12 µg protein	60 µl BSA	40 µl dH_2O
16 µg protein	80 µl BSA	20 µl dH_2O
20 µg protein	100 µl BSA	0 µl dH_2O
Each sample	0 µl BSA 95 µl dH_2O	5 µg of sample protein

- Vortex the solutions thoroughly and let them stand in ice for ±5 min
- Zero the spectrophotometer using the blank and then read the absorbance values at 595 nm using the Simple Reads program
- Once the absorbance readings were recorded, the readings were transferred onto an Excel spreadsheet and a standard curve was created.

Samples:

- Pipette 5 µl from each sample that was centrifuged into a new eppendorf tube and then add 95 µl distilled water and 900 µl Bradford reagent.
- Vortex solution and then read the absorbance values at 595 nm using the Simple Reads program
- Using excel, plot the standard curve with protein concentration on the x-axis and the mean OD on the y-axis (see example below). Add in the absorbance

Protocol 6: Western Blot

BioRad pre-cast gradient gels were used (4-15%).

Loading samples

- Place yellow well guide on top of apparatus in the middle compartment
- Using a 20 µl pipette, add 10 µl peqGOLD pre-stained marker in first well on the left and then your samples from the second well. Use a clean tip for every sample and marker
- Once all samples have been loaded, remove the well guide and add running buffer on the outer compartment up to ½ way from the bottom
- Place green lid on apparatus and attach electrodes – red to red and black to black
- Turn on electrophoresis machine and allow samples to run for 10 min at 400 mA and 100 V (fixed)
- Run samples for a second time for 20 min at 400 mA and 200

Transfer of proteins to membrane

Performed using BioRad transfer packs

- Go back to gel apparatus and remove the U-shaped core-latch. Remove the glass plates and separate them very carefully to avoid tearing the gel. Cut off the wells (stacking gel) and place the remaining (separating) gel in transfer buffer
- Add the gel on top of membrane
- Finally, place another other piece of blotting paper provided on top.
- Close the apparatus and then supply power for electron transfer: 100V, 0.5A

  30 minutes

- Once the time has elapsed, open semi-dry apparatus and remove the blotting papers on top carefully.
- Place membrane in blocking solution for a minimum period of 1hr on the belly dancer on lowest setting or leave in the fridge (4 ºC) overnight

Specific binding of proteins

- Wash membrane 3X (5 min each) with TBS-tween
- Make primary antibody solution in a 50 ml falcon tube. Roll the membrane containing transferred proteins facing the inside and the marker facing the bottom and place inside the falcon tube
- Mix on the rotating machine in the corridor fridge for a minimum period of 8 hr or leave overnight
- Wash membrane 3X (5 min each) with TBS-tween
- Make secondary antibody solution in a 50 ml falcon tube and add to membrane. Mix on the belly dancer or tube roller on lowest setting for 1 hr

Exposure

- Wash membrane 3X (5 min each)
- Mix ECL cocktails (500 µl solution A + 500 µl solution B) in falcon tube Drain excess liquid from membrane using tissue paper and add the ECL on the membrane and leave on for 1min
- Place in Chemi-Doc system tray and roll out bubbles before preparing software for image viewing.

Stripping membranes

- Wash membrane 2X (5 min each) in dH2O at room temperature
- Wash membrane 1X (5 min) in 0.2 M NaOH at room temperature
- Wash membrane 2X (5 min each) in dH2O at room temperature
- Place membrane in blocking solution and carry on as usual for western blotting (This procedure completely removes all antibodies)

Protocol 7: Trypan Blue Cell Exclusion Technique

Three independent experiments were conducted in triplicate.

Method:

- After 24 hour of treatment, 6-well plates containing treated cells were removed from the hypoxic and normoxic incubators.
- Medium was removed from cells in each well, washed with warm PBS and trypsinized (Protocol 1).
- Cell solution containing Trypsin was neutralised with warm growth medium, followed by centrifugation at 1300-1500 rpm for 3 minutes.
- The cells were analysed separately from each well and were re-suspended in 500 µl of warm PBS.
- From this suspension, 10 µl was removed into a 1ml eppendorf and 10 µl of Trypan Blue Dye (Invitrogen) was added to this.
- The cells suspension with the added dye was then pipetted onto counting slides (Invitrogen)

Using the Invitrogen Automatic cell counter, the total numbers of viable cells were calculated automatically and data recorded.

Protocol 8: MTT Cell Viability Assay

Method:

- Three independent experiments were conducted in triplicate.
- An Isopropanol solution (1%): containing 1 ml concentrated HCl and 99 ml Isopropanol was made.
- Triton solution (0.1 %) containing 0.1 ml Triton-X-100 was made up to 100 ml with distilled water.
- An Isopropanol / Triton solution was made in a 50:1 ratio, where 50 ml of 1% Isopropanol was added to 1 ml of 0.1% Triton. 1%
- MTT (0.01 g/1 ml PBS) solution was made up just before use. MTT is photosensitive, thus the solution was covered in foil.
- Medium was removed from treated cells.
- PBS (1.5 ml) and MTT (500 µl) was added and allowed to incubate, in 6 well plates covered with foil for 1 for 1 hour at 37ºC.
- After a hour if no cells had loosened. 2ml of the Isopropanol / Triton solution was added to each well and plates covered in foil were placed on a shaker for 5 minutes.
- The contents of each wells was transferred to 2 ml eppendorf tubes, centrifuged for 2mins at RPM 1500.
- The absorbance values of the supernatant were read at 540 nm using a spectrophotometer with Isopropanol / Triton solution was used as a blank.
- If absorbance was greater than one the supernatant was diluted with the Isopropanol / Triton solution and read at 540 nm again.

Protocol 9: Caspase-Glo 3/7 Assay

For this technique, cells were grown and treated on 96-well flat-bottom (enzymatic assay) plates and caspase activity was measured as follows:

- The Caspase-Glo 3/7 reagent was prepared (mix) following the manufacturer's instructions, and was allowed to equilibrate to room temperature
- The 96-well plates containing cells were removed from the incubator and allowed to equilibrate to room temperature
- 100 µl of the Caspase-Glo 3/7 reagent was added to each well (100 µl) of the plate. The plate was then covered
- The contents of the wells were mixed using a plate shaker at 300-500 rpm for 30 sec. Incubation followed for 30 min at room temperature
- The luminescence of each sample in the plate was measured using a plate-reading luminometer
- In addition, blank (containing only medium) wells were treated with the Caspase-Glo 3/7 reagent. The values from these wells were subtracted from the wells containing cells to remove any background noise.

Protocol 10: GFP-LC3 Transfection and Live Cell Imaging

- Cells were cultured in chamber dishes containing 8 wells.
- 800ng of DNA concentration per sample (well of the 8-chamber dish)
- Lipofectamin is used as chemical transfection reagent. It is a transient transfection, meaning that:

  1. Not all cells will take up the construct and express protein and

  2. The cells will not express the protein for long (usually the plasmid is released during cell cycle or after a few cell divisions).

  - 800ng DNA +50 ul serum free media per sample in one eppendorf tube (A), vortex for 3 sec For 4 wells, use 200 ul media + 2.4 ul DNA for the LC3
  - 12 ul lipofectamin + 200 ul serum free media per sample in one eppendorf tube (B), vortex for 3 sec

- Incubate both at room temperature for 5 min

  1. Combine both A and B, vortex, incubate for 20 min at room temp.
  2. Add the DNA/reagent mixture drop-wise onto the dish (containing normal growth medium) (100 ul per well)

- Image 24 hrs later (or, change media next day, image 48hrs post transfection)

Protocol 11: *In vivo* Model- Cancer cell inoculation.

Adapted from Ewens *et al*. 2006 (doxorubicin plus Interleukin-2 Chemo-immunotherapy against Breast Cancer in Mice).

- Culture E0771 cells until 80% confluent.
- Digest cultured E0771 cells using tyrosin (0.05% trysin-EDTA from 5 minutes at 37˚C).
- Centrifuge at 1500 rpm for 3 minutes.
- Wash cells once with sterile PBS.
- Count cells and dilute with HBSS to a concentration of 1250 cells/µl (2.5×10^5 cells in 200µl)
- Inject the cell suspension in lower abdomen of each mouse, in or near the no. 4 mammary fat pad (Day 0).

***Mice Subcutaneous injection* (SC)**

Adapted from **Guideline for Handing, Restrain, Injections and Blood Collection from Small Laboratory animals (**http://campusvet.wsu.edu/infofac/handing.htm**)**.

SC injections can be administered easily to mice. The needle in inserted between the folds of the skin into the base of the triangle that is form when traction is applied to the skin overlying the animal's scruff. The syringe's plunger should be retraced to verify that a vacuum is created and no blood or tissue fluid can be aspirated. Subsequently, the plunge is depressed releasing the material. In general no greater than 1 ml should be injected per SC injection site in adult mice (> 25 grams). Several sites over the animal's back should be used if large volumes must be administrated. In general, needles should be 0.5-10 long and 23 ga or larger gauge.

Appendix B

Growth Medium

- 500 ml Dulbecco's Modified Eagles Medium (DMEM)
- □56 ml Fetal Bovine Serum (FBS)
- □5.6 ml Penstrep

Hanks Balanced Salt Solution (Used to induce Starvation)

- Contains Magnesium, Calcium and Sodium Bicarbonate, pH 7.0 – 7.4.

Phosphate buffer saline

Weigh the following reagents:

- □16 g NaCl
- □0.4 g KCl
- □2.88 g Na_2HPO_4 (di Sodium hydrogen phosphate)
- □0.48 g KH_2PO_4 (potassium di-hydrogen phosphate)

Adjust pH to 7.4, fill up to the 2 L mark with distilled water and sterilize by autoclaving.

Running buffer (1 L)

- Weight out 3.03 g Tris, 1.44 g Glycine and 1 g SDS into a 1 L beaker.
- Add 500 ml distilled water and stir until dissolved
- Fill up to 1 L with distilled water

10X TBS (5 L)

- Weight out 121 g Tris and 80 g NaCl into a 5 L beaker. Add 2.5 L distilled
- water and stir until dissolved.
- Adjust pH to 7.6 using HCl and then fill up to 5 L with distilled water
- For use in Western blotting, take a 1 L measuring cylinder and add 100 ml
- 10X TBS and dilute with 900 ml distilled water
- To make TBST, add 1 ml tween to 1 L diluted solution of TBS

Transfer Buffer

- In a 1 L cylinder, add 100 ml Biorad 10X TG buffer, 200 ml 100% methanol and 700 ml distilled water

Milk blocking solution (100 ml)

- Weight out 5 g non-fat dry instant milk powder into a beaker. Add 100 ml TBS and mix well
- Finally add 10 µl Tween and mix well. This is sufficient for only one gel

RIPA Buffer

- Tris-HCL 2.5 mM
- EDTA 1 mM
- NaF 50 mM
- NaPPi 50 mM
- Dithiotheitoal 1 mM
- Phenylmethylsulfony floride (PMSF) 0.1 mM
- Benzamidine 1 mM
- 4 mg/ml SBTI
- 10 mg/ml leupeptin
- 1% NP40
- 0.1% SDS
- 0.5% deoycholate

- Add 1000 µl Triton X-1000 to the solution and finally fill up to 100 ml with distilled water and mix thoroughly
- Aliquot 1000 µl of RIPA buffer into eppendorf tubes and store at -20 ºC

BSA (Bovine serum albumin 1 mg/ml)

- For 1 ml BSA, weight out 1mg BSA and add 1000 µl distilled water.
- For use during Western blotting, this BSA needs to be diluted.
- Pipette 100 µl from 1 mg/ml BSA in new eppendorf tube and add 400 µl distilled water.
- Mix well.

Bradford Reagent (1 L)

- Weight out 500 mg Coomassie Brilliant Blue G and add it to 250 ml 95% ethanol
- Add 500 ml phosphoric acid and mix well
- Fill up to 1 L with distilled water and store at 4 ºC
- For use during Western blotting, this solution needs to be filtered twice and then a 1:5 dilution needs to be made

3X Sample buffer

- Measure 33.3 ml stacking Tris (0.5 M) and place in a beaker
- Weigh out 8.8 g SDS and 20 g glycerol and place in the beaker
- Add a pinch of Bromo-phenol blue to the mixture
- Add and make up to 75.47 ml with distilled water

Tris pH 8.8 (500 ml)

- Weigh out 68.1 g Tris (1.124 M) and 1.5 g SDS (0.3%) and place in a beaker.
- Add 400 ml distilled water, stir and then adjust pH using HCl
- Add 100 ml distilled water to make the final volume to 500 ml

Tris pH 6.8 (500 ml)

- Weigh out 30.3 g Tris (0.5M) and 2g SDS (0.4%) and place in a beaker.
- Add 400 ml distilled water, stir and then adjust pH using HCl
- Add 100 ml distilled water to make the final volume to 500 ml

Tris pH 6.8 (100ml) for Sample buffer

- Weigh out 6.06 g Tris (0.5 M) and 4 ml 10%SDS and place in a beaker
- Add 80 ml distilled water, stir and then adjust pH using HCl
- Add 20 ml distilled water to make the final volume to 100 ml